

A HYDRAULIC WAVE ENERGY CONVERTER

by

Jacques du Plessis

*Thesis presented in partial fulfilment of the requirements for
the degree of Master of Science in Mechatronic Engineering
at Stellenbosch University*



Department of Mechanical and Mechatronic Engineering,
University of Stellenbosch,
Private Bag X1, Matieland 7602, South Africa.

Supervisor: Prof. J.L. van Niekerk

March 2012

Declaration

By submitting this thesis electronically, I declare that the entirety of the work contained therein is my own, original work, that I am the owner of the copyright thereof (unless to the extent explicitly otherwise stated) and that I have not previously in its entirety or in part submitted it for obtaining any qualification.

Signature:

J. du Plessis

Date:
1 December 2011

Abstract

As a renewable energy source, wave energy has the potential to contribute to the increasing global demand for power. In South Africa specifically, the country's energy needs may easily be satisfied by the abundance of wave energy at the South-West coast of the country.

Commercially developing and utilizing wave energy devices is not without its challenges, however. The ability of these devices to survive extreme weather conditions and the need to achieve cost-efficacy while achieving high capacity factors are but some of the concerns. Constant changes in wave heights, lengths and directions as well as high energy levels and large forces during storm conditions often lead to difficulties in keeping the complexity of the device down, avoiding over-dimensioning and reaching high capacity factors.

The point absorber device developed as part of this research is based on an innovation addressing the abovementioned issues. An approach is followed whereby standard "off-the-shelf" components of a proven hydraulics technology are used. The size of the device is furthermore adaptable to different wave climates, and the need for a control system is not necessary if the design parameters are chosen correctly.

These characteristics enable low complexity of the device, excellent survivability and an exceptionally high capacity factor. This may lead to low capital as well as low operation- and maintenance costs.

In this paper the working principle of this concept is presented to illustrate how it utilises the available wave energy in oceans. The results obtained from theoretical tests correlate well with the experimental results, and it is proven that the device has the ability to achieve high capacity factors. As the device makes use of existing, "off-the-shelf" components, cost-efficient energy conversion is therefore made feasible through this research.

Opsomming

As 'n hernubare/ herwinbare energiebron bied golfenergie die potensiaal om by te dra tot die bevrediging van die stygende globale energie-navraag. In spesifiek Suid-Afrika kan die oorvloed van beskikbare golfenergie aan die Suid-Weskus van die land gebruik word om aan die land se energiebehoefte te voldoen.

Betroubaarheid en oorlewing in erge weerstoestande, koste-effektiwiteit en die behaal van hoë kapasiteitsfaktore is beduidende struikelblokke wat oorkom moet word in die poging om 'n golfenergie-omsetter wat kommersieël vervaardig kan word, te ontwikkel.

Daarby dra voortdurende veranderinge in golfhoogtes, -lengtes en -rigtings sowel as hoë energievlakke en groot kragte tydens storms by to die feit dat dit moeilik is om die kompleksiteit van die stelsel laag te hou. Dit terwyl daar voorkom moet word dat die toestel oorontwerp en verhoed word dat hoë kapasiteitsfaktore bereik word.

Die puntabsorbeerder-toestel wat in hierdie navorsing ontwikkel is, bestaan uit 'n ontwerp wat spesifiek ontwikkel is om die bogenoemde probleme aanspreek. 'n Unieke benadering is gevolg waardeur standaard, maklik-bekombare komponente gebruik is en die komponent-groottes ook aangepas kan word volgens golfgroottes. Indien die ontwerp-dimensies akkuraat gekies word, is die moontlikheid verder goed dat 'n beheerstelsel nie geïmplementeer hoef te word nie. Hierdie eienskappe verseker lae stelselkompleksiteit, uitstekende oorlewingsvermoë en 'n uitstaande kapasiteitsfaktor. Lae kapitaal- sowel as onderhoudskostes is dus moontlik.

Die doel van hierdie dokument is om die werking van die konsep voor te stel en teoreties sowel as prakties te evalueer. Die resultate van teoretiese toetse stem goed ooreen met eksperimentele resultate, en dit is duidelik dat die toestel hoë kapasiteitsfaktore kan behaal. Aangesien die toestel verder gebruik maak van bestaande komponente wat alledaags beskikbaar is, word die koste-effektiewe omsetting van golfenergie dus moontlik gemaak deur hierdie navorsing.

*To my parents, Abraham and Marietta du Plessis,
my sister, Madelé du Plessis and my
beloved girlfriend, Freda Stander*

Acknowledgements

I wish to thank Professor J.L. van Niekerk for his tireless efforts, valuable comments on the content and support of this project.

I would like to thank my parents, Abraham and Marietta du Plessis, for their support, prayers and encouragement throughout the development of this work. I also wish to thank my sister, Madelé du Plessis (BA Masters) who did the editing and proofreading of this document.

I would like to express my sincere appreciation to Freda Stander who gave me the moral support I required. I am heartily thankful to her for consistently helping me keep perspective on what is important in life.

Last, but not least, all honours to our Creator. Thank you God for the inspiration, wisdom and strength You have given me when I needed it most; for guiding me through the challenges.

It would have been next to impossible to write this thesis without the help and support of these wonderful people.

Contents

Declaration	i
Abstract	ii
Opsomming	iii
Acknowledgements	v
Contents	vi
List of Figures	x
List of Tables	xiv
Nomenclature	xv
Abbreviations	xviii
1 INTRODUCTION	1
1.1 Problem Statement and Motivation	1
1.2 Wave Energy in South Africa	2
1.3 Thesis Objectives and Scope	3
1.4 Thesis Outline	4
2 LITERATURE STUDY	5
2.1 Wave Energy	5
2.2 Wave Energy in South Africa	6
2.2.1 Wave Energy Resource	6
2.2.2 Wave Energy Projects in South Africa	8
2.3 Advantages, Disadvantages and Environmental Impacts of WEC's	9
2.3.1 Disadvantages	9
2.3.2 Advantages	10
2.3.3 Potential Environmental Impacts	11
2.4 Classification of Wave Energy Converters	12
2.4.1 Classification According to Location	13

2.4.2	Classification According to Size, Orientation and Extraction Method	13
2.5	Wave Energy Converters in the World	14
2.6	Point Absorbers	16
2.6.1	Existing Point Absorbers	17
2.6.2	Power Take-Off Methods	18
2.6.3	Modelling of Hydraulic PTO's	20
2.6.4	Control Methodologies for Hydraulic PTO's	21
3	HYDRODYNAMIC MODELLING AND SIMULATION	26
3.1	Forces	26
3.2	Equations of Motion	28
3.3	Desired Movement of Buoy	33
3.4	Analytical Results	35
3.5	Verification of Model	35
3.5.1	Experimental Setup	35
3.5.2	Image Processing	37
3.6	Conclusion	42
4	DEVELOPMENT OF WAVE ENERGY CONVERTER	43
4.1	Sizing of the Buoy	43
4.2	Power Take-off Device	44
4.2.1	Calculation of Power and Energy	44
4.2.2	Control Systems	46
4.2.3	PTO as a Damper	49
4.2.4	Concept Design for PTO	51
4.2.5	Concept Evaluation	51
4.2.6	Comparative Analysis Between Concepts C1 and C2	52
4.2.7	Final Design of PTO	54
4.3	Design Specifications	56
4.4	Conclusion	57
5	MODELLING AND SIMULATION OF HYDRAULIC PTO	58
5.1	Bond Graph Representation	58
5.2	State Equations of the Hydraulic PTO	59
5.2.1	Cylinder	60
5.2.2	Hydraulic Hoses	61
5.2.3	Check Valves	62
5.2.4	Accumulator	63
5.2.5	Hydraulic Motor	64

5.2.6	Damping Force	65
5.3	Analytical Results of Hydraulic Model	66
5.4	Verification of Hydraulic Model	68
5.4.1	Hardware-in-the-loop (HIL) Simulation	68
5.4.2	Experimental Results	69
5.5	Hydraulic Winch System	71
5.6	Combined Hydrodynamic-Hydraulic System	72
5.7	Conclusion	73
6	EXPERIMENTAL SETUP AND RESULTS	74
6.1	Experimental Apparatus and Test Equipment	74
6.2	Test Procedure	75
6.3	Laboratory Results	76
6.3.1	Tests with Pressure Regulator	76
6.3.2	Tests with Flywheel on Shaft	79
6.3.3	Tests with Flow Restrictor at Outlet	79
6.3.4	Tests with Flow Restrictor at Inlet	80
6.3.5	Tests with Smaller Gear Motor	80
6.3.6	Conclusion	80
6.4	Results - Large Wave Flume	81
6.5	Conclusion	82
7	DESIGN IMPROVEMENTS	84
7.1	Shape of Buoy	84
7.2	Spring or Vacuum	85
7.3	Flow and Energy Output	86
7.4	Check Valves and Diameter of Return Line	87
7.5	Conclusion	88
8	CONCLUSION AND FUTURE RESEARCH	89
8.1	Discussion and Conclusion	89
8.2	Recommendations	91
	List of References	92
	Appendices	97
	A Existing Point Absorbers	98
	B Values for design parameters	99

C Concepts	100
D Concept Evaluation	106
E Concepts C1 and C2	108
F Engineering Specifications	114
G Parameter Values	117
H Hydraulic Model	118
I Laboratory Tests - Results	121
I.0.1 Flywheel	121
I.0.2 Flow Restrictor at Outlet	123
I.0.3 Flow Restrictor at Inlet	124
I.0.4 Smaller Motor	126

List of Figures

2.1	Global annual (averaged) wave power distribution in kW/m (Wave Energy Centre (s.a.))	5
2.2	Location of South Africa (De F Retief <i>et al.</i> (1982))	7
2.3	Composite diagram showing important features of surface atmospheric circulation over South Africa (Tyson <i>et al.</i> , (2000))	7
2.4	Classification of WECs according to location (adapted from Falnes (2006)) . .	13
2.5	Classification according to size, orientation and energy-extracting method (adapted from Falnes (2006))	14
2.6	Pelamis (Oregon State University (2011))	14
2.7	CETO (Carnegie Corporation (2011))	15
2.8	LIMPET (The Queen's University of Belfast (2002))	15
2.9	Wave Dragon (Power of Waves (2010))	16
2.10	Definition of six DOF directions	17
2.11	Schematic of hydraulic devices with (a) a double-acting cylinder (Taylor <i>et al.</i> (2009); Engja and Hals (2007)) and (b) a single-acting cylinder	20
2.12	Power bond (Engja and Hals (2007))	21
2.13	Basic bond elements (Engja and Hals (2007))	22
2.14	Model structure	22
2.15	Latching control (Budal and Falnes (1980))	23
2.16	Latching control (Budal and Falnes (1980))	23
2.17	Control system with damping force as reference (Cross <i>et al.</i> (2009))	24
2.18	Control system with angular velocity as reference	24
3.1	Free body diagram	27
3.2	Wave theories (US Corps (2002))	29
3.3	Buoyancy forces acting on submerged sphere	30
3.4	Calculating added mass of a spherical body	31
3.5	Non-dimensionalised heave and surge coefficients of added mass and radiation resistance for a submerged sphere with radius r in deep water (Falnes (2004))	32
3.6	Desired movement of buoy	34
3.7	Desired vertical movement of buoy (Cargo <i>et al.</i> (2011))	34
3.8	Surge response of numerical model	36

3.9	Heave response of numerical model	36
3.10	Wave flume creating waves	37
3.11	Simulated movement of buoy	37
3.12	Movement of physical buoy	37
3.13	Buoy configurations: (a) old and (b) new	38
3.14	Surge response of physical model	38
3.15	Heave response of physical model	39
3.16	Comparison between surge responses of analytical and physical models	39
3.17	Comparison between heave responses of analytical and physical models	40
3.18	Wrong tracking	40
3.19	New comparison between surge responses of analytical and physical models	41
3.20	New comparison between heave responses of analytical and physical models	41
3.21	Position of centre point of buoy: analytical versus experimental	42
4.1	Energy extracted per hour vs. buoy diameter	44
4.2	Velocity vector transformation	45
4.3	Velocities for surge direction	46
4.4	Velocities for heave directions	46
4.5	Velocities along mooring cable	47
4.6	Description of control system	47
4.7	Energy equation derived from desired movement of buoy	48
4.8	Energy for system acting as a damper	48
4.9	Energy for system acting as a spring	49
4.10	Energy for system acting as a constant force	49
4.11	Optimal damping coefficient	50
4.12	Heave response of buoy with damper as PTO	50
4.13	Schematics of concepts C1 and C2	51
	(a) C1	51
	(b) C2	51
4.14	Schematic of the final WEC design	55
5.1	Schematic of hydraulic power take-off system	58
5.2	Bond graph of hydraulic power take-off system	59
5.3	Pressure in accumulator	68
5.4	Speed of rotation of gear motor	68
5.5	Hardware-In-the-Loop	69
5.6	Measured pressure in accumulator	70
5.7	Measured speed and duration of rotation of gear motor	70

5.8	Model structure	71
5.9	Depth of buoy	72
5.10	Heave motion of buoy for second-order stokes waves	72
5.11	Latching effect for second-order stokes waves	73
6.1	Hydraulic PTO	75
6.2	Generated energy for each stroke length and frequency	76
6.3	Shaft speed for each stroke length and frequency	77
6.4	Duration of shaft rotation for each stroke length and frequency	78
6.5	Number of cycles per minute for each stroke length and frequency	78
6.6	Induced voltage and current	79
6.7	Tests in large wave flume	81
	(a) Buoy	81
	(b) Hydraulic PTO	81
6.8	Surge response of combined system	82
6.9	Heave response of combined system	82
7.1	Buoyancy force for a cylinder, sphere and cone	84
	(a) Shapes	84
	(b) Buoyancy force	84
7.2	Surge and heave responses of complete model (with spring)	85
7.3	Accumulator pressure for various size motors	86
7.4	Pressure drop due to friction in hoses	87
A.1	Existing point absorbers	98
C.1	Concept 1 - Mechanical device	100
C.2	Concept 2 - Hydraulic device	101
C.3	Concept 3 - Pneumatic device	101
C.4	Concept 4 - Linear generator device	102
C.5	Concept 5 - MHD device	102
	(a) MHD system	102
	(b) Explanation of MHD	102
C.6	Concept 6 - EAP device	103
C.7	Concept 7 - Friction/ heat device	104
C.8	Concept 8 - Hydrogen device	104
C.9	Concept 9 - Sea water pump device	105
E.1	Schematic of concept C1	108
E.2	Intermittent forces versus gradual force changes	109

E.3	Power output changing with flywheel and torsion spring	109
E.4	Energy capture using only a flywheel	110
E.5	Schematic of concept C2	111
H.1	Sensors	118
	(a) Strain gauge	118
	(b) Load cell	118
H.2	Hydraulic PTO	118
H.3	Sensors	119
	(a) Pressure transducer	119
	(b) Proximity sensor	119
H.4	Pressure devices	119
	(a) Pressure regulator	119
	(b) Pressure relief valve	119
H.5	From left to right: Scope; power supply; PID controller; and signal generator .	119
H.6	Accumulator, gear motor and alternator	120
	(a) Accumulator	120
	(b) Gear motor and alternator	120
H.7	Single-acting cylinder (or pump) connected to actuator	120
	(a) Direct coupling	120
	(b) With rope	120
I.1	Induced voltage and current with 2 kg-flywheel	121
I.2	Normalised energy with 2 kg-flywheel	121
I.3	Speed of rotation with 2 kg-flywheel	122
I.4	Duration of rotation with 2 kg-flywheel	122
I.5	Normalised energy with back-pressure and 2 kg-flywheel	123
I.6	Speed of rotation with back-pressure and 2 kg-flywheel	123
I.7	Duration of rotation with back-pressure and 2 kg-flywheel	124
I.8	Normalised energy with flow restrictor at inlet and 2 kg-flywheel	124
I.9	Speed of rotation with flow restrictor at inlet and 2 kg-flywheel	125
I.10	Duration of rotation with flow restrictor at inlet and 2 kg-flywheel	125
I.11	Induced voltage and current with 6 cc motor and 2 kg-flywheel	126
I.12	Normalised energy with 6 cc motor and 2 kg-flywheel	126
I.13	Speed of rotation with 6 cc motor and 2 kg-flywheel	127
I.14	Duration of rotation with 6 cc motor and 2 kg-flywheel	127

List of Tables

2.2	Weights selected for each environmental impact (Thorpe (1992))	11
2.1	Potential environmental impacts (Petroncini and Yemm (s.a.))	12
3.1	Useful design parameters for a point absorber	34
4.1	Comparison of control systems	49
5.1	Sizes of hydraulic components	67
B.1	Values for design parameters	99
D.1	Decision matrix for wave energy device	106
E.1	Sizes of components: hydraulic vs mechanical	112
E.2	Weights of components: hydraulic vs mechanical	113
E.3	Costs of components: hydraulic vs mechanical	113
F.1	Engineering specifications	114
G.1	PTO model parameters	117

Nomenclature

Constants

$$\pi \approx 3.141\,592\,654$$

$$e \approx 2.718\,281\,828$$

$$g \approx 9.81 \text{ m/s}^2$$

Variables

a	Amplitude of wave	[m]
A_{eff}	Inside cross-sectional area of cylinder	[m ²]
A_{float}	Cross-sectional area of float	[m ²]
A_p	Inside cross-sectional area of cylinder - rod side	[m ²]
β	Bulk modulus	[Pa]
c	Damping coefficient	[Ns/m]
c_v	Transition coefficient	[s/m]
C_A	Added mass coefficient	[]
C_D	Hydrodynamic viscous drag coefficients	[]
$C_{D'}$	Hydrodynamic damping coefficients	[]
d	Depth of water - distance between seabed and SWL	[m]
D_H	Hydraulic diameter of pipe	[m ²]
f	Frequency	[Hz]
f_{cfr}	Coulomb friction coefficient	[N/Pa]
f_{vfr}	Viscous friction coefficient	[N/(m/s)]
F_c	Constant force	[N]

F_{H_2O}	Force of water mass on float	[N]
H	Height of wave	[m]
HP	High pressure	[bar]
k	Spring constant	[N/m]
K	Breakaway friction force increase coefficient	[]
K_D	Flow discharge coefficient	[]
K_s	Shape factor that characterises the cross-section of the pipe	[]
L_g	Geometrical length of pipe	[m]
L_{eq}	Equivalent length of resistance	[m]
LP	Low pressure	[bar]
m_a	Force of water mass on float	[N]
p	Pressure differential across valve	[bar]
P	Generated power	[W]
q	Flow through valve	[m ³ /s]
Q_{acc}	Volume flow into accumulator	[m ³ /s]
Q_{cyl}	Volume flow in and out cylinder	[m ³ /s]
Q_{leak}	Leakage flow from hydraulic motor	[m ³ /s]
Q_{motor1}	Volume flow into motor	[m ³ /s]
Q_{motor2}	Volume flow from hydraulic motor	[m ³ /s]
Q_{res}	Volume flow into reservoir	[m ³ /s]
r	Radius of sphere	[m]
R_s	Hydrodynamic damping coefficient due to added mass in surge	[]
R_h	Hydrodynamic damping coefficient due to added mass in heave	[]
Re	Reynolds number	[]
t	Time	[s]

T	Wave period	[s]
U_1	Water particle velocity in surge	[m/s]
U_3	Water particle velocity in heave	[m/s]
x	Horizontal distance	[m]
X	Surge displacement	[m]
\dot{X}	Surge velocity	[m/s]
\ddot{X}	Surge acceleration	[m/s ²]
z	Vertical distance	[m]
Z	Heave displacement	[m]
\dot{Z}	Heave velocity	[m/s]
\ddot{Z}	Heave acceleration	[m/s ²]
ρ	Fluid density	[kg/m ³]
\forall	Submerged buoy volume	[m ³]

Subscripts

- $1/s$ Surge
- $3/h$ Heave
- am/a Added mass
- b Buoyancy force
- d Drag force
- h/x Surge
- hd Hydrodynamic damping
- v/z Heave

Abbreviations

CECS	Centre for Study of Environmental Change and Sustainability
ESKOM	Electricity Supply Commission (National Electrical Utility of South Africa)
MHD	Magnetohydrodynamics
PSP	Pneumatically Stabilised Platform
PTO	Power Take-off
s.a.	Sine anno ("without year")
s.l.	Sine loco ("without place/ place of publication unknown")
s.n.	Sine nomine ("without a name/ name of publisher unknown")
SEAREV	Syst'eme Autonome Electrique de R'ecup'eration de l'Energie des Vagues
SWEC	Stellenbosch Wave Energy Converter
SWL	Still Water Line
UNFCCC	United Nations Framework Convention on Climate Change
WEC	Wave Energy Converter
WET	Wave Energy Technology

Chapter 1

INTRODUCTION

1.1 Problem Statement and Motivation

As the majority of the earth's population depends on fossil fuels for energy supplies, the world faces major future energy challenges. The exponential growth in human population and resultant rising energy consumption rates will furthermore cause fossil fuel reserves to be depleted within decades. This will lead to a significant increase in fossil fuel prices as it will become increasingly difficult to exploit these natural resources in the deeper layers of the earth's crust.

In addition to these practical implications, the environmental impact of fossil fuels is also of concern. Fossil fuel-fired power plants emit carbon dioxide that alters the greenhouse gas concentrations in the atmosphere. Most of the sun's energy moves through the atmosphere to warm the surface of the earth. In order to keep the earth's energy in balance, most of this energy is radiated back into space while some is (primarily) trapped through the heat-trapping properties of greenhouse gases.

An increase in greenhouse gas amounts (e.g. carbon dioxide, which is the main contributor to climate change), however, enhances the atmosphere's heat-trapping capability, causing it to trap more of the radiated energy (known as the "greenhouse effect") and increases the surface temperature of the earth ("global warming").

The increase in greenhouse gases serves as a forcing mechanism (i.e. it forces the climate to change) that not only increases the temperature, but also depletes the stratospheric ozone layer. The increase in surface temperature in turn causes climates to shift, which affects the weather patterns. This phenomenon is also known as "climate change" (Le Treut *et al.* (2007)).

Due to an increase in environmental concerns as well as the cost of fossil fuels, renewable energy is a contentious issue. Renewable energy resources are currently too costly to

CHAPTER 1. INTRODUCTION

compete with fossil fuels, but as time progresses it will become more economically viable to exploit renewable energy resources such as wave energy.

According to Polinder and Scutto (2004), two French engineers, Pierre-Simon Girard and his son, patented the first wave energy converter in 1799. Since then another 340 patents were filed between 1800 and 1973 (Polinder and Scutto (2004)).

During the 1970's the oil crisis provided an impetus for research into renewable energy. Lord Rothschild wrote a report to the government containing a few recommendations (Wilson (2010)), and included the statement:

"The first stage of a full technical and economic appraisal of harnessing wave power for electricity generation should be put in hand at once."

This statement spurred the creation of wave energy programmes in a few countries in the North Atlantic area, as the area has a large amount of wave energy around the coastlines.

The first wave energy converters were designed to have maximum efficiency (Polinder and Scutto (2004)). The result was a complex mechanism that failed to meet all the necessary requirements, simultaneously including reliability, robustness and cost-effectiveness. When the oil industry regained stability, the need for wave energy devices was reduced, as they were too expensive and could simply not compete with the lower oil prices.

1.2 Wave Energy in South Africa

The energy demand in this country currently outweighs the energy supply. It is estimated that approximately 30% of South African citizens do not have access to electricity (SouthAfrica.info Reporter (2007)). The existing power stations are furthermore unable to supply enough energy to consumers, and energy demand increases cause frustrating intermittent power disruptions. It is accordingly submitted that if nothing is done to balance the energy demand-and-supply-equation, South Africa could expect a serious power crisis (SouthAfrica.info Reporter (2007)) in the years to come.

Fossil fuels currently account for 93% of the country's electricity production. This makes South Africa not only the largest carbon dioxide-emitting country on the continent, but the 13th largest carbon dioxide-emitting country in the world (DEA (2007)). The country is however not only a large contributor to climate change, but is also a victim of it. Studies have shown that the South African landscape is becoming more arid (Vetter (2009)).

CHAPTER 1. INTRODUCTION

Factors such as growth in population, increase in energy demand, energy security, the exhaustion of conventional energy resources and economic stability have all spurred a renewed interest in renewable energy sources.

South Africa has a vast amount of renewable energy resources, including solar power, hydro power, wind energy, biomass and ocean wave energy. To reduce the effect of global warming and climate change, both locally and worldwide, the South African government has set a target of 10 000 GWh (equivalent to two 660 MW units of Eskom's coal fired power stations) to be produced by these renewable energy sources by 2013 (DME (2003)).

Wave energy will have a significant contribution to electricity generation in South Africa. As wave energy features one of the most concentrated forms of renewable energy, it would appear that wave energy may also play a key role in reducing South Africa's carbon footprint in the future.

South Africa has a world class wave power resource due to its close proximity to the storm generation zone in the southern ocean. Measured wave data indicate that the South African South West coast has the greatest resource with an average wave power of approximately 40 kW per meter wave crest. The rest of the South African coast has an average wave power of approximately 18 to 23 kW/m. The wave resource is season dependent. The average wave power for the South West coast is 30 kW/m during the summer and 60kW/m during the winter (Joubert (2010)).

1.3 Thesis Objectives and Scope

To efficiently harness the untapped wave energy around the South African coastline, a wave energy converter is developed as part of this research. This converter should assist the government in reaching its goal of establishing a renewable energy industry, thereby creating a more sustainable and improved standard of living.

The objectives of this research are as follows:

- An offshore point absorber must be developed;
- It must be a scale model that is small enough for it to be tested in the laboratories and for a single person to move it around;
- No attention needs to be paid to the design of the buoy. A spherical-shaped float may be used;

CHAPTER 1. INTRODUCTION

- A mechanical or electromechanical wave energy converter must be developed. The power system could make use of gearboxes, flywheels, hydraulics, generators, etc.; and
- The power take-off system must be mounted on the ocean floor and not in the float. No power cables should run along the mooring cable (as it could easily be damaged).

Apart from the abovementioned objectives, the device also needs to be cost-effective in order to provide a competitive alternative to fossil-based energy technologies. The reliability of the wave energy devices are of critical importance as component failures lead to unplanned maintenance that, in turn, has an impact on the cost of wave energy. Running costs, offshore maintenance and the total number of components should be kept at a minimum.

This wave energy converter must also offer a sustainable, non-subsidised alternative to fossil fuels in South Africa, therefore contributing to the creation of a low carbon economy.

The challenge of this research is therefore to find the best balance between reliability, efficiency and cost-effectiveness when designing a mechanism that can turn the power of waves into a usable form of energy.

1.4 Thesis Outline

This document has been divided into eight chapters. To gain insight into the wave energy field, a literature study was conducted and is documented in Chapter 2.

A mathematical model for the hydrodynamic model is presented in Chapter 3. This model is capable of computing the exact movement of the buoy for any wave profile input, whether it is regular or irregular. Tests were conducted in a small wave flume to verify the results obtained with the mathematical model.

In Chapter 4 the numerical model developed in Chapter 3 is used to find the best method for energy extraction. A few concepts were subsequently developed to determine the technology that should be used for the PTO.

A numerical model that simulates the dynamic behaviour of a hydraulic power take-off system is discussed in Chapter 5. In Chapter 6 the experimental results that have been obtained with a scale model (tested in the laboratory and the large wave flume), are presented. Some design improvements are given in Chapter 7.

Finally, Chapter 8 contains the conclusions and gives some recommendations for future research.

Chapter 2

LITERATURE STUDY

2.1 Wave Energy

The energy contained in the ocean's waves is more than enough to supply at least half of the world's electricity needs: it is estimated that waves possess a total power of 1-10 TW (Wave Energy Group (2005)) or, otherwise stated, 8 000-80 000 TWh/yr, whilst the world's energy requirement is approximately 140 000 TWh/yr (Isaacs and Seymour (1973)) which means that the wave energy could contribute to half of the world's requirements.

Wave energy is unevenly distributed around the world. The highest power levels occur between the latitudes of 30° to 60° (IEA-OES (2007)) in the Southern as well as Northern Hemisphere (see Figure 2.1). These zones, commonly known as "hot spots", have the highest wave activity due to the occurrence of strong storms (CRES (2002)). Other parts of the world located outside of these latitudes also have significant wave climates, but not as substantial as the hot spot zones. The lower power levels are however compensated for by smaller wave power variability (Boud (2003)).

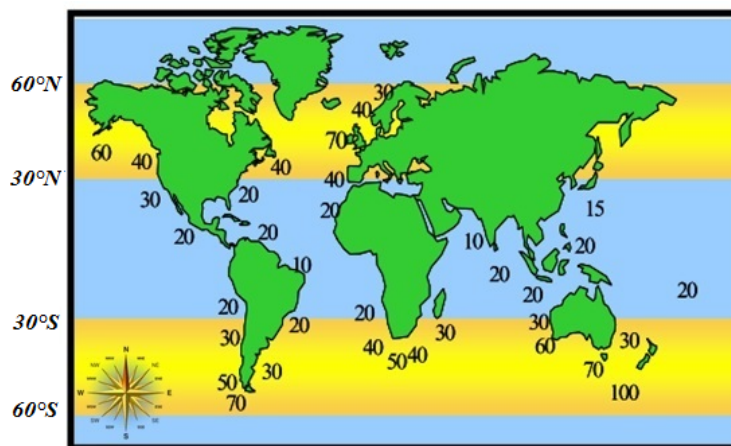


Figure 2.1: Global annual (averaged) wave power distribution in kW/m (Wave Energy Centre (s.a.))

CHAPTER 2. LITERATURE STUDY

Depending on the earth's orientation to the sun, some parts of the earth are heated more than others. The air in the warmer parts becomes less dense, and therefore lighter. Being more dense, cold air displaces the warmer air upwards, causing the air to rise.

When wind blows over the ocean, small ripples form due to friction. As the wind continues to blow, more of the wind energy is converted into wave energy, causing the small ripples to eventually become large waves that can travel over far distances.

Wave energy can therefore be seen as a concentrated form of solar energy. The original solar radiation power levels of $1\ 000\ W/m^2$ of the earth's surface are converted to more concentrated (wave) power levels of 10 to 100 kW per metre crest length (Boud (2003)).

The waves formed within or in close proximity to the storm-generating zones continue to travel in the direction they were formed, even if the wind changes direction or subsides after a period of time. Waves have an irregular pattern at the beginning of formation, but in deep water the waves become progressively regular and can endure for tens of thousands of kilometres from the point of origin (Boud (2003)).

Boud (2003) mentions a few factors that determine the size of the waves and the amount of energy that is transferred across the ocean. These include the speed of the wind, the length of time the wind is blowing as well as the distance over which the wind blows (the so-called "fetch"). Coasts such as the South-West coasts of South Africa, South America, Australia, New Zealand, Europe and the North-West coasts of North America, are exposed to the prevailing wind direction as well as long fetches and consequently tend to have more energetic wave climates than other parts of the world (Figure 2.1).

2.2 Wave Energy in South Africa

2.2.1 Wave Energy Resource

Wave energy has the potential to contribute to an improved environment as well as the increasing demand for power. The southern part of South Africa is located between the latitudes of 30° and 35° South, which is in close proximity of storm-generating zones (see Figure 2.2 and refer to section 2.1).

A few meteorological features have an influence on the wave regime in the South Indian- and South Atlantic oceans. Air that is heated in the tropics at the equator moves in a southward direction and declines at the latitude of 30° , forming the so-called Hadley cell.

The South Indian High and the South Atlantic High, two semi-permanent high-pressure systems, are caused by this declining air that moves in a clockwise direction around the

CHAPTER 2. LITERATURE STUDY

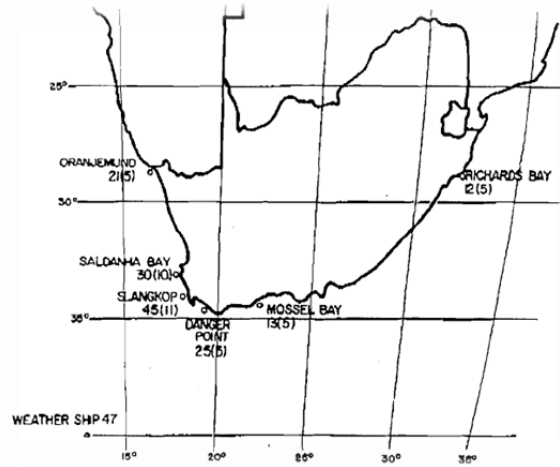


Figure 2.2: Location of South Africa (De F Retief *et al.* (1982))

centre of these high-pressure systems. Air sinks to the south of the Hadley cell and moves towards the poles to create the Ferrel westerly winds. These winds spiral in an easterly direction around the world. Low-pressure systems are created when the Ferrel westerlies is disturbed. The low-pressure systems then migrate from west to east across the country. Figure 2.3 below shows that the ocean waves that approach the South African coastline are mainly caused by this sinking of air with its associated wind fields and cold fronts (Rossouw (1989)).

During the winter months the southern tip of South Africa intersects the low-pressure systems as it moves over the country. In the summer, however, the low-pressure systems shift further south, missing the country. South Africa therefore experiences more severe wave conditions during the winter than in the summer. The South-West coastal region of the country is most exposed to these wave conditions (Rossouw (1989)).

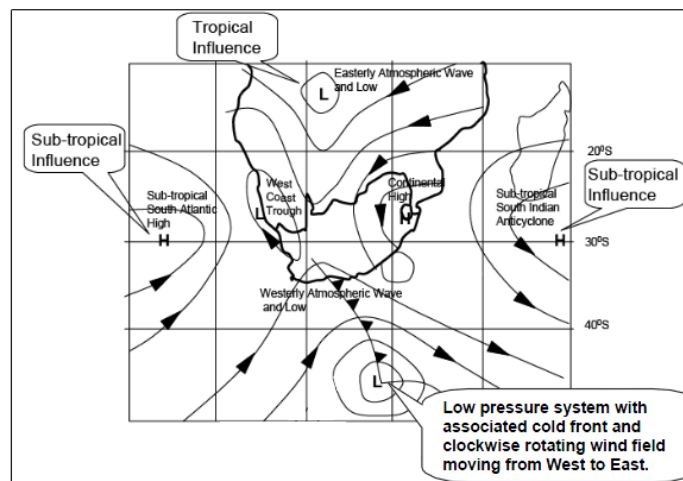


Figure 2.3: Composite diagram showing important features of surface atmospheric circulation over South Africa (Tyson *et al.* (2000))

Compared to the rest of the world, South Africa has a significant wave power resource. As the mean annual power levels of the ocean waves around the Cape Peninsula are roughly 40kW/m wave crest length (Figure 2.1), a total average power of 56 800 MW is available for exploitation (DME (2003)).

2.2.2 Wave Energy Projects in South Africa

High oil prices in the 1980's forced governments across the globe to investigate alternative energy sources. During this period, the University of Stellenbosch conducted research in the field of wave energy conversion and invented the Stellenbosch Wave Energy Converter (SWEC) (De F Retief *et al.* (1982)), which was funded by the mining companies Anglo and De Beers. A pilot plant was however never built as the oil prices regained stability. Model tests were nevertheless completed, and provided valuable data of how such a system will operate.

The ocean waves around the South-West coast (Joubert (2008)) have a significant potential and could greatly contribute to the generation of electricity in South Africa. Due to the high costs of developing this technology, no real efforts have been made to exploit this alternative source of energy.

In 2006 a Scottish company, Ocean Power Delivery, considered a R7 billion investment for the development of a 700 MW wave energy plant off the coast of Mossel Bay (Business Report, (2006)). The company was also interested in installing their devices (known as the Pelamis) near Saldanha, Knysna and Port Elizabeth. This project was however never realised due to the emerging global economic crisis (Joubert, 2010) and a lack of feed-in tariff support in South Africa.

In 2007 a Canadian company, Finavera Renewables, considered the development of a 20 MW wave power plant in two areas off the western coast of South Africa that had been selected. It would have cost more than US\$ 40 million, but the project was never undertaken due to economic losses suffered when one of the company's buoys sank near Oregon (USA). The company cancelled the wave energy operations (Joubert, 2010).

A local South African company, Wave Energy Generation, considered the installation of a 770 MW plant off the western coast near Darling (which would have cost about R15 billion) in 2009. The company is currently seeking investors to secure funding for the development of a 5 MW pilot plant (Davenport (2009)).

According to Business Report (2006), a 30 MW plant that covers an area of a square kilometre, is more than enough to power 20 000 homes. If a wave power plant is to be built near Mossel Bay in the future, it would be enough to supply electricity to approximately

470 000 homes. If another plant is implemented off the Western Coast of South Africa near Darling, almost a million homes could be powered from wave energy.

2.3 Advantages, Disadvantages and Environmental Impacts of WEC's

The development of wave energy is sustainable as it combines environmental, economic, social and ethical factors (Thorpe *et al.* (2002)). In this section the advantages as well as disadvantages are discussed.

2.3.1 Disadvantages

The disadvantages of wave energy power plants include the following:

- High capital costs are needed in constructing and designing of WECs (Petroncini and Yemm (s.a.));
- Offshore devices need long, expensive transmission cables that increase the costs of constructing (Ocean Atlas (s.a.));
- The peak-to-average load ratio for wave converters is high and difficult to predict (Ocean Atlas (s.a.));
- The technology used is restricted to specific sites where the waves are strong (Ocean Atlas (s.a.));
- People have an apparent lack of knowledge about wave energy (Petroncini and Yemm (s.a.));
- Wave energy is an intermittent source (Ocean Atlas (s.a.));
- Power-smoothing systems are needed due to fluctuations in power(Ocean Atlas (s.a.));
- Grid constraints are caused due to fluctuation in power (Petroncini and Yemm (s.a.));
- As with all forms of renewable energy, storing may be problematic (Ocean Atlas (s.a.)); and
- Strong forces exerted on the device lead to low reliability levels (Petroncini and Yemm (s.a.)).

2.3.2 Advantages

The advantages of wave energy power plants include the following:

- No fuel is needed (Haluzan (2010));
- Energy is completely free (Haluzan (2010));
- Wave energy is an inexhaustible energy source (Haluzan (2010));
- The energy supply is secure (Thorpe *et al.* (2002));
- Wave energy has the highest energy density among renewable energies (Ocean Atlas (s.a.));
- The natural seasonal variability follows electricity demand (Thorpe *et al.* (2002));
- There is a limited negative impact on the environment (Thorpe *et al.* (2002));
- There are no carbon dioxide emissions (Ocean Atlas (s.a.));
- Wave energy is suitable for the generation of clean energy carriers such as hydrogen and low carbon fuels (Ocean Atlas (s.a.));
- There is a negligible demand on land use (Thorpe *et al.* (2002));
- Wave energy power plants may serve as artificial reefs (Langhamer and Wilhelmsson (2006));
- WECs can create a calm space behind the wave power plant that could be used for the development of mariculture or even recreational activities (Ocean Atlas (s.a.));
- Converters may be used for remote islands, lighting for navigation, and water pumping for fish farms (Ocean Atlas (s.a.));
- WECs will stimulate declining industries such as shipbuilding, job creation in construction, maintenance and operations, etc. (Thorpe *et al.* (2002));
- WECs can be built into harbour walls, therefore having the dual uses of the protection of harbours and the generation of electricity (Ocean Atlas (s.a.));
- WECs have long operation life time (Ocean Atlas (s.a.));
- The construction and existence of WECs may lead to local economic development (Carter (2005)) and the diversification of employment (Thorpe *et al.* (2002)); and

CHAPTER 2. LITERATURE STUDY

- A WEC may reduce grid stability problems as wave energy converters may make use of synchronous generators that allow reactive power control (Ocean Atlas (s.a.)).

The grid constraints and intermittency problems could easily be solved with hardware. Furthermore, reliability shouldn't be a problem when advanced technology is used. The major disadvantage is therefore the cost of developing a WEC. The advantages clearly outweigh the disadvantages.

2.3.3 Potential Environmental Impacts

Petroncini and Yemm (s.a.) point out that there is little knowledge and experience of the environmental impacts of wave energy converters, primarily because the development of wave energy is still in a nascent stage. In Table 2.1 the researcher provides a summary of the likely environmental impacts envisaged by Petroncini and Yemm (s.a.).

Thorpe (1992) assigned weights to the potential environmental impacts mentioned in Table 2.1. These weights indicate how large of an impact the aspects may have on the environment, and these environmental impacts with, their corresponding weights, are summarised in Table 2.2. Since the student will develop a point absorber, only the environmental impacts with weights for offshore devices are given in this table.

Table 2.2: Weights selected for each environmental impact (Thorpe (1992))

ENVIRONMENTAL IMPACT	WEIGHTS FOR OFFSHORE DEVICES
Land use	-
Visual impact	Small
Construction/ maintenance sites	Small - Medium
Noise	Small
Navigation hazard	Small - Medium
Ecosystems	Small - Medium
Fisheries/ recreation	-
Disturbance of sediment	Small
Disturbance of seabed	Small
Effects on the coast	Small - Medium
Endangered species/ protected areas	Small
Tourism	Small

Table 2.1: Potential environmental impacts (Petroncini and Yemm (s.a.))

ENVIRONMENTAL IMPACT	DESCRIPTION
Land use	Large areas of ocean used
Visual impact	High for onshore and nearshore; low for offshore
Construction/ maintenance sites	Hydraulic fluid losses, accessibility of roads
Noise	Turbine makes noise - behind the waves, but waves usually have a higher noise level
Navigation hazard	Obstacle to shipping
Ecosystems	Interference with the migration routes of fish and mammals
Fisheries/ recreation	Interference with fisheries zones
Disturbance of sediment	Disturbance in sedimentary flow patterns
Disturbance of seabed	Mooring and bottom-standing devices may have an effect on the seabed
Effects on the coast	Smaller waves on beach that influence surfers' activities; may reduce coastal erosion or sediment transportation
Endangered species/ protected areas	There are protected areas where, if disturbed, endangered species may be threatened
Tourism	Leisure activities may be impacted

2.4 Classification of Wave Energy Converters

The variety of wave energy devices are quite large compared to other renewable energy technologies. It is therefore difficult to find a unequivocal classification, but wave energy devices are usually classified according to their location (Polinder and Scutto (2004)). Harris *et al.* (2004) notes that the various wave energy converters can be classified according to three principle areas, namely: location, directional characteristics and operating principles. Wave energy converters may also be classified according to size. A summary of these classifications is provided in the subsections that follow.

2.4.1 Classification According to Location

Wave energy devices can be categorised into three groups, depending on the distance from the shore. These are onshore, nearshore or offshore (Polinder and Scutto (2004)).

Shoreline devices were the first wave energy converters to be developed and are therefore defined as first-generation devices. These devices are normally incorporated into breakwater structures or rocky seaside cliffs.

Nearshore devices, also known as second-generation devices, were later developed and are generally deployed in water depths of one (1) to 25 metres. These depths are generally found at a few hundred metres from the shore.

Offshore- or third-generation devices were only developed at a later stage and evolved from the first- and second-generation counterparts. These devices take longer to develop as result of the harsh environment that they are exposed to.

These devices are portrayed , along with locations, in Figure 2.4

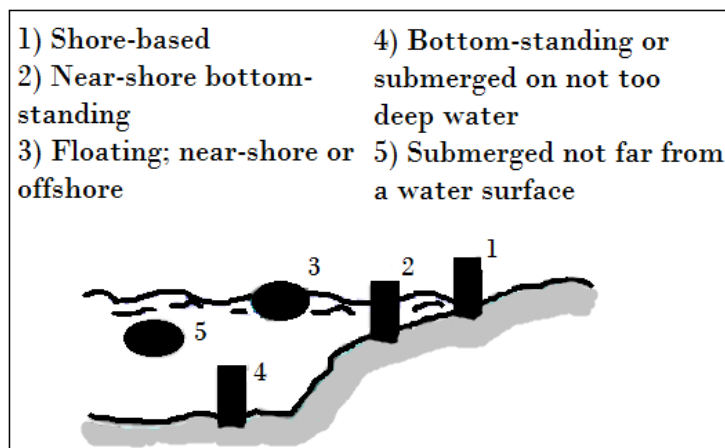


Figure 2.4: Classification of WECs according to location (adapted from Falnes (2006))

2.4.2 Classification According to Size, Orientation and Extraction Method

Other classifications are also possible. The size and orientation affect the way in which the device converts the wave energy to electrical energy (Figure 2.5). The two main groups are known as terminator- and compliant devices. Each group has two subgroups: oscillating water columns and overtopping devices fall under the terminators group, while point absorbers and attenuators fall under the compliant group (Power Projects (2008)).

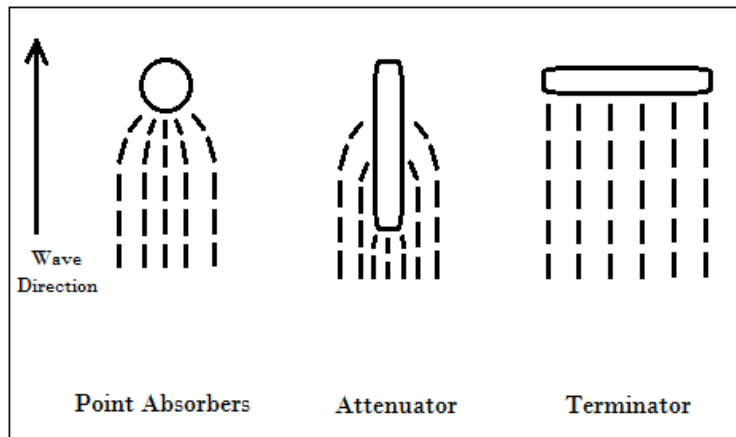


Figure 2.5: Classification according to size, orientation and energy-extracting method (adapted from Falnes (2006))

2.5 Wave Energy Converters in the World

Only a few onshore and offshore wave energy converters, that will also be suitable for electricity generation in South Africa, have been successfully designed and built. These include the Pelamis (attenuator), CETO (point absorber), LIMPET (oscillating water column) and Wave Dragon (terminator). Refer to section 2.4 for the classification of wave energy devices and Van Niekerk and Joubert (2011) for a complete list of current wave energy converter designs.

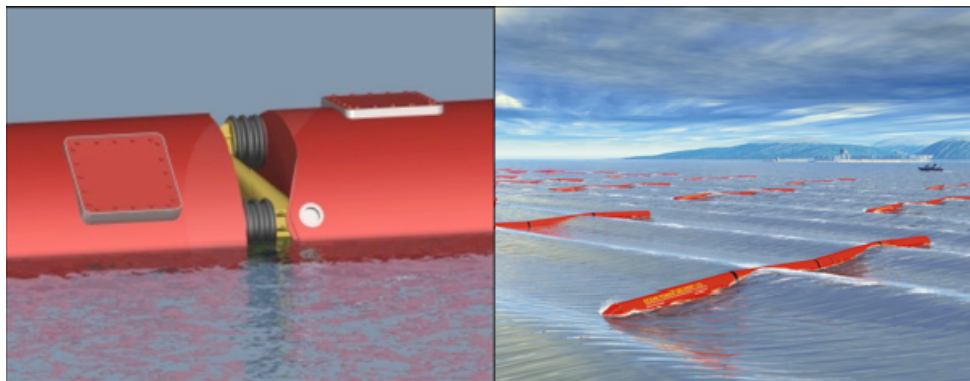


Figure 2.6: Pelamis (Oregon State University (2011))

Attenuators are oriented parallel to the direction of the waves. An example of such devices is the 750 kW Pelamis (Latin for "Sea Snake") developed by the company Ocean Power Delivery. The Pelamis consists of four tubular sections (with a diameter 4.6 m and a total length of 150 m) that are connected with rams. These sections move relative to each other as the wave passes under it. The rams pump hydraulic fluid through a hydraulic system, converting kinetic energy into hydraulic and mechanical energy (Figure 2.6). Due to the fact that the device is slack-moored it is capable of orientating itself into the direction of

CHAPTER 2. LITERATURE STUDY

incoming waves. The Pelamis' narrow profile enables it to survive during extreme weather conditions (Oregon State University (2011)).

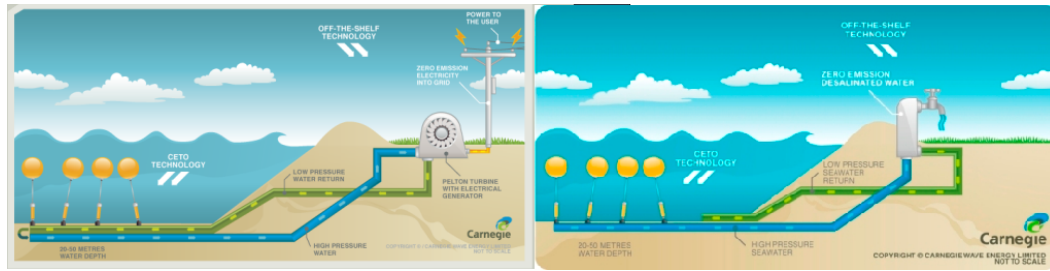


Figure 2.7: CETO (Carnegie Corporation (2011))

Carnegie Corporation's 200 kW CETO is fully submerged and produces high-pressure water. Sea water is delivered via high-pressure pipes either to a Pelton turbine that is located ashore for the generation of electricity; or it is utilised to produce zero-emission freshwater through standard reverse osmosis desalination technologies (Figure 2.7). Only the cylinders and buoys (with diameters of 6 m) are located offshore, and all the other technologies are located onshore, which means that there is no need for underwater transmission. The CETO units are able to adjust their position according to the tide and wave conditions, and because they are point absorbers, they can absorb energy from the waves in all directions (Carnegie Corporation (2011)).

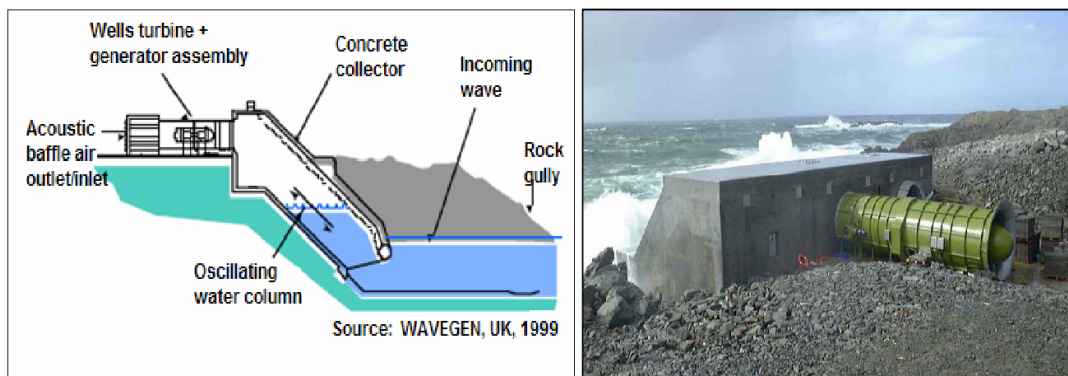


Figure 2.8: LIMPET (The Queen's University of Belfast (2002))

The LIMPET (Figure 2.8), a partially-submerged structure developed by the company WaveGen that is located onshore, is a full-scale 500 kW oscillating water column (OWC). This structure has an opening to the water surface below. Air is trapped inside of the structure above the free water surface and as waves approach the device, the height of the water surface inside the structure oscillates. The trapped air is channeled through to a bi-directional, axial flow Wells turbine (The Queen's University of Belfast (2002)).



Figure 2.9: Wave Dragon (Power of Waves (2010))

An example of a terminator is the Wave Dragon. It consists of two parabolic arms that focus waves over an overtopping ramp into a storage basin. The water that is stored above the sea level rushes out through multiple low-head Kaplan-turbines that generate electricity (Figure 2.9). This four (4) to 11 MW device is capable of orientating itself to face incoming waves (Previsic (2004)).

In this thesis a point absorber will be developed and deployed offshore. Reasons for developing an offshore device rather than other types of wave energy devices, are as follows (Rossouw (s.a.)):

- The visual impact of an offshore device, which is generally not aesthetically pleasing, is lower;
- No contribution to noise levels;
- Limited navigation hazard to shipping;
- The wave power potential is higher;
- Can avoid protected/ sensitive coastal areas;
- These devices will have less of an impact on coastal processes; and
- Water particles in deep waters have less activity closer to the ocean's bed compared to water particles in shallow waters. The particle velocity as well as the radius of the circle (i.e. the circulation of the water particles) decrease rapidly with increasing depth. The buoy can therefore be lowered during extreme weather conditions to protect it from being damaged.

2.6 Point Absorbers

Point absorbers use buoys that harvest the energy of waves from all directions at a specific point in the ocean (Vining (2005)). These devices are usually implemented offshore, but

CHAPTER 2. LITERATURE STUDY

could be deployed near the shore as well, depending on the design of the device and the type of mooring that is used. The most common point absorbers make use of buoys, but other types do exist.

The buoy can float on top of the ocean's surface or it can be fully submerged, depending on the pressure inside the float. To let the buoy float, the cavity inside the buoy needs to be positively buoyant. In other words, there needs to be air or foam inside. To have the buoy fully submerged, the cavity needs to be partially filled with water (Vining (2005)).

According to the company Power Projects (2008), point absorbers mainly have two parts: a large spar that is located on the seabed and a float that reacts to the passing crests and troughs of the waves (as mentioned above).

Generally, a body submerged in water experiences six degrees of freedom: three translational motions (heave, surge and sway) and three rotational motions (roll, yaw and pitch), as shown in Figure 2.10. Point absorbers usually extract the vertical motion (heave) of the kinetic energy from the waves. Modern point absorbers strive to absorb all three translation components, namely heave, surge and pitch.

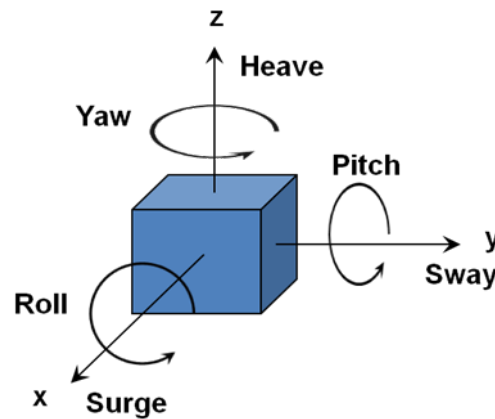


Figure 2.10: Definition of six DOF directions

Point absorbers have a small cross-sectional area compared to other types of wave energy converters. It therefore only extracts a small amount of the ocean's energy. Their size, however, lends it to be deployed in arrays and, as a result, it can achieve utility scale. Point absorbers have generation capacities of 100 kW to 1 MW and can easily form a 700 MW power plant (Power Projects (2008)).

2.6.1 Existing Point Absorbers

A few companies have developed prototype point absorbers over the years, while some are already building point absorbers on a commercial scale. An example of the latter

is the Carnegie Corporation, which deployed its CETO technology (CETO 3) south of Perth, Australia. An offshore test programme was successfully completed in 2010, allowing Carnegie to proceed with its first grid-connected commercial wave power project.

There are currently approximately 45 different point absorbers that have been developed to date. Some are single- and others are multipoint systems (Joubert (2010)). These devices are listed according to location in Appendix A (Wave Energy Centre (2006)).

2.6.2 Power Take-Off Methods

A few power take-off (PTO) methods have been developed over the years to convert the linear motion of a buoy to electrical energy. Forces transferred to the point absorber device can easily exceed one (1) MN, while velocities can exceed two (2) m/s (Vining (2005)). It is necessary to keep this in mind when selecting the appropriate power take-off method.

Intermediaries such as hydraulic systems are used to convert the buoy's linear motion into the rotary motion that is needed to run a conventional electric generator. Mechanical and magnetic systems are also suitable for this conversion, and conversely, direct conversion from linear to rotary motion is possible with linear or MHD generators. Contactless force transmission systems may also be implemented.

2.6.2.1 Linear Generators

Unlike conventional generators, linear generators in buoys move up- and downwards; thus directly converting linear motion into electrical energy. Different linear generator topologies need to be analysed to find the most suitable one for point absorbers.

A large number of different linear machine types are available, but not all machines are suitable for wave energy conversion (McLean (1998); Boldea and Nasar (1999)). According to Polinder *et al.* (2005) field-wound synchronous and induction machines cannot compete with permanent magnetised machines at slow speed. As a result, only five types of machines are used for wave energy applications (Cruz (2008)):

- Asynchronous (induction) generators;
- Synchronous Permanent Magnet Generators (also known as Longitudinal Flux Permanent Magnet Generators - LFPM);
- Air-cored Tubular Permanent Magnet Generators (TAPM);
- Variable Reluctance Permanent Magnet Generators (VRPM); and

- Transverse Flux Permanent Magnet Generators (TFPM).

Of all the devices listed above, the TFPM is considered as the most suitable for a point absorber device as it is the smallest whilst still having the highest efficiency.

2.6.2.2 Magneto hydrodynamic (MHD) Generators

Flowing seawater conducts an electric current in the presence of a strong magnetic field. Seawater flows through a hollow tube that has a flared in- and outlet. These sections work on the Bernoulli principle: it increases the water velocity. Electromagnets generate a magnetic field perpendicular to the flow of water, thereby stimulating an electric current in the passing water. The current is then collected by electrodes that are placed in the tube (Vining (2005)).

2.6.2.3 Hydraulic Systems

In Figure 2.11 two schematics of closed-loop hydraulic power take-off systems are shown. Figure 2.11(a) incorporates a double-acting cylinder while (b) illustrates the incorporation of a single-acting cylinder.

As the crest of the wave passes over the system, the buoy moves upward, causing the single-acting hydraulic cylinder to also move upward and to push hydraulic fluid through the hydraulic circuit. The single-acting cylinder is spring-actuated, which means that as the trough of the wave passes over the buoy, a tension spring pulls the piston downwards and the top chamber is filled with oil, keeping the mooring cable tight and, therefore, preparing the system ready for the next cycle.

Double-acting cylinders, on the other hand, push oil out from the bottom chamber whilst the top chamber is filled with oil during the downward stroke. The hydraulic fluid has a damping effect on the buoy's motion, whether it is on the upward or downward stroke of the cylinder. This linear up-and-down action pumps pressurised hydraulic fluid through an accumulator which, in turn, feeds a hydraulic motor. The hydraulic motor creates the rotary motion that is needed to drive an electric generator.

In both the hydraulic circuits portrayed in Figure 2.11, banks of accumulators are used to minimise pulsations and to absorb shocks. This means that an intermittent or variable input flow will become more smooth. Gas (nitrogen) bottles are connected to the accumulators (with a ratio of approximately 15:1) to increase the effective gas volume whilst keeping the size and cost of the piston accumulator at a minimum.

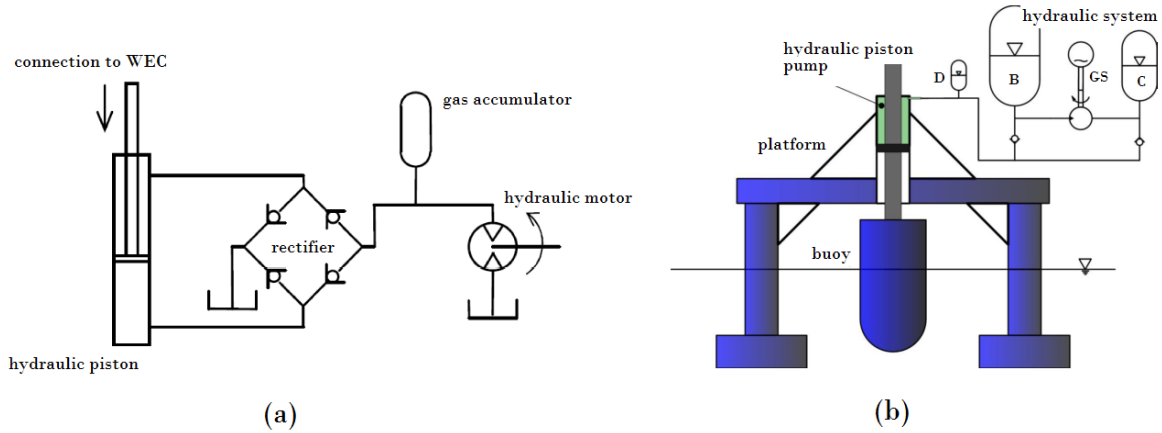


Figure 2.11: Schematic of hydraulic devices with (a) a double-acting cylinder (Taylor *et al.* (2009); Engja and Hals (2007)) and (b) a single-acting cylinder

A high-pressure accumulator and either a low-pressure accumulator or a reservoir are installed on either side of the motor. The pressure difference across the hydraulic motor causes the hydraulic fluid to flow from the high-pressure to the low-pressure accumulator.

A pressure regulator regulates the pressure drop over the hydraulic motor. As it keeps the pressure constant, the hydraulic fluid will be drawn at a constant speed from the high-pressure accumulator. The constant flow through the motor will ensure a constant output shaft speed and therefore a constant power output.

The pressure in the hydraulic system may be lower than the pressure rating of the high-pressure accumulator when the buoy starts moving upward. A smaller accumulator with a lower pre-pressure rating than that of the high-pressure accumulator bank can be installed to absorb this lost energy.

The use of hydraulic components are preferred above other technologies, as it has been proven to be more compact and less expensive for a given power rating.

2.6.3 Modelling of Hydraulic PTO's

2.6.3.1 Bond Graph Basics

Bond graphs (Hals and Engja (2007)) are used to model physical systems such as hydraulic systems. It not only provides a methodical means of formulating state space equations, but also supplies a concise pictorial representation of interacting physical systems that store, dissipate or transport energy. It is a very useful tool for the modelling of power take-off systems in WECs.

Bonds are visual descriptions that represent the bi-directional energy flows through physical systems. Figure 2.12 shows that the conventional direction for positive power flows

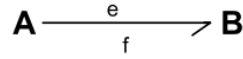


Figure 2.12: Power bond (Engja and Hals (2007))

from A to B, which is indicated by the half arrow. Each bond is associated with an effort variable e and a flow variable f . The short vertical lines (not shown in this figure), also known as the causality strokes, indicate the direction of effort. The power that is exchanged between the two components that is connected by the bond is given as:

$$\text{Power flow} = e(t) \cdot f(t) \quad (2.6.1)$$

Two other energy variables (measures of the stored energy in the system) are the generalised momentum p and generalised displacement q , defined as:

$$p = \int e(t) dt \quad (2.6.2)$$

and

$$q = \int f(t) dt \quad (2.6.3)$$

There are nine basic types of multi-port elements required to represent models. These elements function as idealised mathematical versions of real components. A summary of the constitutive relations for the nine basic 1-port, 2-port and two multiport elements are given in Figure 2.13. In translational mechanics the C , I and R would represent a spring, mass and damper component, respectively. Se and Sf represent the effort (force) and flow (velocity) sources and the zero (0) and one (1) are junction elements that indicate how the components are connected to each other.

Mathematical equations can be formed from a bond graph model and entered into computer algorithms to solve these equations. For basic features of bond graphs, refer to Hals and Engja (2007). For a more detailed explanation of bond graph methodology and associated techniques, refer to Karnopp and Rosenberg (1975).

2.6.4 Control Methodologies for Hydraulic PTO's

Point absorbers need control strategies in order to bring their motion in harmony (or resonance) with the waves. The buoy should therefore oscillate with the same frequency as the waves passing over the device. In order to control the movement of the buoy, some

CHAPTER 2. LITERATURE STUDY

Bond graph element	Elemental relations
$\frac{e}{f} \searrow \text{R}$ Resistor	General: $e = \Phi_R(f)$ Linear: $e = R \cdot f$
$\frac{e}{f} \searrow \text{C}$ Capacitor	General: $q = \Phi_C(e)$ Linear: $q = C \cdot e$
$\frac{e}{f} \searrow \text{I}$ Inertia	General: $p = \Phi_I(f)$ Linear: $p = I \cdot f$
Se $\frac{e}{f} \searrow$ e-source	$e = e(t)$
Sf $\frac{e}{f} \searrow$ f-source	$f = f(t)$
$\frac{e_1}{f_1} \searrow \text{TF}$ $\frac{e_2}{f_2} \searrow$ Transformer	$e_1 = e_2 \cdot m$ $f \cdot m_1 = f_2$
$\frac{e_1}{f_1} \searrow \text{GY}$ $\frac{e_2}{f_2} \searrow$ Gyrator	$e_1 = f_2 \cdot r$ $f_1 \cdot r = e_2$
$\frac{e_1}{f_1} \searrow 0$ $\frac{e_2}{f_2} \searrow$ $\frac{e_3}{f_3} \downarrow$ 0-junction	$e_1 = e_2 = e_3$ $f_1 - f_2 + f_3 = 0$
$\frac{e_1}{f_1} \searrow 1$ $\frac{e_2}{f_2} \searrow$ $\frac{e_3}{f_3} \downarrow$ 1-junction	$f_1 = f_2 = f_3$ $e_1 - e_2 + e_3 = 0$

Figure 2.13: Basic bond elements (Engja and Hals (2007))

means of damping must be incorporated into the system to limit the movement when encountering extreme weather conditions, while still maximising energy capture. Damping methods employed depend on the type of device being operated. Either buoyancy tanks or the resistive forces of the generator may be used for damping (Vining (2005)).

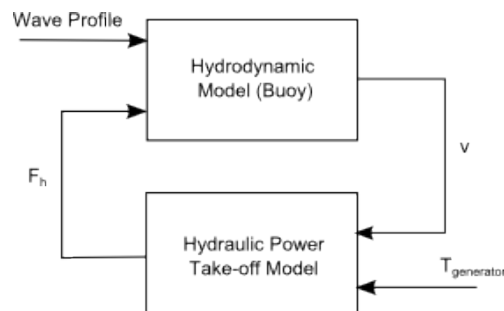


Figure 2.14: Model structure

A control strategy would be to alter the electric generator torque $T_{\text{generator}}$ which, in turn, affects the damping force F_h . Figure 2.14 shows how the hydrodynamic model (buoy) is connected to the power take-off system. The hydrodynamic model requires the ocean profile and damping force of the PTO as a function of the stroke velocity and generator torque as inputs. It then outputs a velocity that supplies the input stroke velocity of the cylinder. The PTO therefore exerts a damping force on the buoy that not only affects the motion of the buoy, but also increases efficiency.

CHAPTER 2. LITERATURE STUDY

2.6.4.1 Control Techniques

Good controlling methods for generator-damping have been established. Budal and Falnes (1980) suggest that a controller must be introduced in the system (Figure 2.15). They introduced a control technique called "latching control", where the velocity is kept in phase with the excitation force.

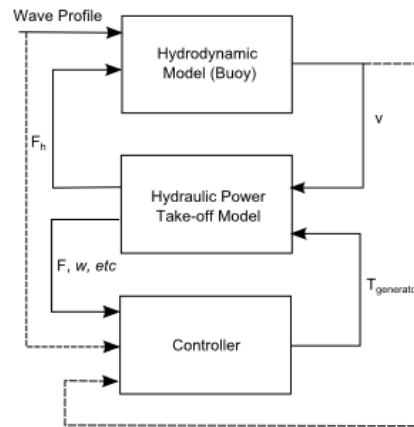


Figure 2.15: Latching control (Budal and Falnes (1980))

As Figure 2.16 illustrates, latching control consists of locking the buoy when the velocity is zero and releasing it again when the most favourable situation (almost maximum buoyancy force) is reached. As long as the velocity vanishes, the forces do not work. This means that latching control does not need to deliver energy to the system while it is engaged. Latching control is therefore a passive method of controlling.

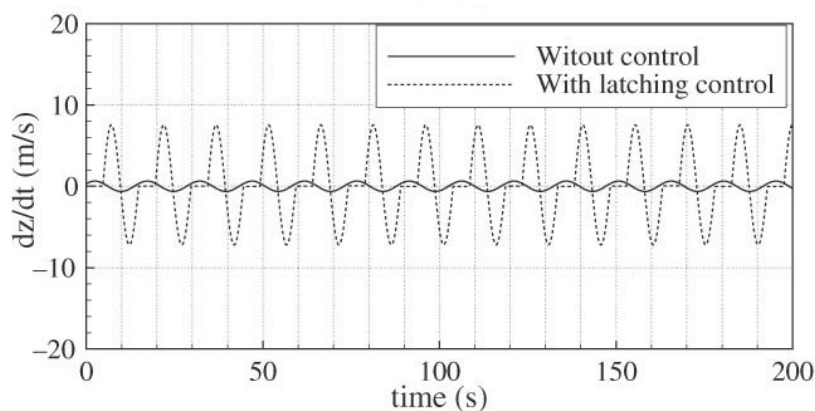


Figure 2.16: Latching control (Budal and Falnes (1980))

In regular waves, half the difference between the wave period and natural period of device can be used as the latching duration. In random seas a Kalman filter can be coupled to the latching control to compute the instantaneous wave period. The input to the Kalman

CHAPTER 2. LITERATURE STUDY

filter in the controller can either be the wave profile or the velocity of the buoy, while the reference input can either be the force in the cable, the damping force due to the hydraulic system or the angular velocity of the motor shaft.

Cross *et al.* (2009) obtained transfer function models statistically and used it to design a Proportional-Integral-Plus (PIP) control system, a logical extension of conventional PID controllers. It implements a feedforward controller that improves disturbance rejection and utilises a piston velocity (disturbance input) as a measured feedforward variable. The generator torque and the damping force represent the control input and controlled output variables, respectively. The optimal damping force is time-varying and is obtained from the optimisation module (Figure 2.17).

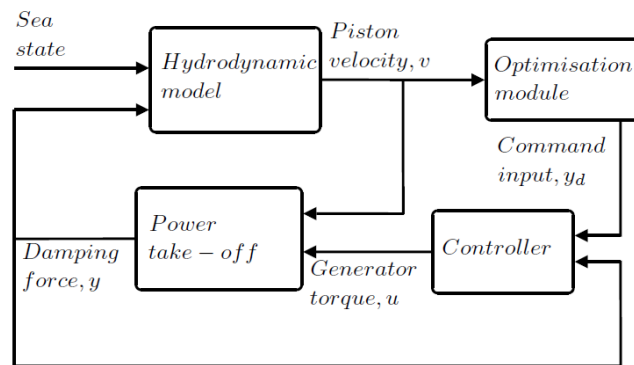


Figure 2.17: Control system with damping force as reference (Cross *et al.* (2009))

Ricci *et al.* (2009) suggest the implementation of a PI controller that controls the rotational velocity of the hydraulic motor output shaft. A reference value for the angular velocity of the hydraulic motor is chosen to be the disturbance input (Figure 2.18). The objective is to have less oscillations in the generator torque.

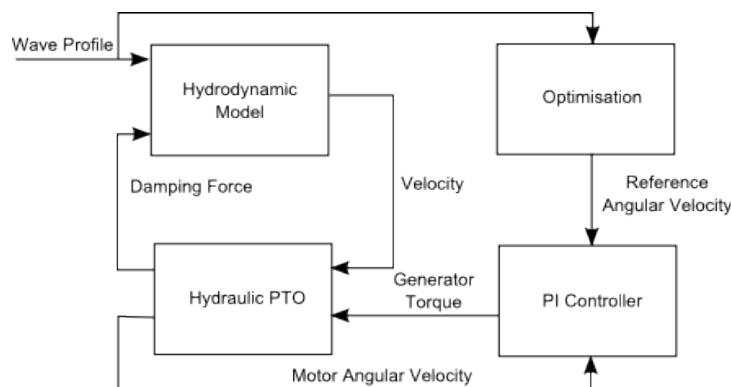


Figure 2.18: Control system with angular velocity as reference

2.6.4.2 Safety Precautions for Hydrodynamic System

If no damage is expected to be caused to the buoy during a storm, the damping of the hydraulic system may be altered by implementing one of the aforesaid control strategies. This limits the movement of the buoy. An excellent example of such a device is the CETO, developed by the company Carnegie Corporations (Carnegie Corporation (2011)).

In extreme weather conditions, the buoy may be sunk to a safe depth where it cannot be damaged. A problematic factor in buoyancy control is however the fact that time is required to pump seawater (and air) into and out of the buoy to alter the buoyancy.

This problem could be overcome by predicting wave conditions rather than reacting to current wave conditions. Sensors could be strategically placed around the point absorber farm, collecting wave data. Usually buoyancy floats are used for large-scale oscillation while generator damping is used to counteract transient forces (Vining (2005)).

Chapter 3

HYDRODYNAMIC MODELLING AND SIMULATION

In this chapter a mathematical model of a spherical buoy is developed. Forces such as drag, buoyancy and the phenomenon known as "added mass" together with its radiation damping component, were included in this model.

The mathematical model is capable of computing the exact movement of the buoy for any wave profile input, whether it is regular or irregular. The model can also be used to determine the optimal size of the buoy, the type of power take-off system that will be responsible for the energy conversion, the size of the different forces acting on the system, the total amount of energy that can be extracted from the ocean waves, and the instantaneous power generated during each cycle.

Tests were conducted in a small wave flume to verify the results obtained with the mathematical model. In the following sections it is shown that the model is a good analytical prediction of the real hydrodynamic model.

3.1 Forces

As previously mentioned, the design of the optimal shape of the buoy is not part of this study's scope. Reference may however be made to De Backer *et al.* (2007), who conducted a study to analyse the performance of a heaving point absorber for different buoy shapes.

In this study the shape of the energy-extracting device (i.e. the buoy) is spherical. This spherical buoy is attached to a single-point mooring cable that enables the buoy to be free to move in all possible directions. Due to the sphere's symmetry, however, it moves predominately in a two-dimensional fashion (Huan Lin *et al.* (2006)): only the heave (vertical motion) and surge (horizontal motion parallel to wave movement) components are considered, and a spherical buoy furthermore has a negligible pitch motion.

CHAPTER 3. HYDRODYNAMIC MODELLING AND SIMULATION

A free body diagram that indicates the different forces acting on the hydrodynamic model, is shown in Figure 3.1. The point absorber-model developed in this chapter can be modeled as a simple spring-mass system: a sphere is attached to a spring that is mounted to the ocean floor.

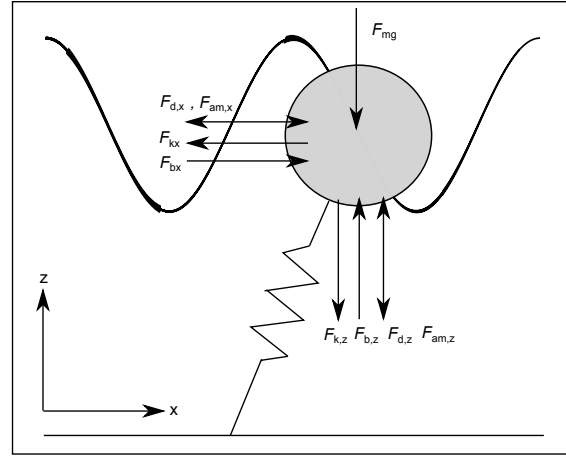


Figure 3.1: Free body diagram

The horizontal forces are known to be the horizontal buoyancy force (due to net pressure distribution, $F_{b,x}$); the spring force ($F_{k,x}$); non-linear drag forces (opposite to direction of movement, $F_{d,x}$); inertial forces (added mass, $F_{am,x}$); and hydrodynamic damping ($F_{hd,x}$). The total wave force on the buoy in the horizontal direction can be written as:

$$F_{b,x} - F_{k,x} - F_{am,x} - F_{hd,x} = F_{d,x} \quad (3.1.1)$$

The vertical forces acting on this system are the vertical buoyancy force ($F_{b,z}$); the spring force ($F_{k,z}$); non-linear drag forces (opposite to direction of movement, $F_{d,z}$); inertial forces (added mass, $F_{am,z}$); the weight of buoy (F_{mg}); and hydrodynamic damping ($F_{hd,z}$). The total wave force on the buoy in the vertical direction can be written as:

$$F_{b,z} - F_{k,z} - F_{am,z} - F_{hd,z} - F_{mg} = F_{d,z} \quad (3.1.2)$$

In this study it is assumed that the weight of the suspension cable has a negligible effect on the buoy's movement. The mass of the cable is therefore taken as zero. When a negatively buoyant cable is used instead of a neutrally buoyant cable, the effects of stiffness, gravity, damping and viscous drag of the cable must be included in this model.

Techniques for modelling the mooring cable are discussed by Driscoll and Nahon (1996). The abovementioned equations can now be rewritten as equations of motion according to Newton's Second Law.

3.2 Equations of Motion

By taking into account the heave-surge coupling effects, the equations of coupled heave-and-surge motion (as stated in Newton's Second Law) of the cable-spring-moored system subjected to deterministic wave excitations are provided by:

$$(m + m_a)\ddot{X} + (R_s)\dot{X} + C_{D,s}'\dot{X}|\dot{X}| + kX - Fh = F_{D,s} \quad (3.2.1)$$

and

$$(m + m_a)\ddot{Z} + (R_h)\dot{Z} + C_{D,h}'\dot{Z}|\dot{Z}| + kZ + mg - Fv = F_{D,h} \quad (3.2.2)$$

In these equations, X and Z denote the displacement in the horizontal and vertical directions; and Fh and Fv the horizontal and vertical buoyancy forces, respectively.

The equations of motion are solved in the presence of regular sinusoidal waves. The simplest wave theory, called linear theory (also known as first-order, small-amplitude or airy wave theory), can be used with reasonable accuracy to approximate this engineering problem. The theory used in the Coastal Engineering Manual (2002) is adopted in this study to provide appropriate guidance during the designing of the point absorber. The wave energy device in this study will be deployed in deep waters where the waves are regular, which means that they have a constant height and period. It can be modeled as two-dimensional, pure sinusoidal waves that are a function of time as well as position:

$$y(c, t) = A0 + (a)\sin(\omega t - kc) \quad (3.2.3)$$

where $A0$ is the height of the SWL above the oceanbed, c the position (function of x and z), k the wave number and ω the wave frequency [rad/s]. The equations for the wave number and wave frequency are given by:

$$k = \frac{\omega}{\nu} \quad (3.2.4)$$

and

$$\omega = 2\pi f \quad (3.2.5)$$

respectively, where ν is the wave velocity and f the frequency [Hz].

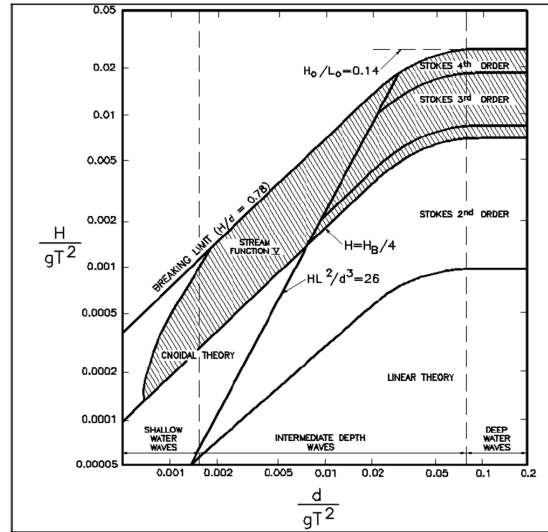


Figure 3.2: Wave theories (US Corps (2002))

According to US Corps (2002) (see Figure 3.2), however, with the given wave conditions around South Africa's South-West coast, the second-order Stokes wave theory may also be implemented. This may be a better approximation of deep-sea ocean waves. The crests have higher and narrower peaks while the troughs are flatter and wider. The second-order Stokes wave theory is characterised by the following equation:

$$y(c, t) = A_0 + (a) \cos(kx - \omega t) + \pi \frac{a^2}{2L} \frac{\cosh(kA_0)}{(\sinh(kA_0))^3} (2 + \cosh(2kA_0)) \cos(2(kx - \omega t)) \quad (3.2.6)$$

where k , the wave number is given by:

$$k = \frac{2\pi}{L} \quad (3.2.7)$$

where L is the wave length.

When the sphere is partially submerged, the water level is not constant over the entire span of the buoy (Figure 3.3). The sphere therefore experiences a vertical as well as a horizontal buoyancy force component at the mass centre point of the submerged volume. The resultant force acts perpendicular to the wave surface through the centre point of the sphere (as indicated with the dotted line).

The vertical and horizontal buoyancy forces may be calculated as:

$$F_v = \rho g \forall \quad (3.2.8)$$

and

$$Fh = \mu_s \rho g h A_{proj} \quad (3.2.9)$$

respectively, where ρ is the density of salt water; \forall the submerged volume; h the height difference between the highest and lowest intersecting points of the wave on the buoy; and A_{proj} the projected area.

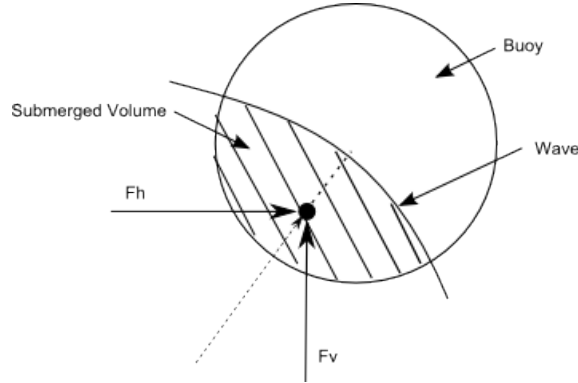


Figure 3.3: Buoyancy forces acting on submerged sphere

As a submerged body moves with an acceleration relative to the surrounding fluid, the submerged buoy imparts an acceleration to some of the surrounding fluid. This phenomenon can be equated to the buoy having an added mass (m_a) of fluid attached to its own physical mass. Added mass can be calculated from the hydrodynamic force that acts on the buoy as it accelerates through the water. The hydrodynamic force in the z -direction is found by integrating the pressure imparted by water particles over the projected area:

$$F_z = \int p dA_z \quad (3.2.10)$$

where p , the pressure, can be found by using the unsteady Bernoulli equation:

$$p = -\rho \left[\frac{\partial \phi}{\partial t} + \frac{1}{2} |\nabla \phi|^2 \right] \quad (3.2.11)$$

Referring to Figure 3.4, the following equations can be obtained:

$$dA_z = \cos \theta dA \quad (3.2.12)$$

$$dA = 2\pi r ds \quad (3.2.13)$$

$$r = R \sin \theta \quad (3.2.14)$$

$$ds = R d\theta \quad (3.2.15)$$

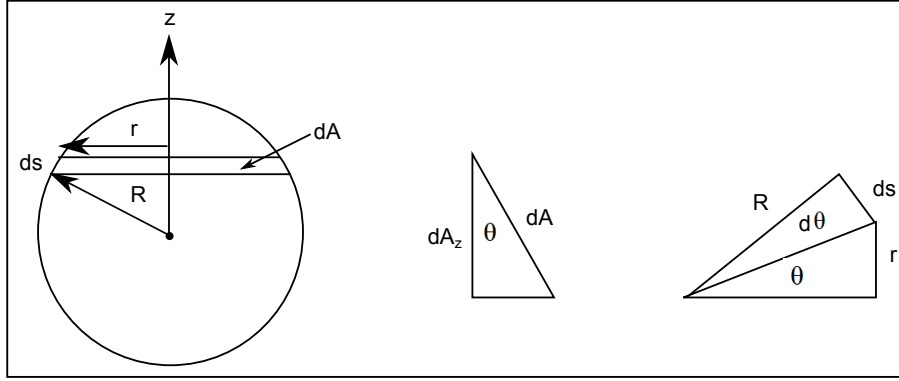


Figure 3.4: Calculating added mass of a spherical body

For axisymmetric flow around a sphere:

$$\phi(r, \theta, U) = U \cos \theta \frac{R^3}{2r^2} \quad (3.2.16)$$

where U is the velocity. The gradient in spherical coordinates is given by:

$$\nabla \phi = \frac{\partial \phi}{\partial r} + \frac{1}{r} \frac{\partial \phi}{\partial \theta} + \frac{1}{r \sin \theta} \frac{\partial \phi}{\partial \phi} \quad (3.2.17)$$

The gradient may then defined as:

$$\nabla \phi = -U \cos \theta \frac{R^3}{r^3} - U \sin \theta \frac{R^3}{2r^3} \quad (3.2.18)$$

Substituting equations 3.2.11 to 3.2.15 into equation 3.2.10, the force may be written as:

$$F_z = -2\rho\pi R^2 \int_0^\pi \left(\frac{\partial \phi}{\partial t} + \frac{1}{2} |\nabla \phi|^2 \right) \cos(\theta) \sin(\theta) d\theta \quad (3.2.19)$$

By simplifying the above equation, it becomes clear that added mass is a function of submerged volume. The simplified equations are given by (Falnes (2004)):

$$Fh = (m_a)_s \ddot{X} \quad (3.2.20)$$

$$Fv = (m_a)_h \ddot{Z} \quad (3.2.21)$$

where the apparent added mass $((m_a)_s$ and $(m_a)_h$) is provided by:

$$(m_a)_s = \mu_s \rho g \nabla \quad (3.2.22)$$

$$(m_a)_h = \mu_h \rho g \nabla \quad (3.2.23)$$

where μ_s and μ_h are the non-dimensionalised added mass coefficients in surge and heave, respectively. This added mass of fluid introduces an additional inertia to the system, and therefore damping, known as radiation damping. The equations for added mass and radiation damping are given by (Falnes (2004)):

$$R_s = \frac{1}{2} \omega \rho \nabla \epsilon_s \quad (3.2.24)$$

$$R_h = \frac{1}{2} \omega \rho \nabla \epsilon_h \quad (3.2.25)$$

where ϵ_s and ϵ_h are the non-dimensionalised radiation damping coefficients in surge and heave, respectively. These parameters are shown by curves portrayed in Figure 3.5.

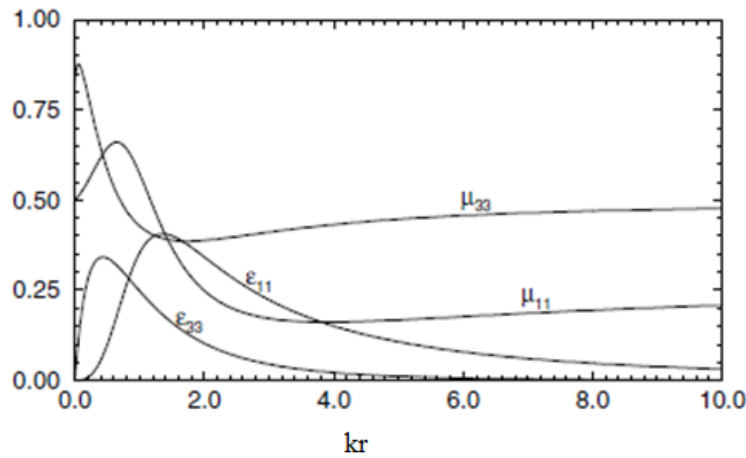


Figure 3.5: Non-dimensionalised heave and surge coefficients of added mass and radiation resistance for a submerged sphere with radius r in deep water (Falnes (2004))

Submerged bodies also experience viscous (non-linear) drag forces opposite to the direction of motion. As the density of air (1.225 kg/m^3) is approximately 830 times less than that

of salt water (1025 kg/m^3), air drag forces may be neglected. The equations for the Morison drag forces are given by:

$$F_{D,s} = \frac{1}{2} \rho C_{D,s} A_p U_1 |U_1| \quad (3.2.26)$$

$$F_{D,h} = \frac{1}{2} \rho C_{D,h} A_p U_3 |U_3| \quad (3.2.27)$$

where A_p is the projected drag area; U_1 and U_3 the surge and heave water particle velocities, respectively. The water particle velocities are given by (US Corps (2002))

$$U_1 = \frac{\pi H}{T} e^{\frac{2\pi z}{L}} \cos \omega t \quad (3.2.28)$$

$$U_3 = \frac{\pi H}{T} e^{\frac{2\pi z}{L}} \sin \omega t \quad (3.2.29)$$

where H is the wave height, T is the wave period and L is the wave length. $C_{D,s}$ and $C_{D,h}$ in equations (3.2.26) and (3.2.27) may be experimentally determined. The wave length may be determined from the wave period:

$$L = \frac{gT^2}{2\pi} \quad (3.2.30)$$

The mooring cable may be modeled as a simple spring system (as shown in figure 3.1). The equations for spring forces in the surge and heave directions are given by:

$$F_{m,s} = kx \quad (3.2.31)$$

$$F_{m,h} = k(z + d) \quad (3.2.32)$$

respectively, where d is the depth of the ocean.

3.3 Desired Movement of Buoy

From the control methodologies discussed in Section 2.6.4, it seems that the desired movement of the buoy in the vertical direction should be similar to the path shown in Figure 3.6. It is known that the most upward/ buoyancy force is generated when the

CHAPTER 3. HYDRODYNAMIC MODELLING AND SIMULATION

buoy is almost completely submerged, as buoyancy is a function of the total submerged volume. In exercising so-called latching control, the buoy is therefore held in the trough until it is completely submerged and then allowed to move upwards until it reaches the crest.

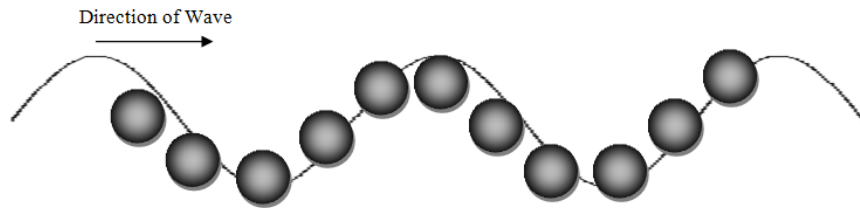


Figure 3.6: Desired movement of buoy

The vertical movement of the buoy will then appear similar to the results shown in Figure 3.7. Cargo *et al.* (2011) is a good source for more detailed information about the desired path of a float in ocean waves.

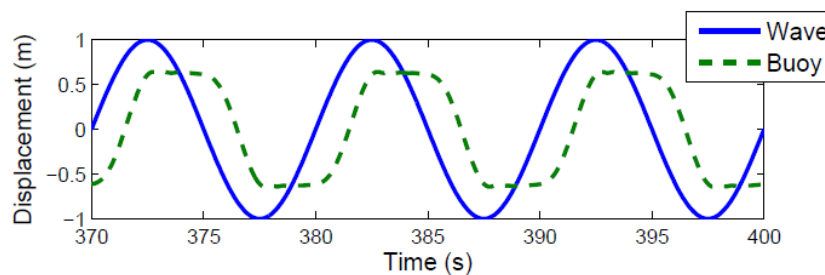


Figure 3.7: Desired vertical movement of buoy (Cargo *et al.* (2011))

In order to achieve this desired movement, it is necessary to optimise the design of the wave energy device according to the design parameters provided in Table 3.1 (Vining (2005)). In order to size the device properly, the designer must know the dominant wavelength at the specific site. The distribution of the wave climate's height and period aids in the choice of the proper control techniques, the correct generator and a suspension cable with the appropriate spring stiffness.

Table 3.1: Useful design parameters for a point absorber

Design parameters
Wave height; wavelength; wave period
Mean water depth
Depth of device below SWL
Diameter of buoy
Stroke length

3.4 Analytical Results

An algorithm that calculates the position of the buoy over a given period of time for any wave profile input was developed. The algorithm, provided in Figure 3.1, was programmed in the computing software programme MATLAB[®], constituting a fast solver and high numerical accuracy.

The integration of the equations of motion is done by a Runge Kutta's 4th Order Method with variable step length. The values for the design parameters for this simulation model are given in Table B.1. The wave profile parameters were arbitrarily chosen while the drag, added mass and radiation damping coefficients were calculated and determined from Figure 3.5.

Algorithm 3.1 Algorithm for hydrodynamic model

Require: *Wave profile, buoy shape, size and weight*

Require: *Spring stiffness, added mass coefficients, drag coefficients*

Require: *Initial conditions for position and velocity in surge and heave*

```

while  $t \leq T_{end}$  do
     $\Rightarrow$  Calculate added mass, damping, drag, buoyancy and spring forces

     $\Rightarrow$  Calculate new positions and velocities

     $\Rightarrow$  Replace old position and velocity values with new values
end while

```

With these values inserted into the algorithm, the surge and heave components of the mathematical model can be calculated. Figures 3.8 and 3.9 show plots of these responses, respectively, where the blue lines are the waves. It is clear that the buoy follows a similar path in the vertical direction as described in Section 3.3. It is not, however, optimal.

3.5 Verification of Model

3.5.1 Experimental Setup

To verify the numerical results, a physical scaled model was built and tests were conducted in a small glass wave flume with dimensions 0.45 x 1 x 40 m (depth x height x length) (Figure 3.10). It was decided to record the movement of the buoy and compare the experimental results with the analytical results. The values for the design parameters

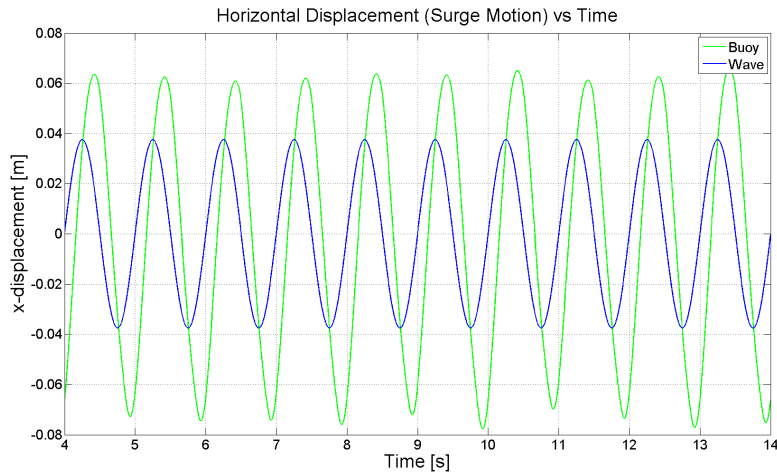


Figure 3.8: Surge response of numerical model

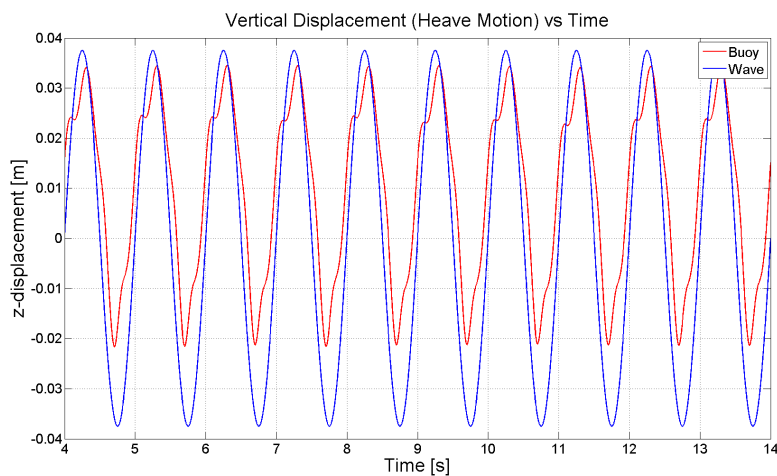


Figure 3.9: Heave response of numerical model

used for the numerical model were inserted into the software Wave Maker[©] which controls the motion of the paddle of the wave flume.

For a particular case, the software was set up for the paddle to create regular waves with an amplitude of 0.0375 m and a period of one (1) second (Figure 3.10). The water depth was always 0.45m (measured from bottom of flume to SWL). The buoy was tightly moored in order to minimise drag forces that may have been caused by a slack cable. This means that the spring connected to the cable was always under tension, even when the trough of the wave passed under the buoy.

The numerical model is even capable of generating a video clip that shows the movement of the buoy in realtime. A few frames of the programmed video clip are provided in Figure 3.11. When the experiments were done, a video camera (mounted at the side of the wave flume) recorded the motion of the buoy in the wave flume. A few frames of the video clip are shown in Figure 3.12. When comparing these two figures, the motion of the



Figure 3.10: Wave flume creating waves

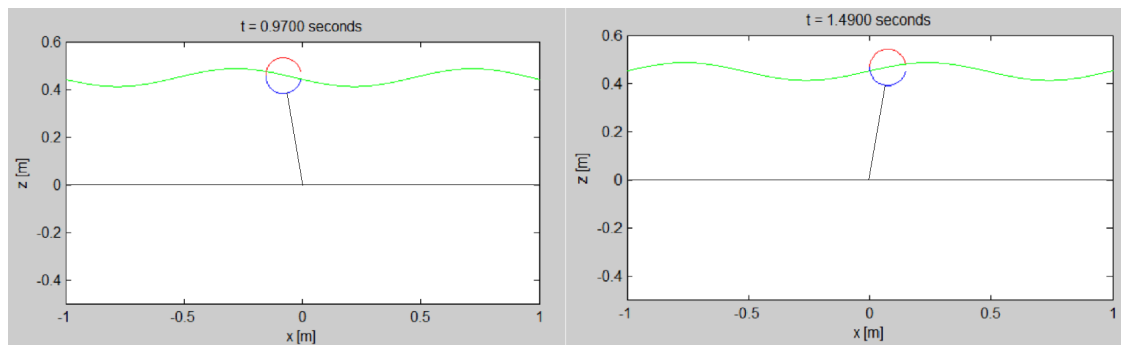


Figure 3.11: Simulated movement of buoy

physical buoy is shown to correlate more or less with the buoy's motion in the numerical simulation.

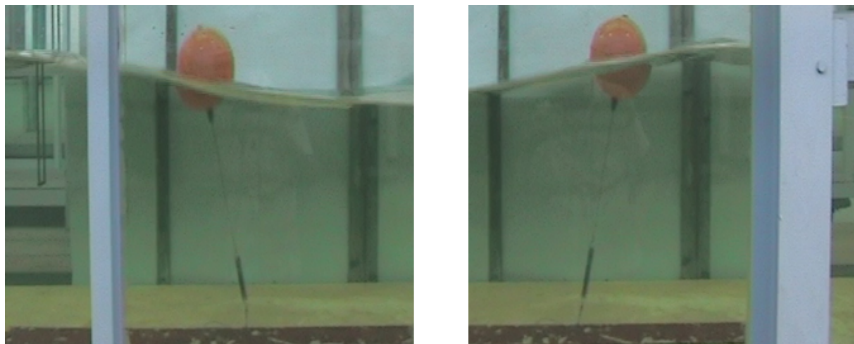


Figure 3.12: Movement of physical buoy

3.5.2 Image Processing

This aforesaid video-recording was used for image processing. An algorithm that is capable of tracking the buoy's motion as the video is fed into the programme frame-by-frame, was created in QT Creator[©] (OpenCV). At the beginning of the tracking simulation, the colour of the body that must be tracked is selected. Throughout the simulation tracking

CHAPTER 3. HYDRODYNAMIC MODELLING AND SIMULATION

only this specific colour will be tracked. The histogram method is used in this study for tracking purposes.

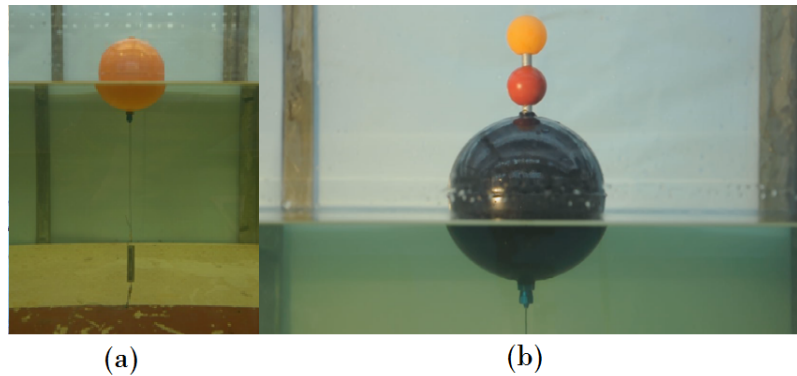


Figure 3.13: Buoy configurations: (a) old and (b) new

The algorithm locates the centre of the buoy over time and stores the coordinates (in terms of pixels) in the form of a text file. A small code was generated in Matlab[®] which reads the information from this text file and converts it into distances (millimeters).

Figure 3.13 shows two buoy configurations. Note the two table tennis balls on top of the buoy and the colour of the buoy in the new configuration. With the old configuration, the surge and heave (Figures 3.14 and 3.15 respectively) components of the physical buoy's motion looked as follows:

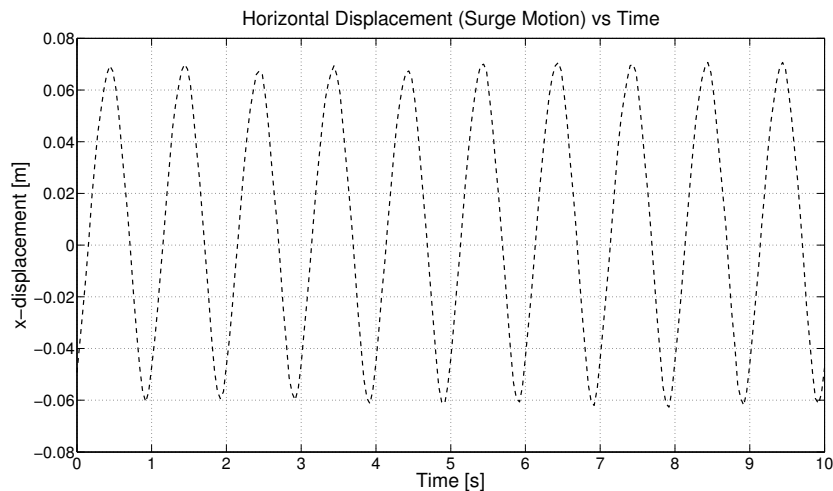


Figure 3.14: Surge response of physical model

The process of comparing the analytical results (Figures 3.16 and 3.17) with the experimental results revealed that the heave component of the experimental model (indicated by dotted lines) has a few higher peaks than the heave component of the analytical model

CHAPTER 3. HYDRODYNAMIC MODELLING AND SIMULATION

(indicated by solid lines). This indicates that the real, physical buoy's movement causes the entire system to have an extra (higher) frequency.

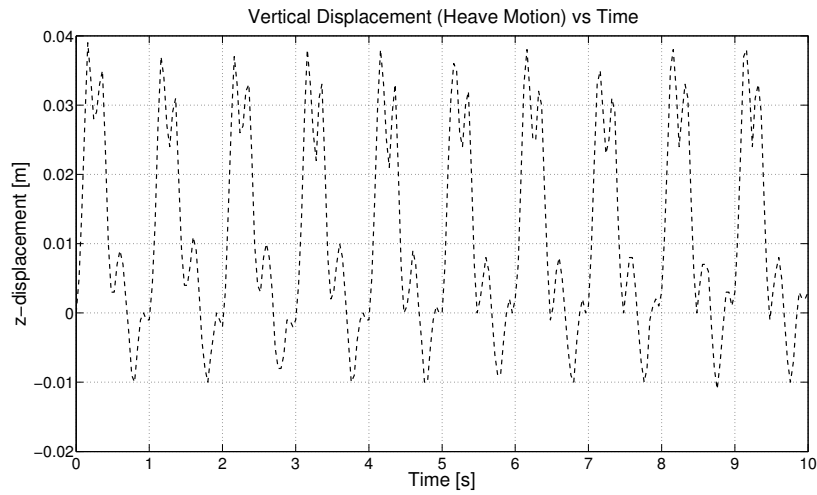


Figure 3.15: Heave response of physical model

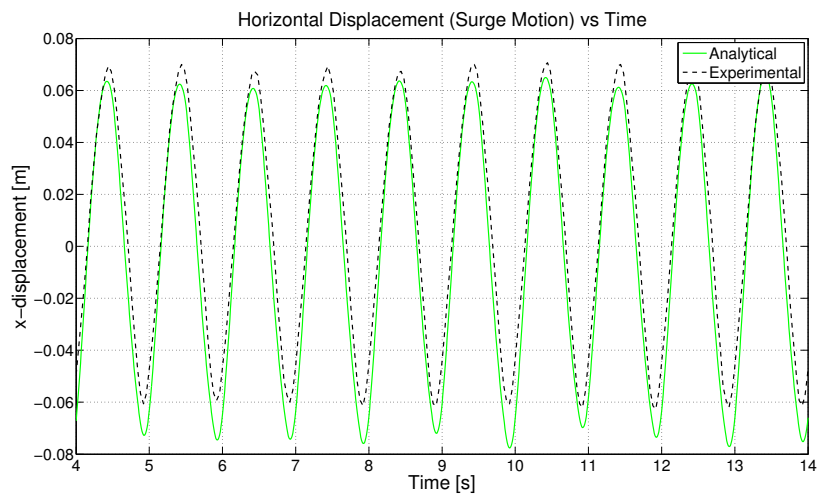


Figure 3.16: Comparison between surge responses of analytical and physical models

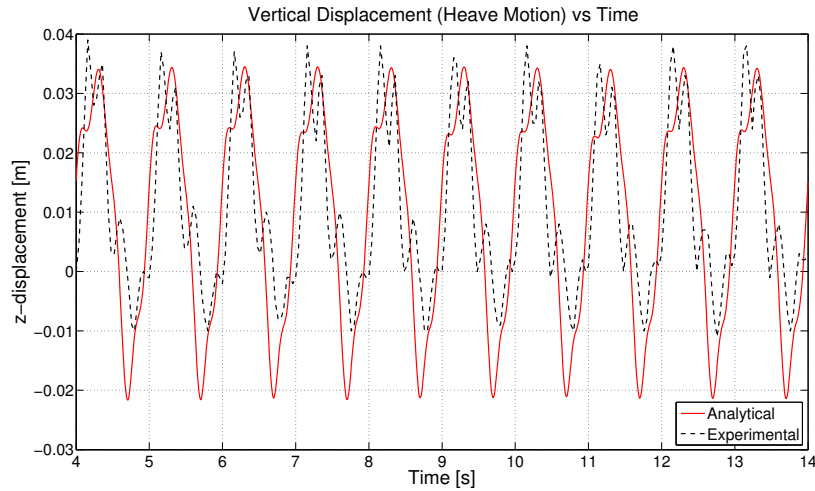


Figure 3.17: Comparison between heave responses of analytical and physical models

A Fast Fourier Transform (FFT) analysis showed that three frequencies are present: one (1) Hz, two (2) Hz and four (4) Hz. The natural frequency of the system was calculated to be two (2) Hz with:

$$\omega_n = \sqrt{\frac{k}{m}} \quad (3.5.1)$$

where k is the spring constant and m the mass of the buoy. The higher four (4) Hz-component, which had a significant impact on the results, was caused by the fact that the tracking software could not track the buoy as it was supposed to. At a certain point on the wave the programme was not able to see the part of the buoy that was submerged under the water. The program then started to track only the part of the buoy that was above the water (Figure 3.18), causing the centre point to jump. This led to the higher peaks in the physical model's heave plot, which is incorrect.

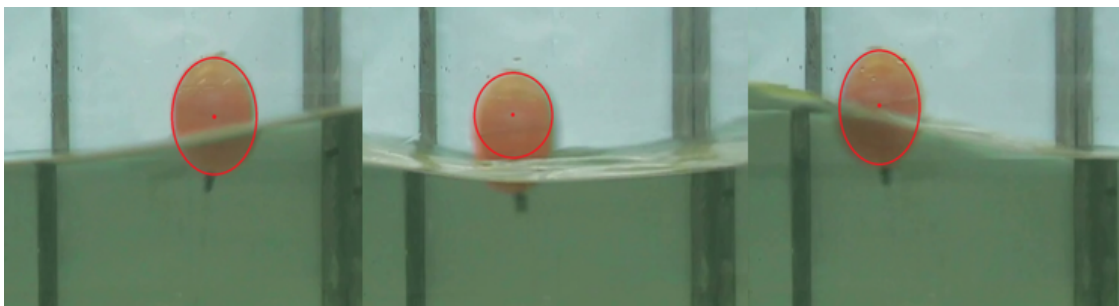


Figure 3.18: Wrong tracking

The buoy in the new configuration had a small aluminum rod with two table tennis balls attached to the top, which barely had an effect on total weight of the hydrodynamic

CHAPTER 3. HYDRODYNAMIC MODELLING AND SIMULATION

system. The water never reaches these balls and therefore has no effect on the tracking. The aluminum rod was furthermore light and did not add another degree of freedom; in this case a pitch component. The orange and red balls were tracked separately. The coordinates of the centre point of the orange and the red ball respectively were used to determine the equation of a straight line that passes through the centre point of the buoy. This equation was then used to determine the centre point of the black buoy at every time interval.

This new set of data of the tracking for the physical model were compared to the analytical results. Figures 3.19, 3.20 and 3.21 show that the analytical results correlate well with the experimental results.

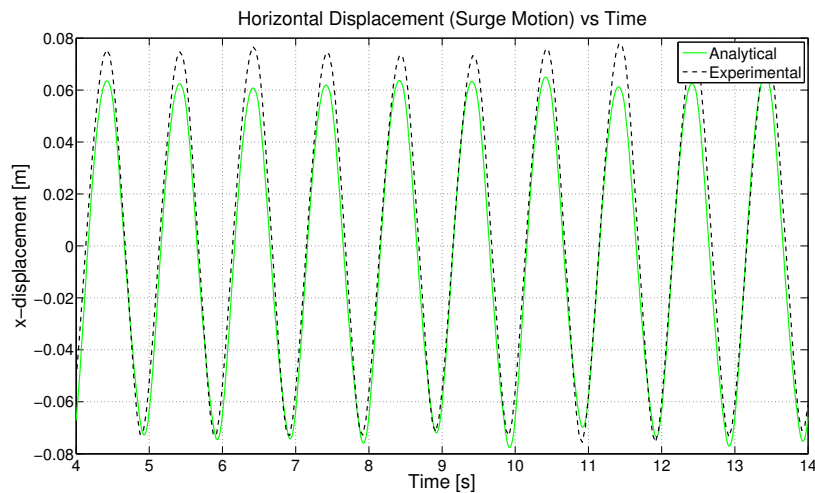


Figure 3.19: New comparison between surge responses of analytical and physical models

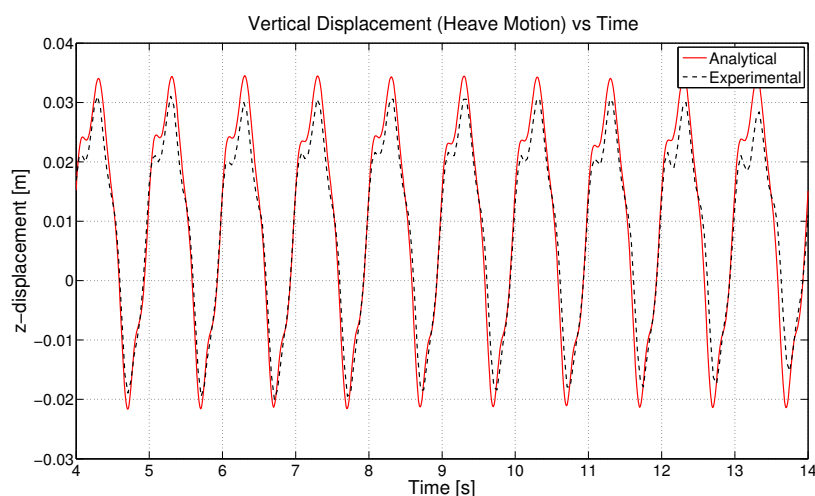


Figure 3.20: New comparison between heave responses of analytical and physical models

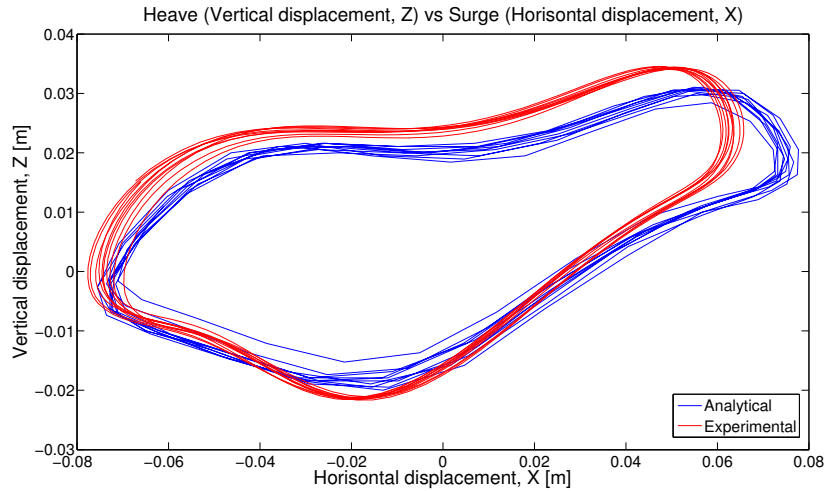


Figure 3.21: Position of centre point of buoy: analytical versus experimental

The numerical model was tested against the physical model for 12 different wave periods and in equal amount of wave heights. All 144 tests provided satisfying results that were similar to those shown in Figures 3.19, 3.20 and 3.21.

3.6 Conclusion

In this chapter a mathematical model of a spherical buoy is developed. Tests were conducted in a small wave flume to verify the results obtained with the mathematical model. It was shown that the model is a good analytical prediction of the real hydrodynamic model.

This model can now be used to determine the type of technology that must be used to extract energy efficiently from the ocean's waves and to find the optimal size of the buoy.

Chapter 4

DEVELOPMENT OF WAVE ENERGY CONVERTER

Wave energy devices should extract energy in an efficient and cost-effective manner without extracting all the wave energy. Such exhaustion will have a negative environmental impact on the ocean or the beach.

In this chapter the type of technology (provided in Section 1.3) that must be used to extract energy efficiently from the ocean's waves, will be determined. This includes finding the optimal size of the buoy. As the wave height of 2.5 m occurs 50% of the time while a wave period of 12 seconds occurs 30% of the time (prevailing conditions - Joubert, 2008), the buoy and power take-off device will be designed for these conditions.

4.1 Sizing of the Buoy

As previously mentioned and prescribed by Section 1.3, a spherical buoy is used in this study. The prevailing wave periods and -heights occurring along the South-West coast of South Africa are 12 to 14 seconds and 2 to 3 metres, respectively (Joubert 2008).

To find the optimum diameter of the buoy in order to extract the maximum energy in these wave conditions, a few simulations were completed using the numerical model developed in Chapter 3. The rated output power was found for various wave periods and -heights while the diameter of the buoy was increased.

The results are shown in Figure 4.1. The wave heights of 2 and 2.5 m correspond with a wave period of 12 seconds, while the wave height of 3 m corresponds with a wave period of 14 seconds. From this figure it is clear that the full-scale buoy should have a diameter of approximately seven (7) metres.

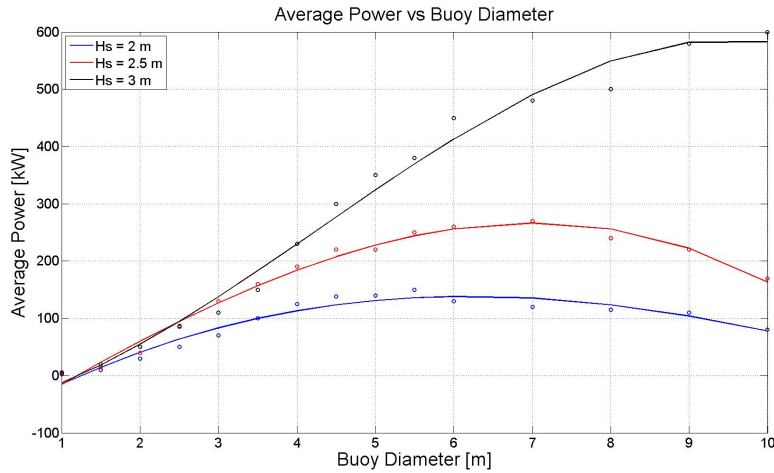


Figure 4.1: Energy extracted per hour vs. buoy diameter

4.2 Power Take-off Device

In order to know how to extract as much energy from the waves as possible, a simple control system was implemented into the numerical model that was developed in Chapter 3.

Three types of control systems were tested: the system acting as a damper; the system acting as a constant force applied to the buoy; and the system acting as a spring. All three control systems were programmed to imitate the latching control strategy discussed in Section 2.6.4. In other words, a force would only be exerted on the buoy when the buoy velocity is positive in the upward direction. Otherwise, it would be zero (0). This ensured that the buoy followed a similar path to the one showed in Figure 3.3 in the vertical direction.

The best control strategy will relate to the system that will ensure the buoy to follow the specific path as described in Section 3.3, with the lowest error. This system would, as a result, extract the most energy from what is available (Equation 4.2.9).

The hydrodynamic numerical model was used to determine the work done by the buoy, the energy available in the waves, the work done by the control system and the output power of the control system.

4.2.1 Calculation of Power and Energy

Before the control systems can be tested, it is necessary to find the velocity along the mooring cable. Vector transformation of a single point in a two-dimensional space is used to transform the velocity vectors, as shown in Figure 4.2.

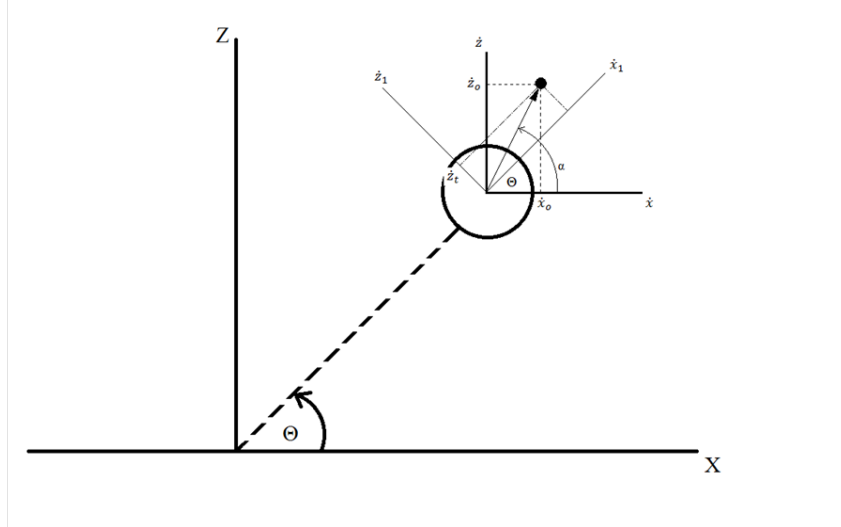


Figure 4.2: Velocity vector transformation

The resultant velocity vectors in the local coordinate system, at the centre point of the buoy, have a different direction (indicated by the angle α) than the resultant position vectors in the global system at the mooring point (indicated by the angle θ). This means that the resultant velocity vector cannot be used to accurately predict the velocity of the buoy. Vector transformation allows the local coordinate system to be transformed to the global coordinate system. These new velocity vectors may then be used to accurately predict the buoy's velocity.

From Figure 4.2, the transformed vectors can be written as:

$$\dot{x}_t = \dot{x}_o \cos\theta + \dot{z}_o \sin\theta \quad (4.2.1)$$

$$\dot{z}_t = \dot{z}_o \cos\theta - \dot{x}_o \sin\theta \quad (4.2.2)$$

where \dot{x}_o and \dot{z}_o are the original velocity vectors in the horizontal and vertical direction of the local coordinate system respectively; and \dot{x}_t , \dot{z}_t the transformed velocity vectors in the transformed, but also global coordinate system. \dot{x}_t can simply be taken as the velocity v along the mooring line.

The velocities in the surge and heave directions (Figures 4.3 and 4.4) for a spherical buoy that is only connected to a spring, were calculated using the numerical model developed in Chapter 3. No control system was implemented to determine these velocities.

Using Equations 4.2.1 and 4.2.2, these velocity vectors can be transformed to the global coordinate system. The transformed velocity is provided in Figure 4.5.

The power extracted by the PTO is portrayed by

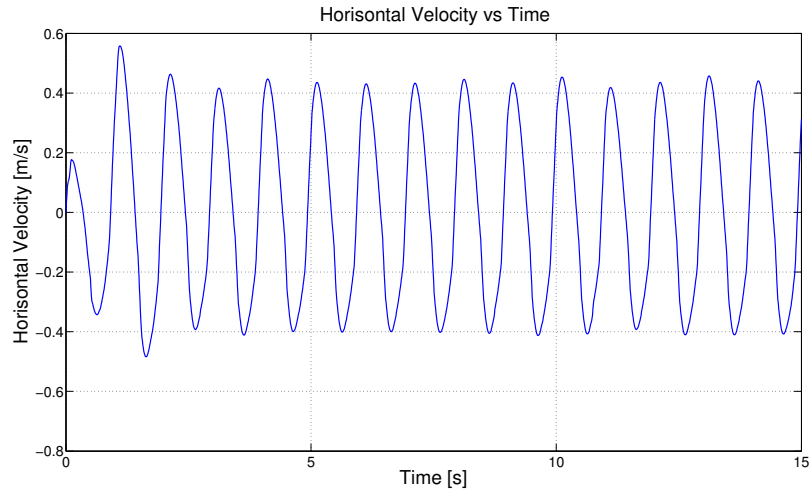


Figure 4.3: Velocities for surge direction

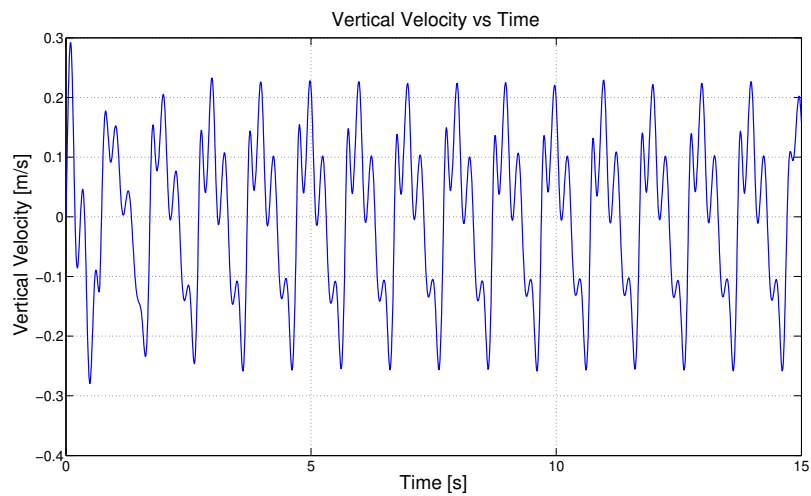


Figure 4.4: Velocities for heave directions

$$P = F\nu \quad (4.2.3)$$

where F and ν are the forces in the cable experienced by the control system and the transformed velocity, respectively. The energy can be calculated as:

$$E = \int P dt \quad (4.2.4)$$

4.2.2 Control Systems

As mentioned in the beginning of this section, a small control system was implemented into the model (Figure 4.6) to determine in which manner the wave energy device should

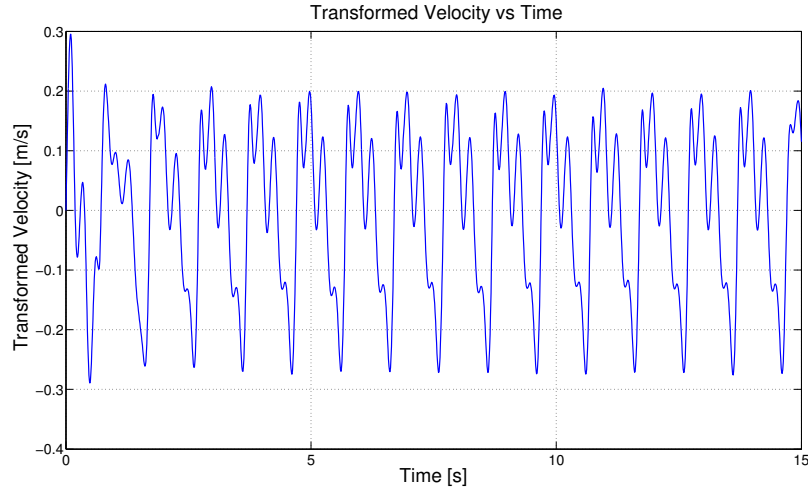


Figure 4.5: Velocities along mooring cable

function, i.e. as a damper, a constant force, or a spring. The spring, with spring stiffness k , in parallel with the control system, was used to keep the mooring cable tight.

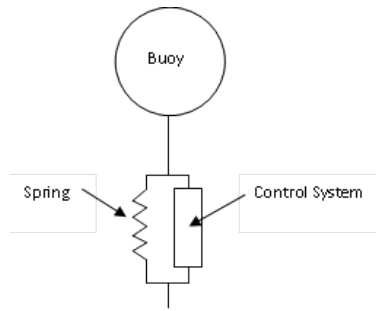


Figure 4.6: Description of control system

The equation of energy when the buoy moves in an upward direction, from one to two in Figure 4.7), can be written as:

$$W_b = W_T + E_g + losses \quad (4.2.5)$$

where W_b , W_T and E_g are the work done by the buoyancy force; work done by the control system; and energy due to gravitation, respectively. The losses-term includes the hydrodynamic damping, drag, friction in mooring cable and control system.

From Figure 4.7 the work done by the buoyancy force, work done by the control system and energy due to gravitation can be written as:

$$W_b = F_b(A - d) \quad (4.2.6)$$

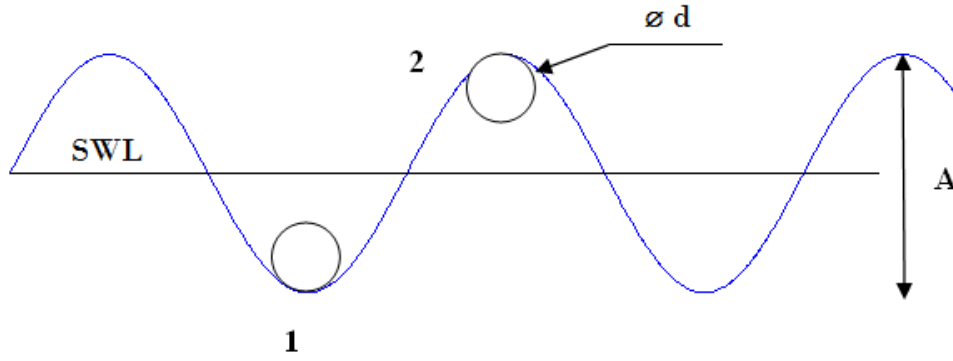


Figure 4.7: Energy equation derived from desired movement of buoy

$$W_T = F_c(A - d) \quad (4.2.7)$$

$$W_g = mg(A - d) \quad (4.2.8)$$

These equations were implemented in the numerical model to calculate the extracted, generated and wasted energy (all cumulative) as well as the instantaneous power for each control system. The results are provided in Figures 4.8, 4.9 and 4.10.

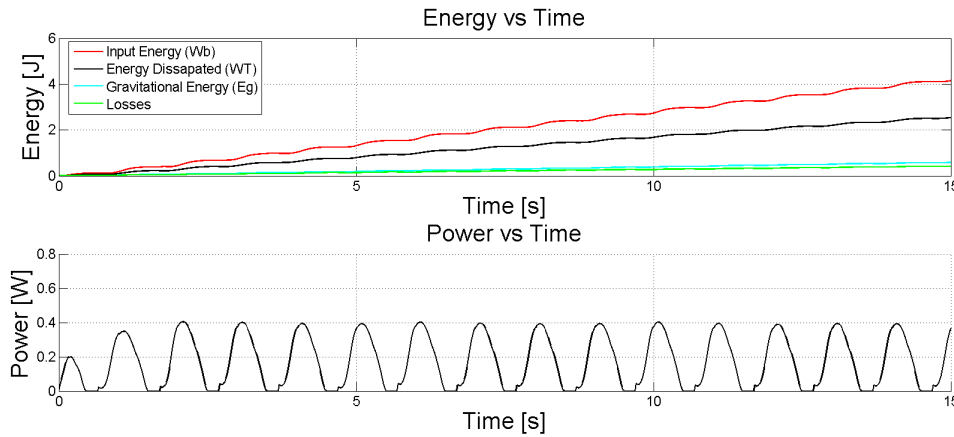


Figure 4.8: Energy for system acting as a damper

In order to compare the three different control systems, the work conducted by the control system was taken as a fraction of the work done by the buoyancy force:

$$\frac{W_T}{W_b} \times 100\% \quad (4.2.9)$$

The values for the design parameters in Table G.1 were used for all three control systems and the results are tabulated in Table 4.1. In this table the "Energy extracted" refers to

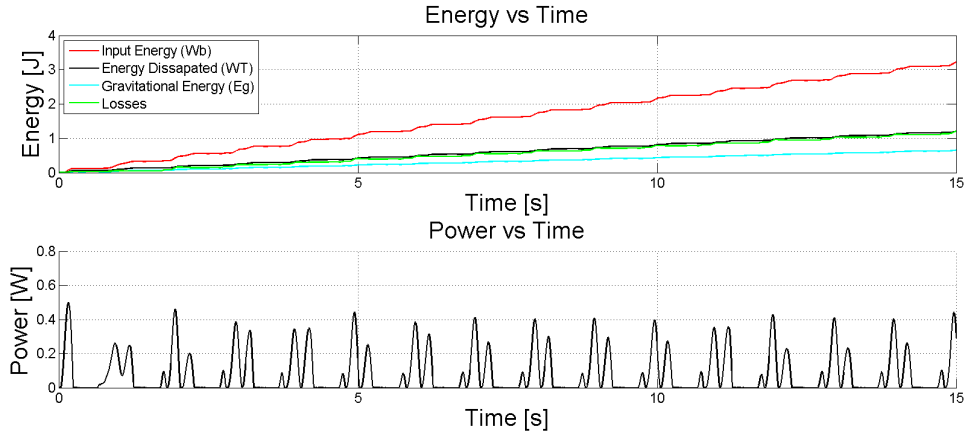


Figure 4.9: Energy for system acting as a spring

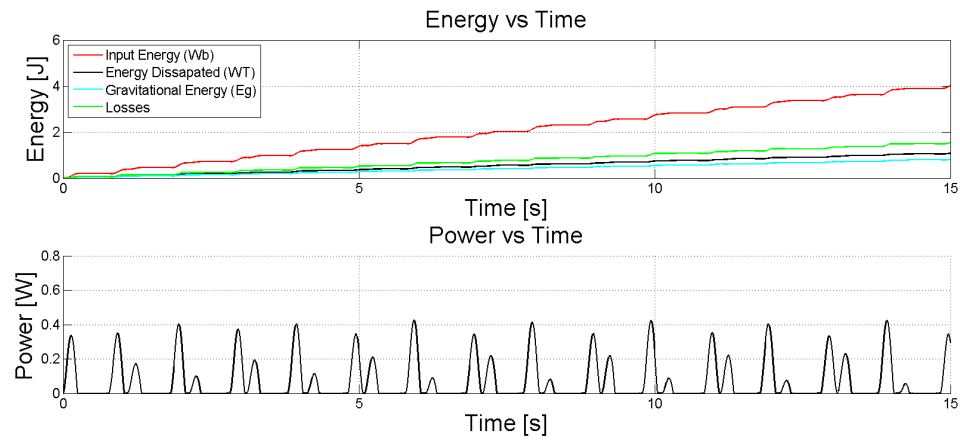


Figure 4.10: Energy for system acting as a constant force

the percentage of available energy that was extracted (with the help of Equation 4.2.9) and the output power was simply the time derivative of the energy that was extracted by the control system (W_T).

Table 4.1: Comparison of control systems

System	$v > 0$	$v < 0$	Energy extracted	Average power [W]
Damper	$c = 90$	$c = 0$	62%	0.19
Constant force	$Fc = 1.5$	$Fc = 0$	40%	0.09
Spring	$k = 100$	$k = 0$	30%	0.07

4.2.3 PTO as a Damper

From Table 4.1 it is clear that the system should function as a damper and that damping should only occur during the upward stroke. It extracts most of the wave energy while

CHAPTER 4. DEVELOPMENT OF WAVE ENERGY CONVERTER

the losses are minimal.

Further simulations with this spring-damper system, which is connected to the buoy, revealed that the damper should have an optimal damping coefficient as shown in Figure 4.11; in this case 90 Ns/m. Anything above or below this value would result in less energy being captured. The power take-off should therefore be optimised to have an optimal damping coefficient.

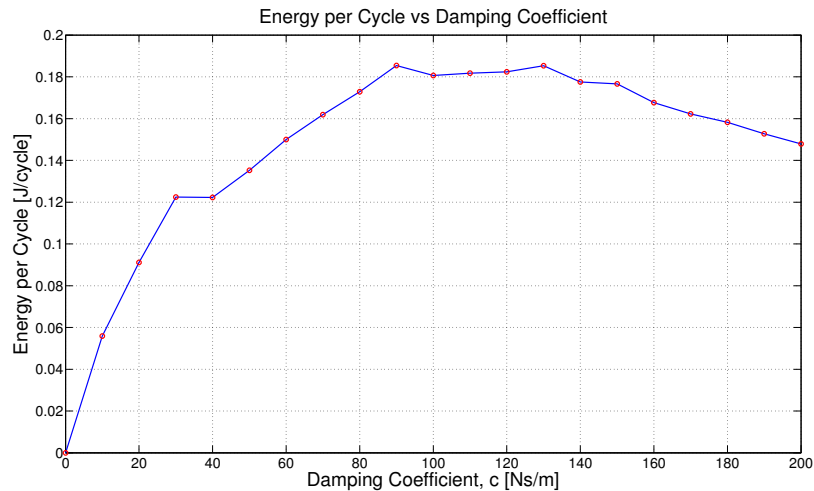


Figure 4.11: Optimal damping coefficient

A simulation of the buoy's movement in the vertical direction is shown in Figure 4.12. As noted in section Section 3.3, the damper causes the buoy to have a more desired movement in the waves, which will result in higher energy capture.

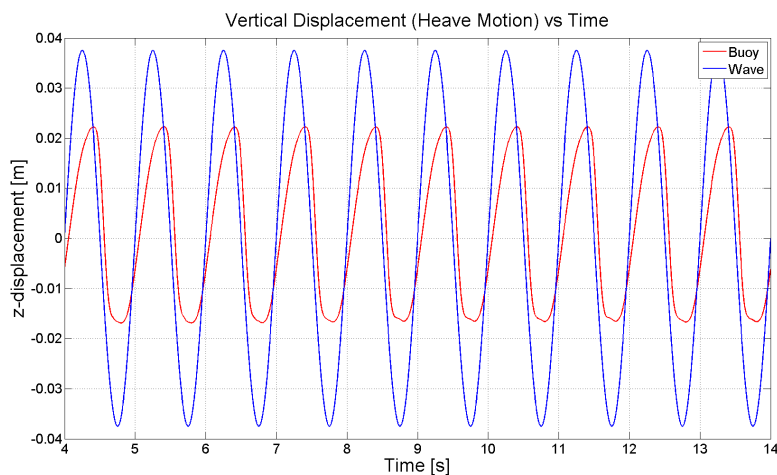


Figure 4.12: Heave response of buoy with damper as PTO

4.2.4 Concept Design for PTO

With the results obtained in the previous section, the power take-off system can now be designed. As noted in Sections 4.2.2 and 1.3, the system should act as a damper and it should be mounted on the ocean floor. Fifty-five concepts were generated in order to find a suitable device that would give optimum results. Similar devices were grouped together in nine categories according to the type of technology the devices would make use of (i.e. devices implementing hydraulics under "Hydraulics", etc.). The top concept in each group is discussed in Appendix C.

4.2.5 Concept Evaluation

In this study the decision-matrix method, also known as Pugh's method, is used for comparing the alternative concepts discussed in Section 4.2.4 and to find the best alternative. This method provides a means of scoring each alternative concept relative to another in its ability to meet specific criteria established according to the customers' requirements. This method not only tests the completeness and understanding of the requirements, but also provides insight to the best alternatives. It rapidly identifies the strongest alternative and helps foster new alternatives.

One of the concepts is used as a datum (or reference) and all the other alternatives are compared with this datum as measured by each of the customer requirements. Each alternative concept being evaluated is judged to be either better than (+ score) approximately the same ("0"), or worse than (- score) the datum. The overall score is the difference between the number of plus and minus scores, while the weighted score is the sum of each plus score and minus score multiplied by the corresponding importance weighting.

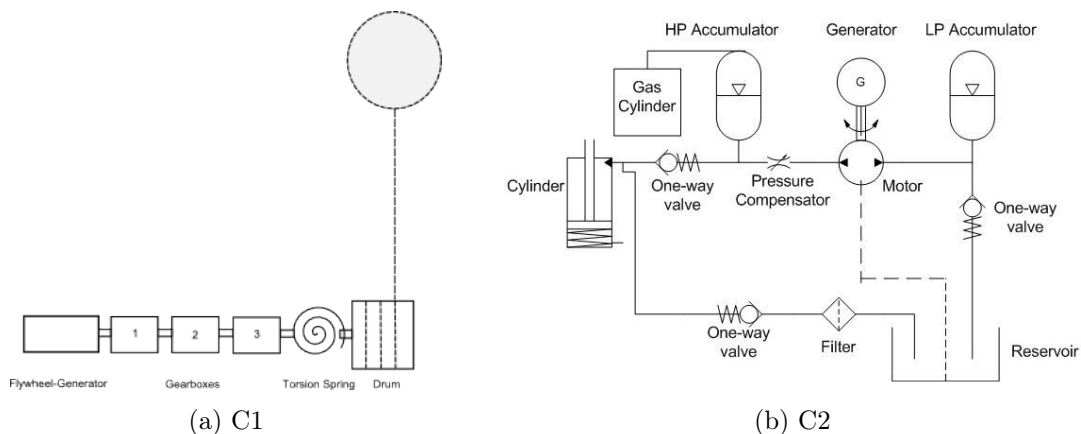


Figure 4.13: Schematics of concepts C1 and C2

The concepts mentioned in Section 4.2.4 are compared in Table D.1 in Appendix D. Pugh's method yielded two concepts in this study: Concept C1, a mechanical system, and Concept C2, a hydraulic system (Figure 4.13). It cannot be said with certainty which concept would be the best solution, and detailed studies must be done in order to reveal the best solution.

4.2.6 Comparative Analysis Between Concepts C1 and C2

Before any comparisons could be made, more detailed designs were generated for both concepts (see Appendix E). These designs were then used to compare the two concepts in terms of cost, size, mass, overall efficiency, lifetime, environmental impact, method for retracting the buoy, method for transferring intermittent forces, complexity, availability of components and manufacturability.

4.2.6.1 Size, Mass and Cost

From Appendix E the cost of the hydraulic system is half of the mechanical system's cost. It weighs much less than the mechanical system and it is almost a fifth of the mechanical system's size.

4.2.6.2 Adaptability to Wave Conditions

A continuously variable transmission (CVT) system can be used together with the three gearboxes in the mechanical system. The gearboxes will have a constant multiplication speed factor, but the CVT system has an infinite number of gear ratios. The generator speed could be kept constant.

The flow restrictor in the hydraulic circuit regulates the hydraulic flow through the system. It allows the system to have a constant flow through the hydraulic motor, which means that the output shaft will turn at a constant speed.

4.2.6.3 Efficiencies

As mentioned in table 4.1, the system can only extract 60% of the available energy. Both systems will have an approximate efficiency of 60%. This means that both systems can capture and convert roughly 40% of the total wave energy into electrical energy.

4.2.6.4 Lifetime and Maintenance

The mechanical system has many moving parts. The gears in the industrial gearboxes must be able to handle large pulsating forces. A planetary gearbox instead of straight helical gearboxes can be used. Each gear will only need to transfer a third of the total force. Not only will the gearbox be smaller, but the gears' lifetime will definitely be extended. If the gearboxes are sufficiently lubricated, the expected lifetime may also be increased.

The spring, however, cannot handle the large pulsating forces, which means that the expected lifetime of the machine is decreased. The bearings and one-way bearings are lubricated for life and only needs to be replaced approximately every 10 years. It does not affect the expected lifetime of the overall system. As the CVT system's size however increases, friction and lubrication becomes a problem that reduces the lifetime.

The mooring cable is wound onto a drum that introduces rope friction and affects the lifetime negatively. Regular maintenance should be done on mechanical systems to ensure that the system will be operable for as long as possible. Unplanned maintenance should be avoided at all costs.

The hydraulic system only has a few moving parts. The accumulators absorb pulsating shocks, thereby avoiding pump-, pipe- and system failures in order to achieve a longer life expectancy. It not only provides fail-safe conditions, but lowers operating and maintenance costs. As long as the hydraulic fluid is free of contamination, the system can operate approximately for 100 000 hours (roughly 10 years).

Hydraulic technology has proven to operate very well in offshore conditions. The mooring cable is connected to the piston rod that follows the movement of the buoy. As a result, no rope friction is present. It will not be necessary to do regular check-ups as in the case of mechanical systems, which means that maintenance costs are reduced and the systems will be operable at all times.

4.2.6.5 Environmental Impact

The large buoy will not have an aesthetic impact on the environment as the PTO device will be located offshore. Whereas both systems have low noise and vibrations, it may leak oil or lubricant that could affect the environment. Both will however serve as artificial reefs and the hydraulic equipment is sprayed with a special coating which has no impact on the environment.

4.2.6.6 Method for Retracting Buoy During Inclement Weather Conditions

In the mechanical system it is easy to reverse the system and to retract the buoy by winding it onto the drum during inclement weather conditions.

In the hydraulic system the distance with which the buoy can be lowered is equal to the stroke length. A winch may be used to lower the buoy.

4.2.6.7 Complexity, Availability of Components and Manufacturability

The mechanical system has a high complexity and a low manufacturability as special rollers and tools are needed to build the device. Not all of the components are standard and readily available. Some must be manufactured to specification.

All of the hydraulic components are standard and readily available, or could be manufactured with ease. The hydraulic system therefore has a low complexity and high manufacturability.

4.2.6.8 Conclusion

Research indicates that a hydraulic wave energy converter is perfect for this type of application.

Not only is it sustainable, but can also act as a damper (Section 4.2.2). Power smoothing is furthermore one of the main concerns due to the stochastic nature of the ocean environment. Wave energy converters that make use of hydraulic power take-off devices have a relatively smooth power output, easing connection between the WEC and the grid.

4.2.7 Final Design of PTO

The wave energy converter developed in this study can be divided into three parts: the buoy, the hydraulic power take-off system and the winch system. This is illustrated in Figure 4.14. The partially submerged and positively buoyant float will be connected to a single-acting cylinder in this design. When a crest passes over the buoy, the piston is extracted and oil is pumped from the top chamber of the cylinder via high-pressure pipes running across the ocean floor to the accumulator on the high-pressure side through the hydraulic gear motor to a reservoir on the low-pressure side.

During this operation a vacuum or air-spring is formed in the bottom chamber. When the trough of the wave passes under the float, the vacuum retracts the piston and the

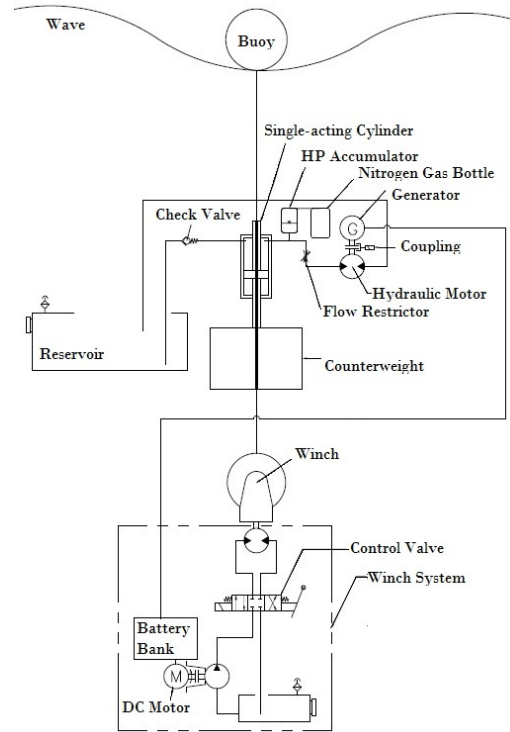


Figure 4.14: Schematic of the final WEC design

top chamber is filled with oil. A counterweight could be used to assist the vacuum. A damping force will therefore only be applied when the buoy velocity is positive, damping the upward movement of the buoy (Section 4.2.2). Low friction seals are used in the cylinder to minimise the friction force that could work against the buoyancy force of the float.

A pressure regulator, which is placed between the accumulator and motor, regulates the pressure on the high pressure side. When the pressure is however lower than the precharge pressure, the flow will also be less, leading to a less gradual power output. A flow restrictor can be used to ensure a constant flow supply, but this will increase the energy losses. As result the use of an accumulator is therefore proposed. The motor will turn at a more constant speed and the alternator, or DC generator, that is connected via a flexible coupling to the gear motor, will then have a continuous and more gradual power output.

A winch system protects the entire system during inclement weather conditions. A hole is drilled through the piston rod and the cylinder so that the rigid, neutrally buoyant mooring cable can be directly connected to the winch system (that is located below the cylinder). A hydraulic clamp positioned just above the cylinder clamps the cable during normal operation. Before any power is fed into the national grid, the wave energy device charges the battery pack that is connected to the winch system. During inclement weather

conditions a proxy sensor senses that the piston has reached maximum stroke length and it communicates with the hydraulic clamp, telling it to release the cable. The winch which is powered by the battery pack, then lowers the buoy to a safe depth where less water particle activity takes place. After 24 hours the winch will release the buoy, allowing it to return to its normal operating position.

A ball-joint is welded to the bottom of the cylinder so that the cylinder can pivot around a point and follow the buoy's movement (as indicated in Chapter 3). Both the vertical and horizontal components of the waves' kinetic energy will be extracted. This allows the piston in the cylinder to experience smaller sideward forces and, as a result, an extended lifetime. Instead of placing the winch below the cylinder, it could be placed inside the buoy. Only the cylinder will then be located below the water. Maintenance could be done from a boat, which not only saves time, but a lot of money that would have been spent on divers to enable maintenance below water.

4.3 Design Specifications

A list of engineering specifications for a full-scale prototype model can now be compiled. Froude's scaling laws are implemented to determine the parameters for the scaled model (Gerike, 1982). The length relationship for geometric similarity can be written as:

$$L_r = \frac{x_m}{x_p} \quad (4.3.1)$$

where x_m and x_p denote the measurements of the model and full-scale prototype, respectively. The wave period relationship can be written as:

$$T_r = \sqrt{L_r} \quad (4.3.2)$$

and

$$T_r = \frac{T_m}{T_p} \quad (4.3.3)$$

where T_m and T_p denote the wave period of the model and full-scale prototype, respectively. The power scale relationship can be written as:

$$P_r = T_r^{\frac{7}{2}} \quad (4.3.4)$$

and

$$P_r = \frac{P_m}{P_p} \quad (4.3.5)$$

where P_m and P_p denote the power of the model and full-scale prototype, respectively.

The PTO device must be optimised for wave conditions at a deployment site off the South African South-West coast. The list of engineering specifications is provided in Appendix F. The prevailing wave conditions of this coast is listed under "Prototype" in this list.

4.4 Conclusion

In this chapter it was shown that a damper would extract energy efficiently from the ocean's waves. Research indicated that a hydraulic system is sustainable and is able to act as a damper. A detailed design for the hydraulic system was developed in this chapter. Together with the engineering specifications provided, this detailed design can be used for simulation purposes.

Numerical models for the hydraulic power take-off components and for the winch system may now be developed. These models will provide a better understanding of the dynamic behaviour of the hydraulic system.

The numerical model for the hydrodynamic model developed in Chapter 3 and the numerical model for the hydraulic power take-off system developed in the following Chapter, may then be combined to determine the behaviour of the entire system in the ocean.

Chapter 5

MODELLING AND SIMULATION OF HYDRAULIC PTO

In this chapter numerical models for the hydraulic power take-off components and for the winch system are developed. These models will provide a better understanding of the dynamic behaviour of the hydraulic system. The numerical model of the power take-off system is capable of computing the oil pressures in the pipes, the gas pressure in the accumulator, pressure losses due to friction, the instant at which the hydraulic motor will turn, how fast and long it will turn as well as the damping force created by the hydraulic system.

Tests were conducted in the laboratory to verify the results obtained with the mathematical model of the power take-off system. To demonstrate the winch system's basic working principle, only simulations of the system are included.

5.1 Bond Graph Representation

Bond graphs are used to model the hydraulic power take-off system shown in Figure 5.1.

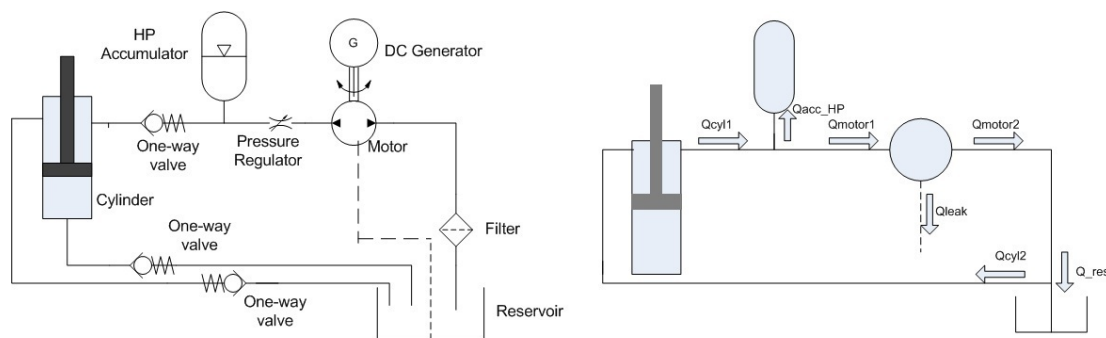


Figure 5.1: Schematic of hydraulic power take-off system

CHAPTER 5. MODELLING AND SIMULATION OF HYDRAULIC PTO

The bond graph of Figure 5.1 is given in Figure 5.2. A transformer (TF) represents the interface between the mechanical domain (hydrodynamic model) and the hydraulic domain. The area A_{piston} of the hydraulic piston pump is the transformer modulus.

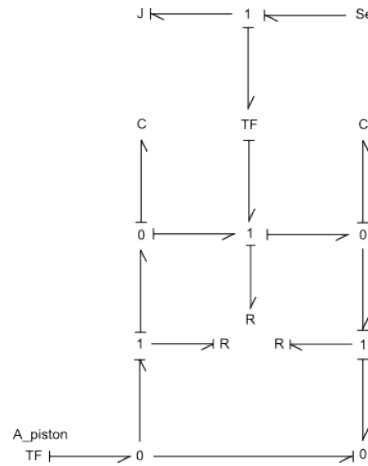


Figure 5.2: Bond graph of hydraulic power take-off system

In order to model the hydraulic domain, the 0-junctions and 1-junctions must be established. There are four 0-junctions and four 1-junctions. The two 0-junctions at the bottom of the graph represent the output pressure from the cylinder. The gas accumulator and reservoir (indicated by the letter C) are connected to their appropriate 0-junctions. Two resistance elements (R) that represent the check valves are connected to 1-junctions and inserted between the appropriate 0-junctions. The hydraulic motor is represented as a transformer. It is connected to a 1-junction that represents the flow between the high- and low-pressure accumulators. A resistance element that represents the hydraulic leakage of the motor is connected to this 1-junction. A 1-junction that represents the rotational velocity of the motor is furthermore also connected to this junction. The motor inertia (J) and the load torque of the generator (effort source Se) are connected to the latter junction.

5.2 State Equations of the Hydraulic PTO

The bond graph provided in Section 5.1 can now be used to formulate the state equations. It is assumed that there are internal losses and leakages in the system. The system is however a closed-loop system, which means that the total mass is constant. It is also assumed that the hydraulic fluid is incompressible, meaning that the rate of change of volume or volumetric flow in the accumulators are:

$$Q_{acc,HP} = Q_{cyl} - Q_{motor1} - Q_{leak} \quad (5.2.1)$$

$$Q_{res} = Q_{motor2} - Q_{cyl} \quad (5.2.2)$$

where Q_{cyl} is the oil flow into and out of the cylinder chamber:

$$Q_{cyl} = A_p \cdot v \quad (5.2.3)$$

where v is the stroke velocity of the piston rod.

5.2.1 Cylinder

The position of the piston, r , is given by:

$$r = \sin(2\pi ft) \quad (5.2.4)$$

and the disturbance input, the stroke velocity, is simply the derivative of the position:

$$v = (2\pi f)\cos(2\pi ft) \quad (5.2.5)$$

For a full-scale model a spring is not sufficient to retract the piston and a counterweight should be added. For a 1:7 scale model (as used in this research) however, an air-spring is more than efficient for this purpose. The bottom chamber of the cylinder is connected to the reservoir with a one-way valve. The one-way valve is connected in such a way that, when the piston moves upward and forces fluid out of the top chamber (on the rod side), a vacuum is formed in the bottom chamber. This vacuum acts as a spring and is known as an "air spring". When the buoy reaches the crest of the wave, the vacuum pulls the piston down and air is forced out towards the reservoir. The mathematical stiffness of the air spring is derived from below. It is known that a spring force is the product of pressure in this chamber and the effective area. Therefore, the spring stiffness:

$$k_s = \frac{dF}{dx} \quad (5.2.6)$$

can be written as:

$$k_s = A_{eff} \frac{dP}{dx} \quad (5.2.7)$$

Using equation 5.2.26 and rearranging it, the derivative of the pressure relative to the volume can be calculated as:

$$\frac{dP}{dV} = -nP_0V_0^nV^{-(n+1)} \quad (5.2.8)$$

For infinitesimal piston displacement, the following relation can be obtained:

$$dV = -A_{eff}dx \quad (5.2.9)$$

The minus indicates that the variation of air volume decreases as the piston moves downwards. Substituting equations 5.2.9 and 5.2.8 into equation 5.2.7, the spring stiffness expression of the air spring is obtained and given as:

$$k_s = nA_{eff}^2 \frac{P}{V} \quad (5.2.10)$$

where V is the air volume in the bottom chamber and P the gauge pressure in this chamber. The force of the air spring can now be calculated as:

$$F_{airspring} = k_s dx \quad (5.2.11)$$

The pressure in the cylinder chamber during the up and down stroke can now be calculated as:

$$P_{piston,up} = P_{drop,pipes} + P_{acc,HP} \quad (5.2.12)$$

$$P_{piston,down} = P_{res} - P_{drop,pipes} \quad (5.2.13)$$

5.2.2 Hydraulic Hoses

The pressure drop in the pipes $P_{drop,pipes}$ can be modeled using the Haaland approximation of the Darcy equation:

$$P_{drop,pipes} = f \frac{L_g + L_{eq}}{D_h} \frac{\rho}{2A^2} q_p |q_p| \quad (5.2.14)$$

where f , the friction factor, is characterised by:

$$f = \frac{Ks}{Re} \quad (5.2.15)$$

Hydraulic fluid is an important element of hydraulic systems and can influence the dynamic behaviour of the system. The bulk modulus is affected by the system pressure and entrapped air. For accurate system dynamics, these parameters influencing the bulk modulus must be included in the model. The variable bulk modulus of a fluid-air mixture in a flexible hose is given by the following equation (McCloy and Martin (1980)):

$$\frac{1}{\beta_v} = \frac{1}{\beta_f} + \frac{1}{\beta_h} + \frac{V_a}{V_t} \cdot \frac{1}{\beta_a} \quad (5.2.16)$$

where subscripts v , f , h and a refer to variable, hydraulic fluid, hose and air, respectively. The total volume V_t is the sum of the fluid and air volumes.

5.2.3 Check Valves

The purpose of the one-way valve, also known as a check valve, is to block the flow in one direction and permit flow in the opposite direction. The valve remains closed while the pressure differential across the valve is lower than its cracking or opening pressure. When the cracking pressure is reached, flow is permitted between the inlet and outlet. As the pressure continues to rise, the area of the opening is further increased until the maximum area is reached. The flow rate is determined according to the following equations (Matlab, Simulink):

$$q = \begin{cases} K_D \cdot A \sqrt{\frac{2}{\rho}} \cdot \text{sign}(p) & \text{for } Re \geq Re_{cr} \\ 2C_{DL} \cdot A \frac{D_H}{\nu \cdot \rho} p & \text{for } Re < Re_{cr} \end{cases} \quad (5.2.17)$$

where ν and ρ are the fluid kinematic viscosity and fluid density, respectively. The instantaneous orifice passage area is a function of pressure:

$$A(p) = \begin{cases} A_{leak} & \text{for } p \leq p_{crack} \\ A_{leak} + K \cdot (p - p_{crack}) & \text{for } p_{crack} < p < p_{max} \\ A_{max} & \text{for } p \geq p_{max} \end{cases} \quad (5.2.18)$$

where p , p_{crack} , p_{max} are the pressure differential; valve cracking pressure; and pressure needed to fully open the valve, respectively. The pressure differential across the valve is given by:

$$p = p_A - p_B \quad (5.2.19)$$

where p_A and p_B are the gauge pressures at the block terminals. The non-dimensional constants K and C_{DL} can be written as:

$$K = \frac{A_{max} - A_{leak}}{p_{max} - p_{crack}} \quad (5.2.20)$$

and

$$C_{DL} = \left(\frac{K_D}{\sqrt{Re_{cr}}} \right)^2 \quad (5.2.21)$$

where K_D is the flow discharge coefficient and Re , the Reynolds number, may be written as:

$$Re = \frac{q \cdot D_H}{A(p) \cdot \nu} \quad (5.2.22)$$

The instantaneous orifice hydraulic diameter is given by:

$$D_H = \sqrt{\frac{4A(p)}{\pi}} \quad (5.2.23)$$

5.2.4 Accumulator

The accumulator is initially filled with pressurized nitrogen gas. The rate of change of hydraulic fluid volume must be equal and opposite to the rate of change of nitrogen volume, because the total volume of the accumulator are fixed:

$$Q_{acc, Ni} = -Q_{fluid} \quad (5.2.24)$$

Assuming the nitrogen gas to be isentropic, the pressure in the accumulator can be calculated using

$$P_{Ni}(0)V_{Ni}(0)^n = P_{Ni}(t)V_{Ni}(t)^n \quad (5.2.25)$$

The pressure in the reservoir is always the same as atmospheric pressure. This equation can be rewritten as:

$$P_{acc,HP} = \frac{P_{pre}}{\left(1 - \frac{V}{V_{init}}\right)^n} \quad (5.2.26)$$

where $P_{acc,HP}$ is the hydraulic fluid in the accumulator and reservoir at a specific given time; n is the specific heat ratio (1.4 for nitrogen gas); V_{init} is the total volume of the accumulator; and P_{pre} is the gas pressure when the oil volume in the accumulator is zero (pre-charge pressure). The oil volume V is the integral of the fluid volume that flows into the accumulator:

$$V = \int Q_{acc,HP} dt \quad (5.2.27)$$

5.2.5 Hydraulic Motor

The pressure difference across the hydraulic motor can be written as:

$$\delta P = P_{acc,HP} - P_{res} \quad (5.2.28)$$

where P_{res} is the (atmospheric) pressure in the reservoir. Once the pressure difference is known, it can be used to calculate the loss due to leakage flow in the hydraulic motor, the hydraulic motor torque and the damping force. The hydraulic flow and the losses in the hydraulic motor are respectively given by:

$$Q_m = D_m \omega \quad (5.2.29)$$

$$Q_{leak} = k_l \cdot \delta P \quad (5.2.30)$$

where k_l is the motor leakage coefficient and ω_m the motor angular velocity:

$$\omega_m = \frac{L}{J} \quad (5.2.31)$$

where L is the angular momentum of the hydraulic motor shaft and J is the momentum of inertia. The motor torque and loss due to rotational friction are given by:

$$T_m = D_m \nu_m \delta P \quad (5.2.32)$$

$$T_f = B \omega \quad (5.2.33)$$

where B is the rotational friction coefficient. The torque on the shaft between the hydraulic motor and generator can now be calculated as:

$$T_s = T_m - T_f - T_g \quad (5.2.34)$$

where T_g is the generator torque and T_s can be described by:

$$T_s = \dot{L} \quad (5.2.35)$$

The output power of the hydraulic motor is a function of speed:

$$P_{out} = \frac{q_v \cdot \delta p}{600 \cdot \eta_v} \quad (5.2.36)$$

where δp is the pressure differential across the motor; η_v the total efficiency; and q_v the flow through the motor, which is given by:

$$q_v = \frac{D_m \cdot n \cdot \eta_v}{1000} \quad (5.2.37)$$

where n is the speed of rotation and η_v the volumetric efficiency, respectively. The output power is also a function of the pressure differential across the motor and the duration of rotation.

5.2.6 Damping Force

The piston in the cylinder experiences frictional forces during movement. These frictional forces are characterised by the following equation (Matlab, Simulink):

$$F_f = F_c(1 + (K - 1)e^{(-c_v|v|)})\text{sign}(v) + f_{vfr}v \quad (5.2.38)$$

where F_c is given by

$$F_c = F_{pre} + f_{cfr} \cdot P_r \quad (5.2.39)$$

where P_r is the pressure in the cylinder chamber.

The damping force acting on the hydrodynamic model or buoy, due to the hydraulic system can finally be calculated for the upward and downward strokes:

$$F_{h,up} = A_p \cdot P_{acc,HP} + A_p \cdot P_{drop} - F_f - F_{cw} \quad (5.2.40)$$

$$F_{h,down} = A_p \cdot P_{acc,LP} - A_p \cdot P_{drop} - F_f + F_{cw} \quad (5.2.41)$$

where F_{cw} is the force due to the counterweight, an air spring or a normal spring.

5.3 Analytical Results of Hydraulic Model

An algorithm (Table 5.1) that incorporates the equations obtained in Section 5.2, was developed and programmed in MATLAB[©] to simulate the nonlinear hydraulic system. It calculates the pressures in the accumulator and reservoir, the flows through the entire system, the power output at the generator, the torque and angular momentum of the shaft, and the damping force on the buoy due to the hydraulic system.

Algorithm 5.1 Algorithm for the hydraulic model

Require: *Buoy velocity*

Require: *Cylinder size, pipe diameters and lengths, size of accumulator*

Require: *Pre – pressure of accumulator, Size of motor*

while $t \leq T_{end}$ **do**

if $v \geq 0$ **then**

Calculate flow from cylinder; damping force

Leakage through check valve = 0

else

Flow from cylinder = 0

Calculate leakage through check valve; damping force

end if

Calculate pressure in accumulator and pipes; leakage through gear motor

if *Pressure in accumulator* ≥ 250 bar **then**

Open relief valve

else

if *Pressure in accumulator* \geq *startup pressure of motor* **then**

Calculate shaft speed, duration shaft turns, power output

Calculate new pressure in accumulator

end if

end if

end while

The algorithm was tested for a 1:7 scale model. An iterative approach was followed in this study, namely that the size of the hydraulic motor was determined first (with the known output power and rotational velocity), followed by determining the sizes of the accumulator, hoses and lastly, the cylinder. Knowing what the force must approximately

be for the buoy to follow the certain path, the size of the cylinder could be verified using the equations in the previous section. The necessary adjustments were made to resize the other components (Table 5.1). From this value, the flow through the system, knowing the wave velocity, and the pressure could be calculated. These values were then used to size the accumulator and hydraulic motor. The parameter values used in this study are shown in Table G.1 in Appendix G.

Table 5.1: Sizes of hydraulic components

Component	Size
Cylinder	Stroke 0.4 m; area 0.0015 m^2
HP accumulator	Volume 0.005 m^3 ; pressure 20 bar
Reservoir	Volume 0.04 m^3 ; pressure 1 bar
Gear motor	10 cc
Alternator	1450 rpm; T_g 1 Nm
Check valve (supply)	25 mm
Check valve (return)	12,5 mm

Figure 5.3 illustrates the way in which the oil pressure in the accumulator builds up with every upward stroke of the piston. When the piston retracts and the top chamber is filled with oil again, no oil is pumped to the accumulator, which results in a slight drop of oil pressure in the accumulator (and hoses). This is due to leakages around the gears of the hydraulic gear motor. The pressure builds up until it reaches a certain value, i.e. the pressure is high enough for the motor to overcome its startup torque, and it starts turning.

When the pressure in Figure 5.3 reaches 25 bar, it quickly drops to one (1) bar, which is equal to the atmospheric pressure on the low-pressure side of the motor. This means that the motor not only turns at a very fast speed, but needs a high volume flow, and the cylinder cannot keep up with supplying enough oil. The motor keeps turning until no fluid is available in the accumulator to supply the motor.

The motor will turn and come to a standstill within a few milliseconds. Figure 5.4 shows that the motor turns at an average speed of 1050 rpm and turns for approximately 0.8 seconds. It is clear that an intermittent power output will occur, which is a substantial problem as a continuous output would be more desirable. Simulations were done with a smaller, 6 cc motor, but the results were similar to the results obtained with the 10 cc motor. With the 6cc motor, however, the motor turned on average approximately 1.5 times longer than the 10 cc motor.

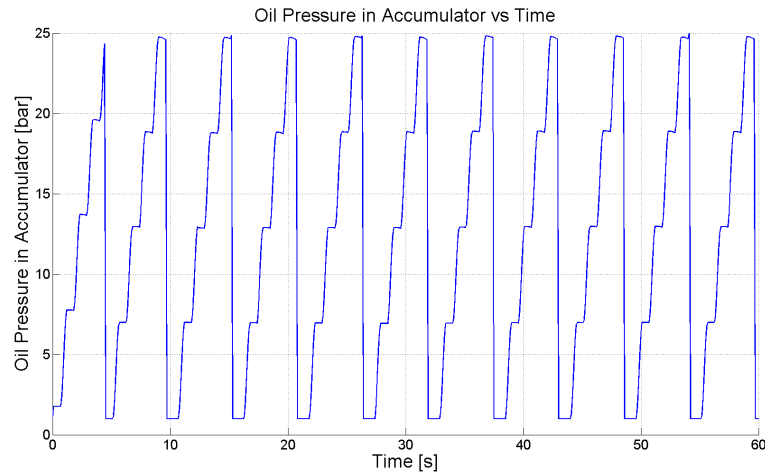


Figure 5.3: Pressure in accumulator

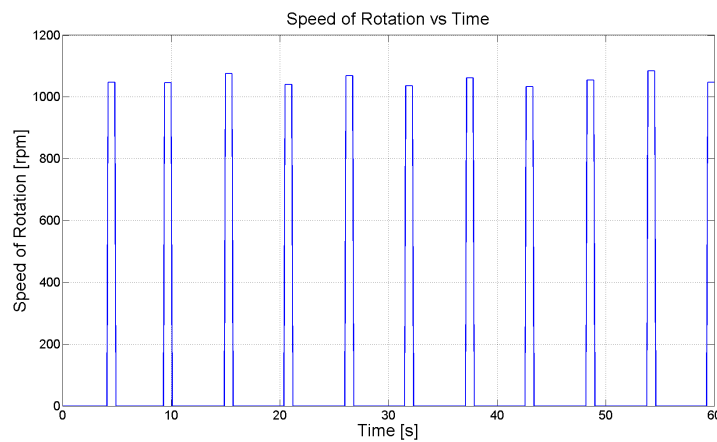


Figure 5.4: Speed of rotation of gear motor

5.4 Verification of Hydraulic Model

To verify the results obtained with the numerical model, a scale model was built and tested. Hardware-in-the-loop simulation is a technique that was used to mimic the movement of the buoy in ocean waves in the development and testing of the complex hydrodynamic-hydraulic system.

5.4.1 Hardware-in-the-loop (HIL) Simulation

The complexity of the buoy is included in the development and testing by adding a mathematical representation of this dynamic system. This mathematical representation is referred to as the "plant simulation" and portrayed in Figure 5.5. The embedded system, or hydraulic PTO, that must be tested interacts with this plant simulation (see Signorelli *et al.* (2011) for more information). This is a very efficient way of testing

embedded systems, as it is used during tight development schedules; it enhances the quality of testing; and it identifies human errors at an early stage.

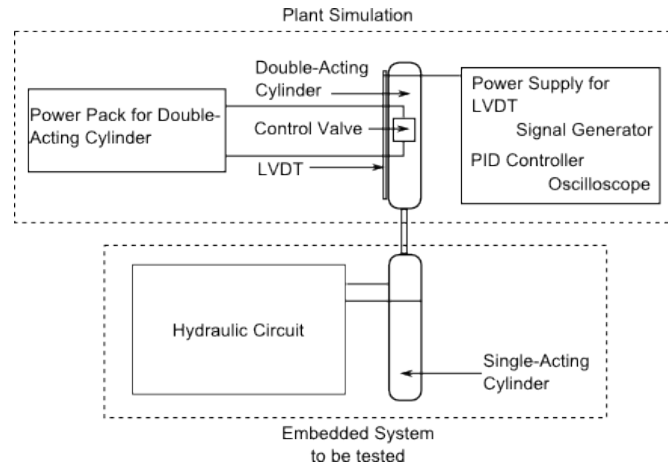


Figure 5.5: Hardware-In-the-Loop

In this study a double-acting cylinder or plant simulation that mimicked the movement of the buoy, was connected to the single-acting cylinder (Figure H.7 in Appendix H) of the PTO system or embedded system under testing. The position of this double-acting cylinder was controlled with a Linear Variable Displacement Transducer (LVDT) together with a four-way control valve, a signal generator and a PID controller. The signal generator could also determine at what frequency the piston of the double-acting cylinder must actuate the single-acting cylinder. The power pack supplied oil to the double-acting cylinder while the PID controller ensured that the error between the reference input (signal generator) and the actual output (position of LVDT) was minimised. The position of the piston could be read on an oscilloscope.

5.4.2 Experimental Results

Figure 5.6 shows the results that were obtained with the experimental setup. The measured pressure appears to be similar to the numerical model's pressure, but there are slight differences. As the motor uses all of the oil inside of the hoses before it comes to a standstill, the physical model takes longer to build up pressure inside the accumulator than the numerical model. The pressure is thus longer at one (1) bar as the hoses must be filled with oil before pressure can be built up.

When no fluid is supplied to the accumulator, the oil pressure inside the accumulator also decays drastically. It is clear that the leakage through the gears of the motor, which is a function of pressure, drops exponentially rather than quadratically - as modelled. When the cylinder pumps oil, the check valve opens, and the pressure inside the accumulator

CHAPTER 5. MODELLING AND SIMULATION OF HYDRAULIC PTO

reaches the desired value before the piston reaches the end stop, the pressure of the cylinder is transferred through the open check valve to the motor. This results in the narrow spikes of pressure.

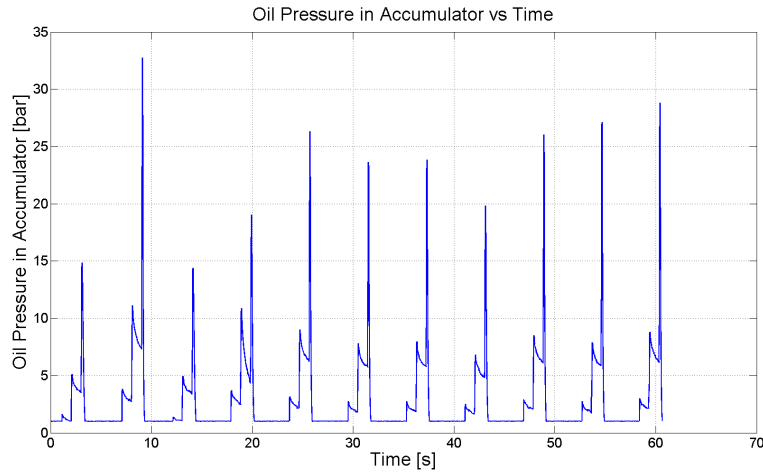


Figure 5.6: Measured pressure in accumulator

The speed at which the gear motor turns and the period of time it turns for, are provided in Figure 5.7. The gear motor turns at an average speed of 986 rpm for approximately 0.77 seconds, which is very close to the results of the numerical model.

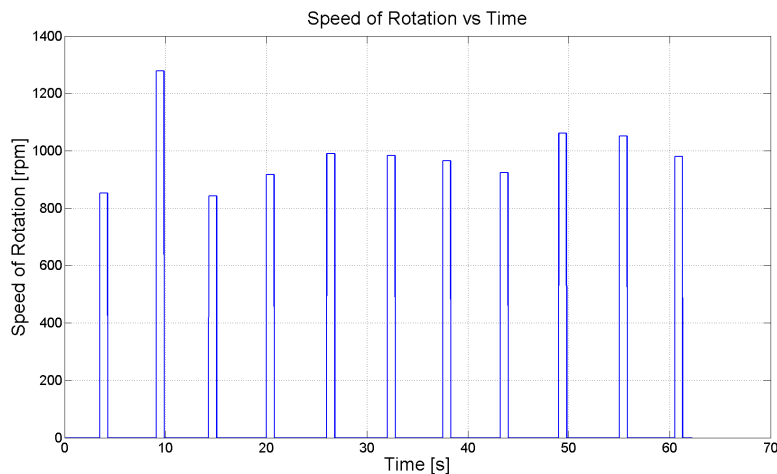


Figure 5.7: Measured speed and duration of rotation of gear motor

The numerical model is not a perfect representation of the physical system, but it is accurate enough to obtain a general idea of how the hydraulic system will react to certain inputs.

5.5 Hydraulic Winch System

During inclement weather conditions, the winch will lower the buoy to a certain depth so that the buoy will be protected from potential damage. This system was modelled in Simulink as illustrated in Figure 5.8.

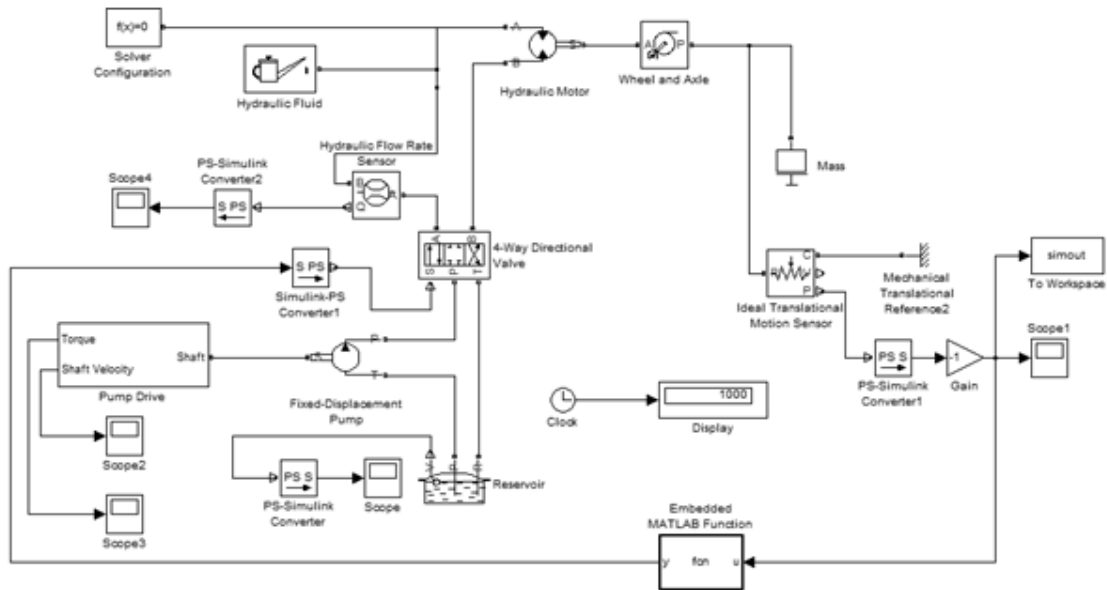


Figure 5.8: Model structure

When the wave height reaches five (5) metres, the clamp releases the cable and the four-way directional valve is opened. The battery pack, which is initially charged, drives an electric motor that, in turn, drives a hydraulic pump. The pump drives a motor that is connected to the drum. During operation the cable is wound around the drum. When the buoy reaches a certain depth, the four-way valve closes and the pump stops pumping fluid to the motor.

For a full-scale model it will take approximately 16 minutes to lower the buoy (Figure 5.9). After 24 or 48, depending on designer's choice, hours, the buoy is released to its normal operating position. When the WEC starts to operate, the generator charges the battery pack first before it feeds power via an inverter into the grid.

The design aspects of this winch system are outside the scope of this study. Hence no further detailed studies were conducted regarding this part of the hydraulic device.

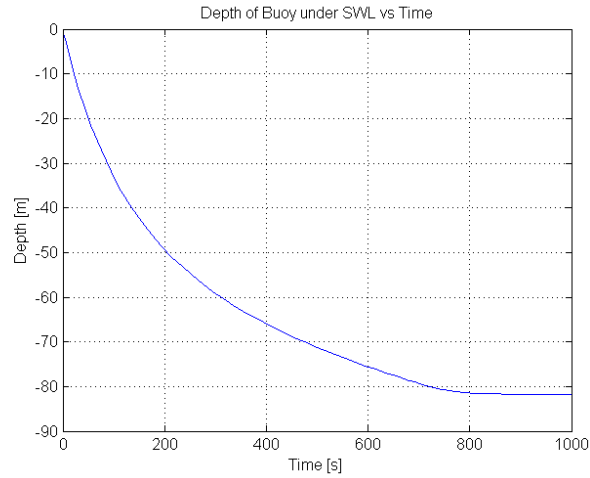


Figure 5.9: Depth of buoy

5.6 Combined Hydrodynamic-Hydraulic System

Both models were combined during this simulation. There is not a significant difference between the two wave profiles' buoy motions, but with the second-order stokes wave profile the buoy tends to follow the desired path better than in the case of the linear wave profile. In Figure 5.10 the red line indicates the position of the centre point of the buoy and the blue line illustrates the incoming waves from right to left. Only the heave data is given in these figures as the surge data are similar to the results shown in Chapter 3.

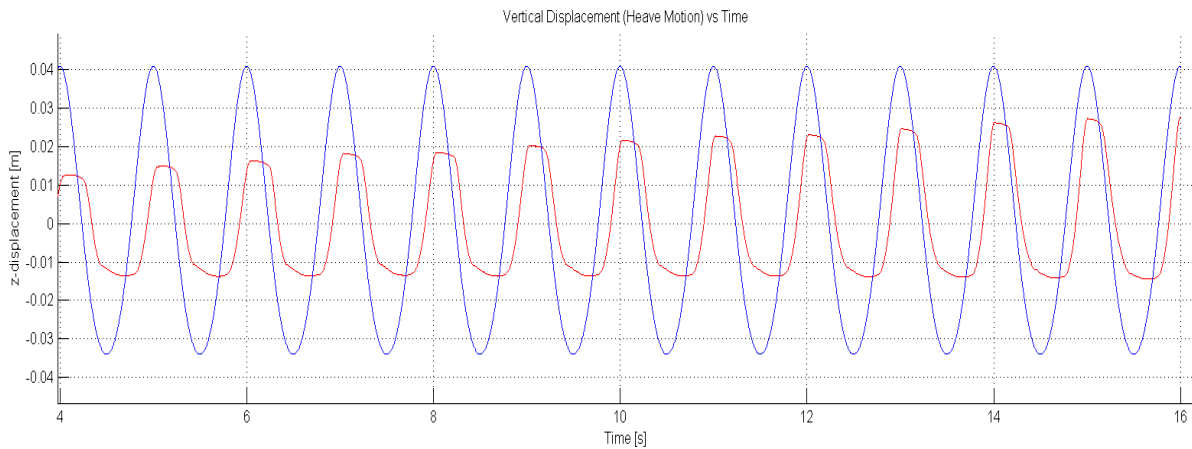


Figure 5.10: Heave motion of buoy for second-order stokes waves

Another remarkable finding is that with the hydraulic system connected to the buoy, the velocity profile almost fits the profile described by Budal and Falnes (1980) if the design variables are chosen correctly. Figure 5.11 shows the latching effect the hydraulic system

has on the buoy's motion due to the damping force. This means that no controller is needed for this wave energy converter.

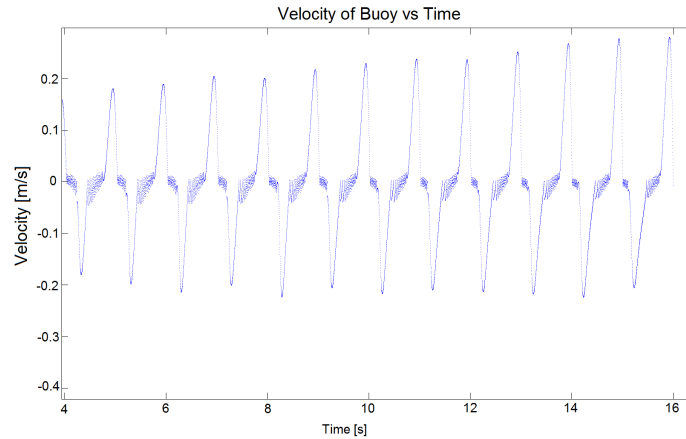


Figure 5.11: Latching effect for second-order stokes waves

5.7 Conclusion

In this chapter numerical models for the hydraulic power take-off components and for the winch system were developed. Tests were conducted in the laboratory to verify the results obtained with the mathematical model of the power take-off system. To demonstrate the winch system's basic working principle, only simulations of the system are included.

The results obtained with the experimental setup appeared to be similar to the numerical model's results, but there were slight differences. Nevertheless, the numerical model was a relatively good approximation of the experimental model.

The combined hydrodynamic-hydraulic numerical model showed that latching control is possible when the design parameters are chosen correctly and that no controller is needed to control the position of the buoy.

A number of tests may now be performed in the laboratory to determine the hydraulic system's performance and in the large wave flume to determine the performance of the combined hydrodynamic-hydraulic system.

Chapter 6

EXPERIMENTAL SETUP AND RESULTS

A number of tests were performed to determine the hydraulic system's performance. The aim was to test the system for various wave profile inputs and to determine the influence of flow restrictors, pressure regulators and flywheels. The winch system was not tested.

More tests were conducted in the large wave flume to determine the performance of the combined hydrodynamic-hydraulic system. The behaviour was investigated using test instrumentation.

In this chapter the test equipment, experimental apparatus and testing procedures, together with the results of these, are discussed for both the hydraulic and combined hydrodynamic-hydraulic systems.

6.1 Experimental Apparatus and Test Equipment

The hydraulic components were mounted on a wooden platform while the two cylinders were bolted horizontally to the floor and connected directly to each other. The equipment - PID controller, signal generator and oscilloscope - that was necessary for control, or for the plant simulation, were placed on a table next to the double-acting cylinder. A computer, together with the Spider data-acquisition system, were placed on a separate table next to the hydraulic system. Figure 6.1 shows the PTO setup, and more images of the PTO are provided in Appendix H.

A strain gauge and a 20 kN load cell measured the force necessary to move the piston; a pressure transducer measured the oil pressure in the pipes and accumulator; and an inductive proximity sensor (normally open) measured the speed of rotation of the shaft. All these sensors were connected to a Spider data-acquisition system that provided an interface between the test equipment and computer. The Catman Easy Software, installed on the computer, was used to log and analyse all the sensors' measured data.

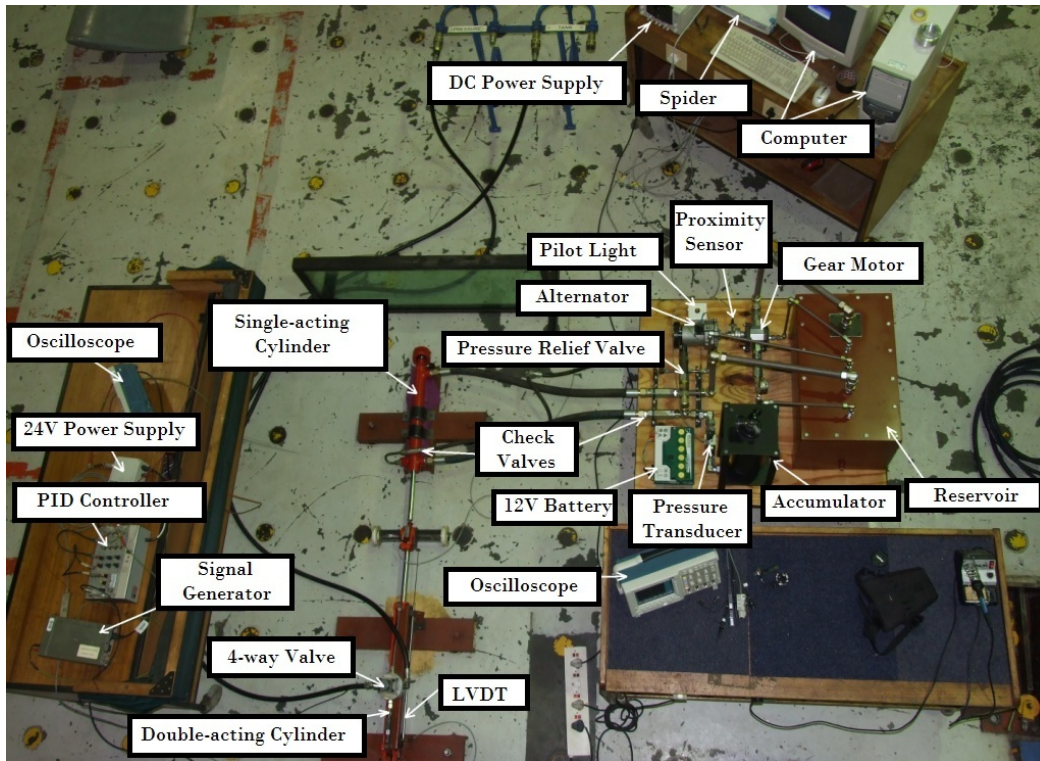


Figure 6.1: Hydraulic PTO

Probes that measured the induced current and voltage at the terminals of the alternator as well as the voltage of the battery, were connected to an oscilloscope. The scope logged the data and stored it frame-by-frame. When the motor turned, a voltage and current were induced. The induced voltage was slightly higher than the battery voltage, causing the induced current to flow from the alternator to the battery. When this happened, the pilot light switched off and the battery, or the load, was charged.

6.2 Test Procedure

A hydraulic system consisting of a cylinder, accumulator, gear motor, generator and reservoir, together with the HIL plant simulation discussed in Section 5.4.1, were used for experiments. The hydraulic system was tested by its own in the laboratory. Tests were initially executed with only a pressure regulator mounted at the motor's inlet. The behaviour of the system was then tested with a flow restrictor mounted at the motor's inlet. The opening was just wide enough for the motor to rotate at a desirable speed. A flow restrictor was then mounted at the motor's outlet to create a back-pressure. More tests were done with two flywheels (with mass of 1 kg and 2 kg, respectively) mounted on the motor's shaft. Lastly a combination of flow restrictors and flywheels were used to determine the system's behaviour.

A buoy, or hydrodynamic model, was connected to the hydraulic system and tests were conducted in the large wave flume. The behaviour of the combined system was recorded and analysed, including the pressures in the accumulator and hoses and the shaft speed.

6.3 Laboratory Results

The hydraulic system was tested for various combinations of wave heights, or stroke lengths, and wave velocities, or buoy velocities. The stroke lengths varied between 0.05 and 0.35 metres whilst the velocities varied between 0.1 and 1.0 Hz. This allowed for more repeatable experiments. With the sensors connected to the system, the input energy, output energy, oil pressure in accumulator, shaft speed and duration of rotation could be calculated or measured.

6.3.1 Tests with Pressure Regulator

The input power and energy can be calculated from the measured force and known input velocity, provided by the signal generator, and are described by Equations 4.2.3 and 4.2.4. The output energy, on the other hand, is calculated as:

$$E_{out} = \int V(t)I(t) dt \quad (6.3.1)$$

where $V(t)$ and $I(t)$ are the induced voltage and current, respectively. The measured instantaneous output energy for each stroke length and frequency is given in Figure 6.2.

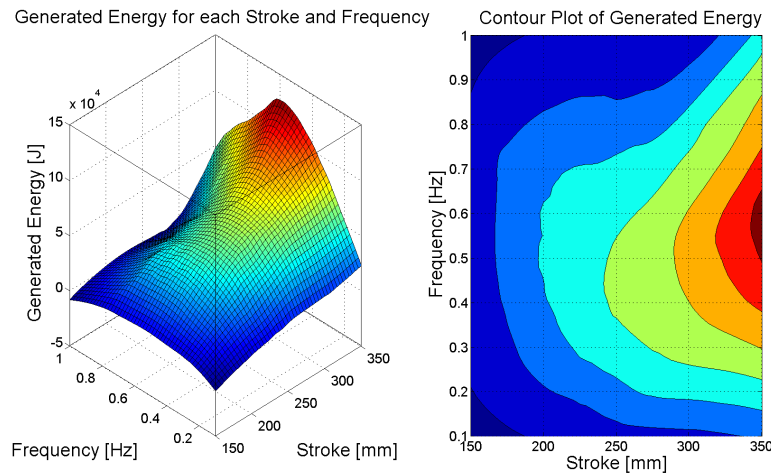


Figure 6.2: Generated energy for each stroke length and frequency

The energy in Figure 6.2 can be normalised with the following equation:

CHAPTER 6. EXPERIMENTAL SETUP AND RESULTS

$$E(i, j) = \frac{E(i, j)}{\max(\max(E(i, j)))} \quad (6.3.2)$$

where $E(i, j)$ refers to a specific element in the energy matrix; the i 'th element, or row, refers to frequency and the j 'th element, or column, to stroke length. The $\max(E(i, j))$ establishes the row vector with the maximum value in the matrix, and $\max(\max(E(i, j)))$ finds the maximum value in that specific vector. Figure 6.2 indicates that the system has an optimal operating range: when the stroke length is anything between 250 and 350 mm and the frequency between 0.4 and 0.6 Hz, the system produces a maximum energy output.

The measured speed of rotation of the hydraulic motor's shaft, the measured duration of shaft rotation and the measured number of times the shaft turns and come to a standstill in a minute, are given in Figures 6.3, 6.4 and 6.5, respectively.

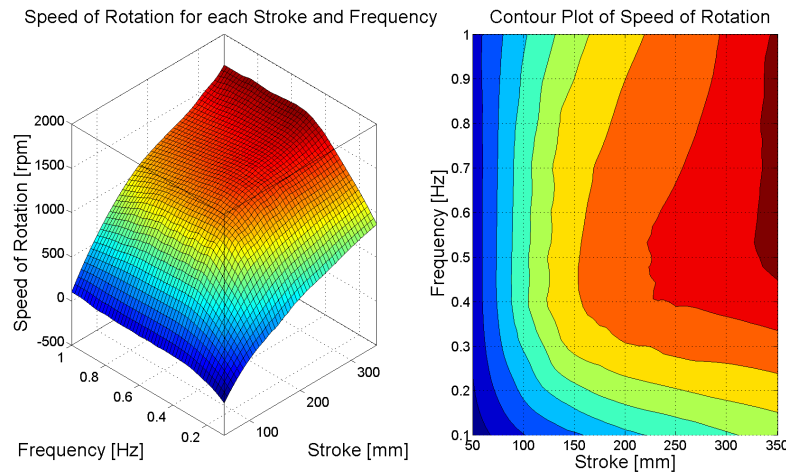


Figure 6.3: Shaft speed for each stroke length and frequency

It is interesting to note that at low- and at high stroke lengths the shaft turns for only a few milliseconds before it comes to a standstill. At low stroke lengths, the small amount of oil volume that is pumped to the accumulator ensures that the startup torque is overcome with a small fraction. This causes the pressure differential across the motor to be very low. The volume flow through the motor and, as a result, the speed at which the motor turns, are therefore very low. The friction of the gears causes the motor to come to a standstill within a very short period of time (a few milliseconds). At high stroke lengths the motor turns at a very high speed and the pressure differential is very high, therefore needing high volume flows. Within a few milliseconds all the oil in the accumulator and pipes flows through the motor. No oil is available to keep the motor turning and the friction of the gears brings it to a standstill.

CHAPTER 6. EXPERIMENTAL SETUP AND RESULTS

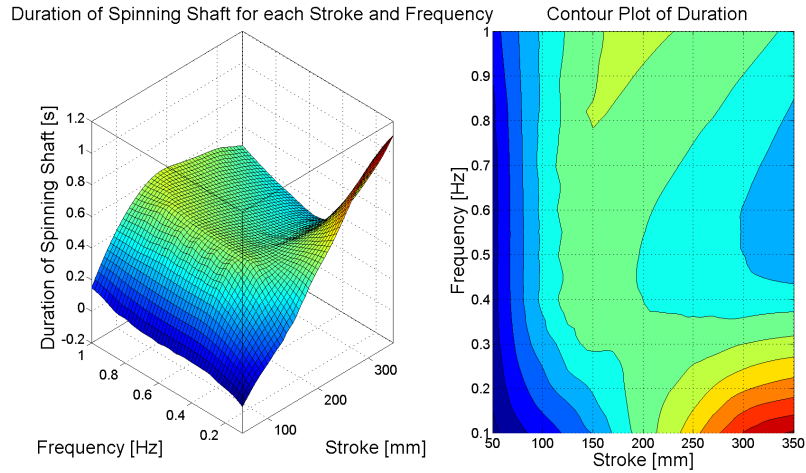


Figure 6.4: Duration of shaft rotation for each stroke length and frequency

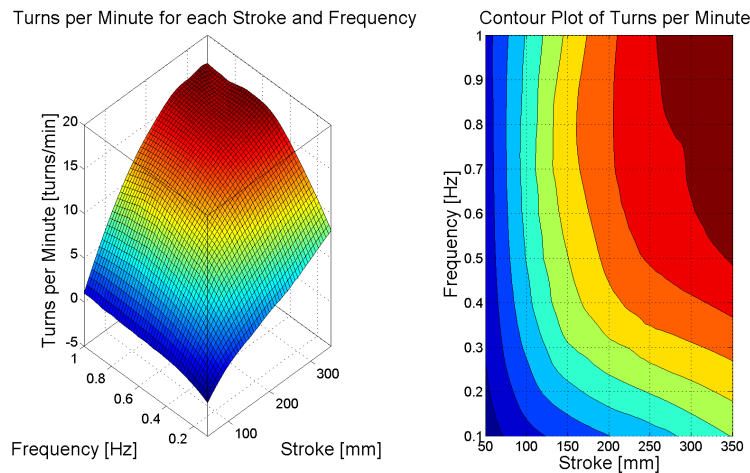


Figure 6.5: Number of cycles per minute for each stroke length and frequency

At low frequencies, the motor turns every other stroke, but at higher frequencies and stroke lengths the motor turns with every single upward, pumping, stroke. More oil is therefore pumped at higher strokes and frequencies; the startup torque is overcome more frequently and a more frequent turning of the shaft is the result.

An alternator must turn at least 500 to 600 rpm before it generates electricity. The higher the speed, the higher the induced voltage. When it reaches 1200 rpm, the alternator induces a maximum voltage. The induced voltage remains constant for any speed above 1200 rpm. The average shaft speed was found to be 975 rpm and it turns on average for 0.55 seconds. During this short period of time, a voltage is induced in the alternator. If the induced voltage is higher than the battery voltage, a current flows from the alternator to the load, or battery, and the battery gets charged. An example where the battery is charged is provided in Figure 6.6.

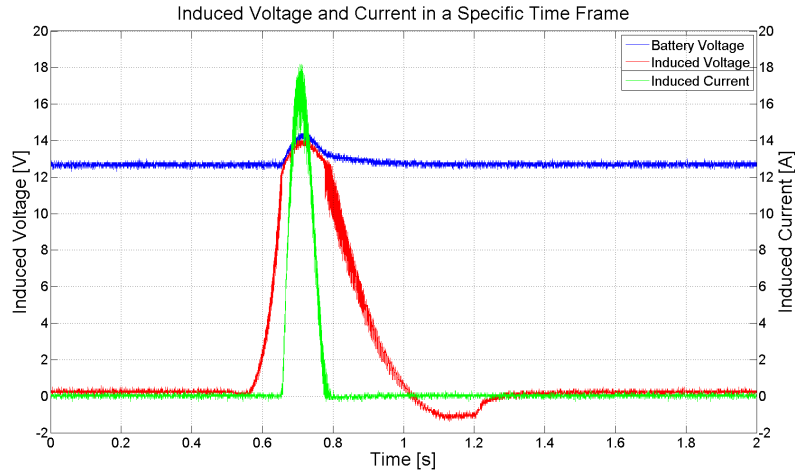


Figure 6.6: Induced voltage and current

After this short period of time, there is no energy output, and the output energy will be "instantaneous". For the next few tests the energy, shaft speed and duration of rotation were normalised with respect to the maximum values found for these values in Section 6.3.1. Tests were done with stroke lengths of 250 to 350 mm and frequencies of 0.4 to 0.6 Hz as these were the "optimal" operating conditions for the PTO. The figures are provided in Appendix I.

6.3.2 Tests with Flywheel on Shaft

A two-kilogram flywheel was mounted on the alternator's shaft to widen the narrow peaks of the induced voltage and current (Figure I.1). The energy output almost doubled (Figure I.2), while shaft speeds of one-and-a-half times the original speed were not uncommon (Figure I.3). The higher shaft speeds require higher oil flow rates through the motor. The inertia of the flywheel however kept the alternator turning for almost twice as long at an average of 1.45 seconds, even if there was no oil supply to the motor (Figure I.4). As the flywheel improved the output, the rest of the tests discussed here were done with a flywheel mounted on the shaft.

6.3.3 Tests with Flow Restrictor at Outlet

A back-pressure of three (3) to five (5) bar was now applied to the motor. The back-pressure lowers the pressure differential across the motor, which lowers the shaft speed (Figure I.6). As result of the lower pressure differential, the upstream pressure approaches

the downstream pressure of the motor in less time. The duration of rotation is therefore lower (Figure I.7), as is the output energy (Figure I.5).

6.3.4 Tests with Flow Restrictor at Inlet

The back-pressure was removed and a flow restrictor was placed in front of the motor. The flow restrictor was adjusted to the point where the hydraulic motor turns the alternator fast enough to generate electricity. In this case the output energy and shaft speed is lower (Figures I.8 and I.9), but the hydraulic motor turns for longer periods (Figure I.10).

6.3.5 Tests with Smaller Gear Motor

The 10 cc motor was replaced with a 6 cc motor. The average shaft speed was found to be approximately 650 rpm (Figure I.13). Due to the fact that the smaller motor displaces less volume of oil per minute, the average time duration of rotation (Figure I.14) was 1.6 seconds, which is three times the time duration of a 10 cc motor. This caused the peaks of the induced voltage and current to be even wider than the 10 cc motor with the flywheel (Figure I.11) and the energy to be 2.5 times the maximum energy found in Section 6.3. Note that the optimal operating conditions have shifted from 0.4 to 0.6 Hz to 0.1 to 0.3 Hz for the 6 cc motor, which is closer to the optimal wave periods that the system must be designed for (Table F.1).

6.3.6 Conclusion

The ideas that were explored showed that a flywheel and a smaller motor improves the performance of the system. Questions that however arose included why there is an optimum frequency range and why the energy output did not increase with increasing frequency.

Further investigations revealed that it takes the oil three (3) to ten (10) seconds to flow into the top chamber through the check valve. When the frequencies become too high, the oil cannot flow fast enough through the check valve in the return line, which means that by the time the piston is pulled out again, the top chamber of the cylinder is not completely full. Only a small volume of oil, together with air, is pumped to the accumulator. This results in a low increase of pressure. Above a certain frequency, therefore, the energy output drops.

The intermittent power output indicates that the system has a flow problem. In this study an instantaneous power output was found to be anything between 300 and 500 W

(rms). It is far less than what was initially aimed for (Table F.1), but the size of the alternator used in this model did limit the power output. The induced voltage remains constant; thus limiting the electricity that could be generated.

6.4 Results - Large Wave Flume

An inflatable, conical-shaped buoy was connected to the single-acting cylinder of the hydraulic PTO (combined hydrodynamic-hydraulic system). Tests were conducted in a large wave flume (Figure 6.7) with dimensions 2 by 2 by 60 m (depth \times height \times length).

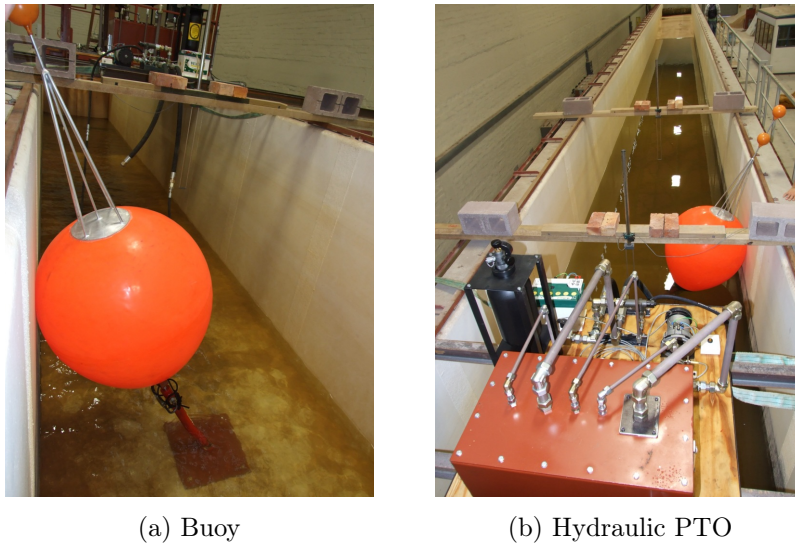


Figure 6.7: Tests in large wave flume

The algorithm used in Chapter 3 for image processing was used here to track the movement of the large float. To ensure that the same problems were not encountered as in Chapter 3, two smaller floats were attached to an aluminium rod that was mounted vertically on top of the large float. Figures 6.8 and 6.9 respectively show the surge and heave components of the buoy's movement.

It is clear that the buoy only moves from side to side as a wave passes over it, and not vertically. This means that oil was not pumped from the top chamber, and nor was the top chamber filled with oil. No pressure was therefore built up in the accumulator; the motor did not turn; and no energy output could be measured.

When the water level was however raised and lowered at a low rate, the piston did move slowly up and down. This indicates that the system could not react fast enough to short wave periods.

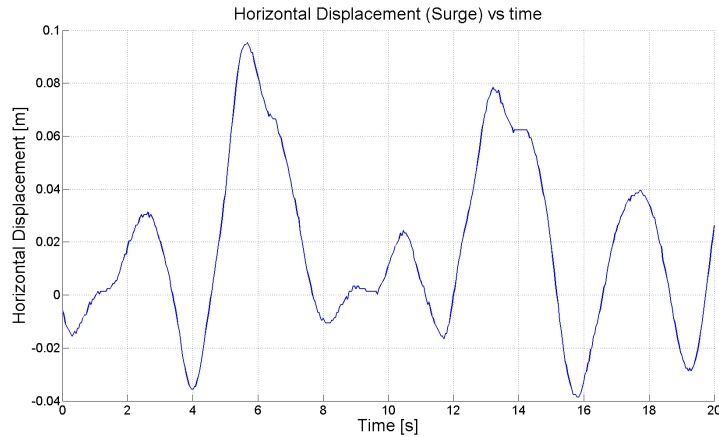


Figure 6.8: Surge response of combined system

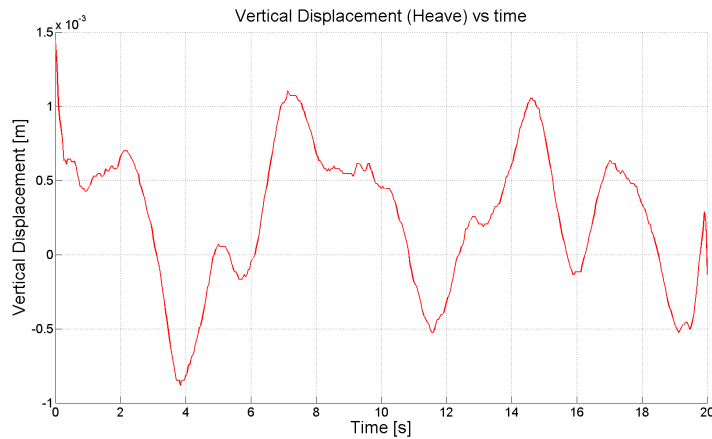


Figure 6.9: Heave response of combined system

The large wave flume could furthermore only make waves with a wave height of 100 mm between 3.5- and 6-second wave periods - the frequency range in which tests had to be conducted. With the shape of the buoy being conical, a small buoyancy force that was not large enough for the piston to be pulled out was created. At higher frequencies, or shorter wave periods, however, the wave flume could create waves that have a height of 500 mm.

As the large wave flume could not create the desired wave heights at specific frequencies and the system could not react to shorter wave periods, the tests were abandoned.

6.5 Conclusion

A number of tests were performed to determine the hydraulic system's performance. More tests were conducted in the large wave flume to determine the performance of the combined hydrodynamic-hydraulic system.

CHAPTER 6. EXPERIMENTAL SETUP AND RESULTS

The hydraulic system did not, however, function efficiently. Design changes should be made to the hydraulic system so that it can function properly. A few design improvements are suggested in the following chapter.

Chapter 7

DESIGN IMPROVEMENTS

In this chapter a few suggestions are made to potentially improve the wave energy developed in this study.

7.1 Shape of Buoy

Tests in the large wave flume were done with a conical-shaped float as a spherical one could not be found. This conical-shaped float has low drag and when the buoy is submerged, the apex of the cone displaces a small volume of water resulting in a low buoyancy force. This shape and the low drag furthermore cause the water to flow around the buoy.

It must also be mentioned that the large wave flume can only make waves with a wave height of 100 mm between 3,5 and 6 second wave periods. It is, however, necessary to have larger waves so that the desired buoyancy force can be created.

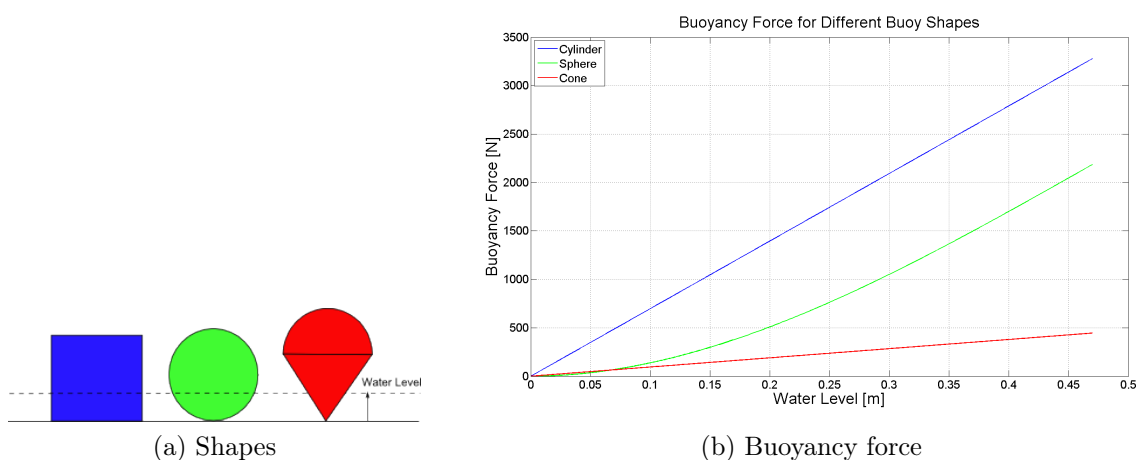


Figure 7.1: Buoyancy force for a cylinder, sphere and cone

The shape of the buoy may be altered so that a bigger buoyancy force is created with small displacements. Figure 7.1 shows that the buoy should have an almost cylindrical shape, but this could also impose problems as slamming may occur. All three shapes in

CHAPTER 7. DESIGN IMPROVEMENTS

this figure have a diameter of 0.94 metres. The cylinder has a height of 0.94 metres and the cone has a height of 1.2 metres. The shape of the buoy should be a combination of the sphere and the cylinder. The new shape will have higher drag and buoyancy forces. This will ensure that the buoy will react faster to passing waves, water will not simply flow around the buoy and the piston will be pulled out.

7.2 Spring or Vacuum

It was not possible to create a good vacuum as low friction seals caused some oil to flow from the top chamber around the seals to the bottom chamber or vacuum. Either seals with higher friction should be used or the vacuum must be replaced with a spring. If the latter approach is chosen, and using an optimal spring coefficient 6000 N/m, the buoy will have a movement similar to the results of a simulation shown in Figure 7.2. In this simulation a spherical-shaped buoy together with the hydraulic model was used. Note that the surge response of this simulation appears to be similar to the measured results provided in Figure 6.8.

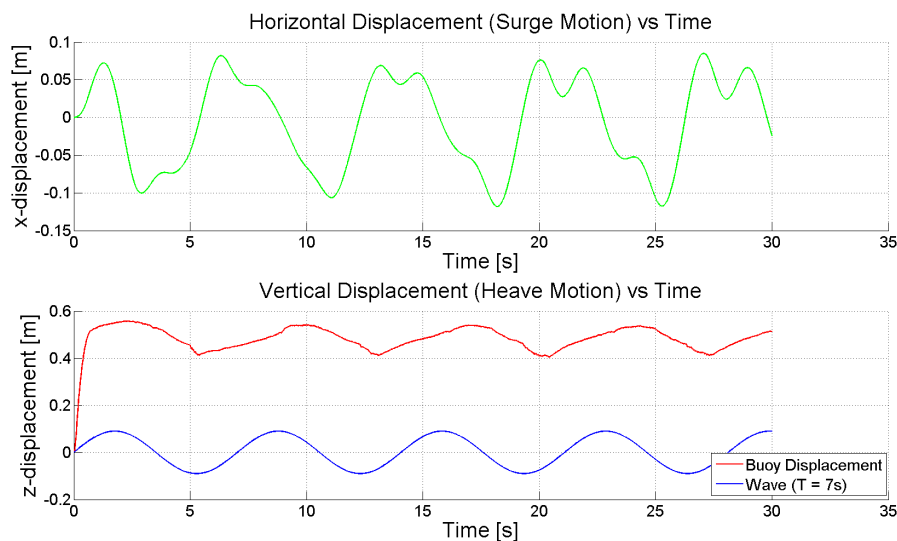


Figure 7.2: Surge and heave responses of complete model (with spring)

It is interesting to note that this buoy has a vertical displacement of approximately 100 mm when a wave with a wave height of 200 mm passes over it. A larger wave flume is therefore necessary to test the physical model.

7.3 Flow and Energy Output

Results in Chapters 5 and 6 indicate that there is a flow problem in that there is not enough oil supply for the motor to turn continuously. A smaller motor, 6 cc instead of the 10 cc, caused the alternator to rotate for at least three times longer. If an even smaller motor, e.g. a 2 cc gear motor, is used, the alternator will turn at least six (6) to eight (8) times longer than an alternator connected to a 10 cc motor; causing the alternator to turn more continuously. The 6 cc motor turned at a much lower speed (just enough to generate electricity) than the 10 cc motor, however. This means that a 2 cc motor, which needs less oil volume flow, will turn even slower than the 6 cc. The speed could, however, be increased with a gearbox with at least 1:5 gear ratio that is mounted between the motor and alternator. The alternator will then generate electricity.

This setup will only partially solve this power output problem. As there is no constant oil supply, the oil pressure in the accumulator will drop relatively fast when no oil is pumped to the system. The oil pressure in the accumulator will have large fluctuations; looking similar to the oil pressure shown in Figure 7.3. The lowest point will however be much lower than 24 bar (but higher than 1 bar, which is the pressure on low-pressure side). This will cause the alternator's speed to fluctuate and, as a result, the power output too. These fluctuations could be smoothed with the use of electronics.

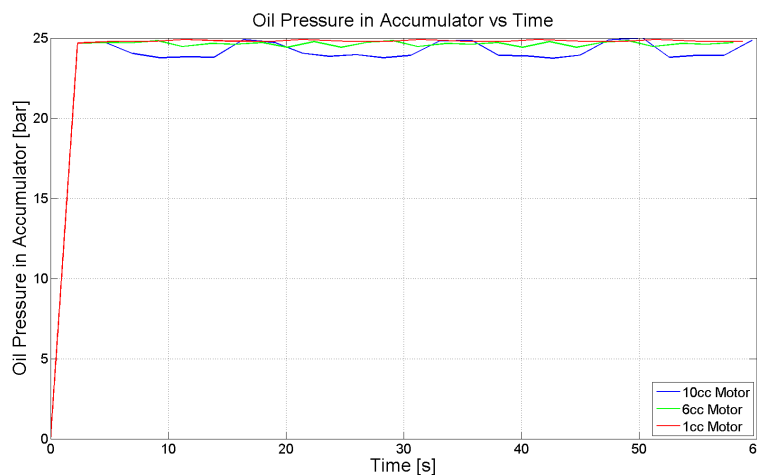


Figure 7.3: Accumulator pressure for various size motors

A simulation was done where two single-acting cylinders work 180° out of phase with each other. This means that when the one cylinder pumps oil to the accumulator, the other is filled with oil. When the first cylinder's piston is retracted and is filled with oil, the second cylinder pumps oil to the accumulator. This ensures a more constant oil supply to the hydraulic motor and solves the flow problem. Figure 7.3 indicates that a more constant

CHAPTER 7. DESIGN IMPROVEMENTS

pressure in the accumulator will occur when a smaller motor is used as a smaller motor needs less volume flow and therefore does not cause the pressure to drop dramatically.

The more constant pressure ensures a more constant pressure differential across the motor. This means that the motor will be turning at all times, forcing the alternator to generate uninterrupted electricity. In real-life applications more than two cylinders should be used as it is almost impossible to get two cylinders to work 180° out of phase in the ocean.

7.4 Check Valves and Diameter of Return Line

In-line ball check valves with no spring should rather be used than poppet check valves with springs. The cracking pressure will be reduced from one (1) bar to zero (0) bar. This means that the slightest increase in oil pressure will open the valve, allowing oil to flow. Oil will be pumped more easily to the accumulator and the top chamber will be filled more readily with oil when the piston retracts. This will allow an increase in the system's reaction time to oncoming waves with smaller wave periods.

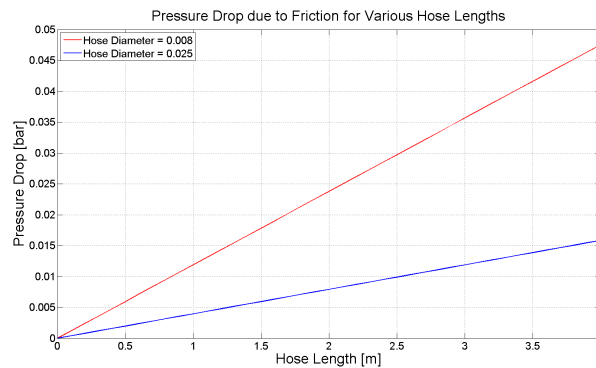


Figure 7.4: Pressure drop due to friction in hoses

Increasing the hose diameter of the return line from 0.008 m to 0.025 m means that a one (1) inch instead of a half inch check valve must be used. Not only does the increase in hose diameter result in a lower pressure drop along the hose due to reduced friction (Figure 7.4), but the flow will be increased from 5.3 to 22.7 litres per minute. The top chamber could be filled much faster. By the time the piston is pulled out again, a full chamber of oil with no air present will be pumped to the accumulator. This will mean that the energy output will increase with frequency and not decrease after a certain frequency (Section 6.3.6).

7.5 Conclusion

The hydraulic system did not function efficiently, but if the design improvements mentioned in this chapter are implemented, the system may function as desired. The system will then have a more continuous power output.

Chapter 8

CONCLUSION AND FUTURE RESEARCH

In this chapter the most important findings are emphasized and a few recommendations are made regarding future work on the WEC model.

8.1 Discussion and Conclusion

Several design aspects of a combined heave-and-surge hydraulic point absorbers have been investigated in this research. A reliable point absorber WEC with a mechanical or hydraulic PTO, coupled to a spherical buoy, had to be designed, built and tested. It should have the capacity to capture energy from ocean waves and convert it to electrical energy efficiently.

A numerical model for the hydrodynamic system, or buoy, was first developed. This model could almost exactly predict the movement of the buoy for any wave profile input, whether regular or irregular. The numerical model could also be used to calculate the forces acting on the buoy; the available energy that; the amount of energy that the buoy could capture from the waves; and the approximate power output. Tests were conducted in a small wave flume to verify the results obtained with the mathematical model. The results of the numerical and experimental models correlated very well.

This numerical model could then be used to determine the optimal diameter of the spherical buoy that should be used around the South-West coast of South Africa. It was furthermore used to determine how the power take-off system should react and it was found that the PTO should be something similar to a damper. It was also noted that the PTO must damp the buoy's movement in the upward direction only, and not in the downward direction. This ensures that the buoy follows a certain "optimal" path to capture the maximum energy from the ocean waves.

CHAPTER 8. CONCLUSION AND FUTURE RESEARCH

Concepts for the PTO were subsequently generated. In the end, a comparative analysis between a mechanical and a hydraulic system had to be conducted. Research indicated that the hydraulic system would be perfect for this application, being more compact, less heavy and less expensive than a mechanical system. It can also act as a damper. A numerical model was then developed for the hydraulic system and experimental tests were conducted in large wave flumes at the University of Stellenbosch to validate this model. The results of the numerical and the experimental models for the hydraulic PTO, however, did not seem to match perfectly. It was nevertheless sufficient enough to predict the dynamic behaviour of the hydraulic power take-off device.

Unfortunately the PTO did not function in an efficient manner. The motor turned for a few seconds and then came to a standstill. The shaft speed remained zero (0) until enough pressure was built up to drive the motor. The system was found to have a flow problem as the cylinder did not supply enough oil to keep the motor turning and the motor, which was too large, needed a substantial oil volume flow. This problem could be solved partially with a smaller hydraulic gear motor, replacing the bigger one, and a flywheel that was mounted on the alternator's shaft. It kept the motor turning for longer periods, but an intermittent power output still occurred. Due to time and money constraints, this problem could not be further addressed.

The numerical models for the hydrodynamic and hydraulic systems were subsequently combined. The numerical results indicated that the hydraulic model would have a latching effect on the buoy's movement; thereby maximising energy capture. When tests were however conducted in the large wave flume, nothing happened. The buoy did not pull the piston out and the piston did not retract. As a result the motor did not turn and no electricity was generated.

The large wave flume could unfortunately not generate waves with a sufficient wave height. The small wave heights, together with the conical shape of the buoy, caused the system to experience small buoyancy forces. The piston could therefore not be pulled out, and a vacuum was also not formed in the bottom chamber of the cylinder. This caused the piston not to retract when a trough passed under the buoy. The system did not work in the large wave flume and tests were therefore abandoned.

The error that was made in the laboratory tests was that the double-acting cylinder of the Hardware-In-the-Loop model was connected directly with a rod to the single-acting cylinder of the PTO. If a rope (Figure H.7) was used instead of a rod, it could have been predicted that the piston would not retract. The impact of the buoy's shape and the wave flume's inability to generate large enough waves could unfortunately not have been predicted.

The point absorber developed in this study is promising. An instantaneous power output was found to be anything between 300 and 500 W (rms). It is far less than what was initially aimed for (Table F.1), but the size of the alternator used in this model limited the power output. Above a certain speed the induced voltage remains the same, thus limiting the electricity that could be generated.

As this converter resides below the ocean surface, it may be less obtrusive than other wave energy converters. This location also means that the point absorber is less likely to be damaged during a storm. Tests in the large wave flume have shown that the complete model built in this study was able to withstand any wave conditions, indicating that the system is reliable.

The scale model developed in this study can easily be scaled up to a full scale prototype model using the scaling laws. The size of the buoy should be scaled first. Knowing what the buoyancy force and the power output should be, the size of the cylinder, hydraulic motor and accumulator can be calculated. The hose diameters can then be sized according to the velocity of oil that is needed throughout the system, keeping flow laminar and losses at a minimal.

With the necessary design improvements the device can offer a sustainable alternative to fossil fuels. Whereas the device does make use of oil that could contaminate the ocean, but with the proven technology used in this study, the possibility of a leak occurring is considered to be extremely unlikely. With the proven technology used in this study, the device could therefore contribute to the improvement of the living standard of many South Africans in providing electricity-deprived homes with power.

8.2 Recommendations

Apart from the design improvements suggested in Chapter 7, the following recommendations are made regarding future work on the WEC model:

1. A more complex hydraulic system should be developed. This is to enable the piston to be retracted; but also to get a continuous power output.
2. Studies should be done regarding the optimal shape of the buoy.
3. In this study the buoy was directly coupled to the cylinder (due to size constraints in wave flume). In real applications a mooring cable should be used. The mooring design and its influence on power extraction should further be addressed.

List of References

- Boldea, I. and Nasar, S. (1999). Linear electric actuators and generators. *IEEE Trans Energy Conversion*, vol. 14, no. 3, pp. 712–717.
- Boud, R. (2003). Status and Research and Development Priorities: Wave and Marine Current Energy. *This report was prepared for the UK Department of Trade and Industry by Richard Boud of Future Energy Solutions.*
- Budal, K. and Falnes, J. (1980). Interacting Point Absorbers with Controlled Motion. *Power from Sea Waves.*
- Business Report (2006a). Pilot wave energy investment likely. [online].
Available at: <http://www.businessreport.co.za>. [Accessed: 27 May 2010]
- Business Report (2006b). Sa's wave energy potential. [online].
Available at: <http://www.businessreport.co.za>. [Accessed: 27 May 2010]
- Cargo, C., Plummer, A., Hillis, A. and Schlotter, M. (2011). Optimal Design of a Realistic Hydraulic Power Take-off in Irregular Waves. *Centre of Power Transmission and Motion Control.*
- Carnegie Corporation (2011). CETO Technology. [Online].
Available at: <http://www.carnegiwave.com/index.php?url=/ceto/what-is-ceto>
[Accessed: 1 August 2011]
- Carter, R. (2005). *Wave Energy Converters and a Submerged Plate*. MScEng, Honolulu: University of Hawaii.
- CRES (2002). Wave Energy Utilization in Europe: Current Status and Perspectives. Marathonos Avenue, Pikermi. Greece.
- Cross, P., Taylor, C. and Aggidis, G. (2009). Feedforward Control of a Power Take-off Simulation for Wave Energy Conversion. Engineering Department, Lancaster University, UK.
- Cruz, J. (2008). *Green Energy and Technology: Ocean Wave Energy - Current Status and Future Perspectives*. Bristol (United Kingdom): Springer.
- Davenport, J. (2009). Big wave energy project under investigation in the Western Cape. [Online].
Available at: <http://www.engineeringnews.co.za/article/770-mw-wave-energy-project-under-investigation-2009-09-18>. [Accessed: 27 May 2010]

- De Backer, G., Vantorre, M., Banasiak, R., Beels, C. and De Rouck, J. (2007). Numerical Modelling of Wave Energy Absorption by a Floating Point Absorber System. *Proceedings of the Sixteenth International Offshore and Polar Engineering Conference, Lisbon (Portugal)*.
- De F Retief, G., Prestedge, G. and Muller, F. (1982). A Proposal for Wave Energy Conversion near Cape Town. *Proceedings of 18th Conference on Coastal Engineering, Cape Town, South Africa*.
- DEA (2007). State of the Environment. [Online].
Available at: <http://soer.deat.gov.za> [Accessed: 25 May 2010]
- DME (2003). Simulated Response of a Linear Generator Wave Energy Converter. *White Paper on Renewable Energy*, pp. vii–ix.
- Driscoll, R. and Nahon, M. (1996). Mathematical Modeling and Simulation of a Moored Buoy System. *IEEE*.
- Engja, H. and Hals, J. (2007). Modelling and Simulation of Sea Wave Power Conversion Systems. *Proceedings of the 7th European Wave and Tidal Energy Conference, Porto (Portugal)*.
- Falnes, J. (2004). Ocean Waves and Oscillating Systems. p. 133. University of Cambridge, United Kingdom.
- Falnes, J. (2006). Havbolgje-Energi. Norwegian University of Science and Technology.
- Hals, J. and Engja, H. (2007). Modelling and Simulation of Sea Wave Power Conversion Systems. *EWTEC*.
- Haluzan, N. (2010). Wave Power - Advantages and Disadvantages. [Online].
Available at: <http://www.renewables-info.com> [Accessed: 27 May 2010]
- Harris, R., Johanning, L. and Wolfram, J. (2004). Mooring Systems for Wave Energy Converters: A Review of Design Issues and Choices.
Available at: <http://www.supergen-marine.org.uk/documents> [Accessed: 28 May 2010]
- Huan Lin, A., Yim, M. and Solomon, C. (2006). Coupled Surge-Heave Motions of a Moored System. *Journal of Engineering Mechanics; Technical Papers*, vol. 132, no. 6.
- IEA-OES (2007). *Annual Report*. IEA-OES Executive Committee.
- Isaacs, J. and Seymour, R. (1973). The Ocean as a Power Resource. *International Journal of Environmental Studies*, vol. 4, no. 3, pp. 201–205.
- Joubert, J. (2008). *An Investigation of The Wave Energy Resource on the South African Coast, focusing on the Spatial Distribution of the South-West Coast*. MScEng, University of Stellenbosch.

- Joubert, J. (2010). Personal Communication relating to Projects undertaken in South Africa. [18 November 2010].
- Karnopp, D. and Rosenberg, R. (1975). *System Dynamics: A Unified Approach*. *EWTEC*.
- Langhamer, O. and Wilhelmsson, D. (2006). *Wave Power Devices as Artificial Reefs*. Swedish Centre for Renewable Electric Energy Conversion, Uppsala. Uppsala University, Sweden.
- Le Treut, H., Somerville, R., Cubasch, U., Ding, Y., Mauritzen, C., Mokssit, A., Peterson, T. and Prather, M. (2007). *Historical Overview of Climate Change*. *Climate Change 2007: The Physical Science Basis*. Contribution of Working Group I to the Fourth Assessment Report of the Intergovernmental Panel on Climate Change. Cambridge University Press, Cambridge, United Kingdom and New York, NY, USA.
- McCloy, D. and Martin, H. (1980). *Control of Fluid Power, Analysis and Design*. New York (USA): John Wiley and Sons.
- McLean, G. (1998). Review of recent Progress in Linear Motors. *IEE Proc B Electric Power Applications*, , no. 135, pp. 380–416.
- Ocean Atlas (sa). Advantages and Disadvantages of Wave Energy. [Online]. Available at: <http://www.oceansatlas.com> [Accessed: 26 May 2010]
- Oregon State University (2011). Pelamis Attenuator. [Online]. Available at: <http://nmmrec.oregonstate.edu/pelamis-attenuator> [Accessed: 1 August 2011]
- Petroncini, S. and Yemm, R. (sa). Introducing wave energy into the renewable energy marketplace. *CECS*.
- Polinder, H., Mecrow, B., Jack, A., Dickinson, P. and Mueller, M. (2005). Conventional and TFPM Linear Generators for Direct-Drive Wave Energy Conversion. *IEEE Trans Energy Conversion*, vol. 20, no. 2, pp. 260–267.
- Polinder, H. and Scutto, M. (2004). *Wave Energy Converters and their Impact on Power Systems*. (s.l.):(s.n.), Delft University of Technology, Netherlands.
- Power of Waves (2010). Wave Dragon. [Online]. Available at: <http://powerofwaves.blogspot.com/2010/03/wave-dragon.html> [Accessed: 26 May 2010]
- Power Projects (2008). *Development of Marine Energy in New Zealand*. Prepared for Electricity Commission Energy Efficiency and Conservation Authority and Greater Wellington Regional Council.
- Previsic, M. (2004). *Offshore Wave Energy Conversion Devices*. Technical Paper Published as an Assessment by E2I EPRI.

- Ricci, P., Lopez, J., Santos, M., Ruiz-Minguela, P., Villate, J., Salcedo, F. and de Falcao, A. (2009). Control Strategies for a Wave Energy Converter Connected to a Hydraulic Power Take-off. Institution of Engineering and Technology, Derio (Spain). vol. 5, no. 3.
- Rossouw, C. (sa). Offshore Wave Energy Converters. *ZLH Consulting Engineers (Pty) Ltd.*
- Rossouw, J. (1989). *Design Waves for the South African Coastline*. Phd (Eng), University of Stellenbosch.
- Signorelli, C., Villegas, C. and Ringwood, J. (2011). Hardware-In-The-Loop Simulation of a Heaving Wave Energy Converter. *Centre of Power Transmission and Motion Control. University of Bath.*
- SouthAfrica.info Reporter (2007). Sustainable Development USD40m Wave Energy Plant for SA. [Online].
Available at: <http://www.southafrica.info/about/sustainable/finavera.htm>
[Accessed: 25 May 2010]
- Taylor, C., Stables, M., Cross, P., Gunn, K. and Aggidis, G. (2009). Linear and Nonlinear Control of Power Take-off Simulation for Wave Energy Conversion. *Proceedings of the 8th European Wave and Tidal Energy Conference, Uppsala, Sweden.*
- The Queen's University of Belfast (2002). Islay Limpet Wave Power Plant. Technical Report. (s.l.): (s.n.).
- Thorpe, T. (1992). *A Review of Wave Energy*. Energy Technology Support Unit, Great Britain. Department of Trade and Industry. ETSU-R-72.
- Thorpe, T., Clement, A., McCullen, P., Falcao, A., Fiorentino, A., Gardner, F., Hammerlund, K., Lemonis, G., Lewis, T., Nielsen, K., Petroncini, S., Pontes, M., Schild, P., Sjoström, B. and Sorensen, H. (2002). Wave Energy in Europe: Current Status and perspectives. *Renewable and Sustainable Energy Reviews: ETSU-R-72*, vol. 6, no. 5, pp. 405–431.
- US Corps (2002). Coastal Engineering Manual (CEM).
- Van Niekerk, J. and Joubert, J. (2011). Wave Energy Converters. University of Stellenbosch: Centre for Renewable and Sustainable Energy Studies.
- Vetter, S. (2009). Drought, Change and Resilience in South Africa's Arid and Semi-Arid Rangelands. *South African Journal of Science*. vol. 105. Department of Botany, Rhodes University, Grahamstown 6140, South Africa.
- Vining, J. (2005). Ocean Wave Energy Conversion. Advanced Independent Study Report. Electrical and Computer Engineering Department University of Wisconsin, Madison.

Wave Energy Centre (2006). Wave Energy Technologies. [Online].

Available at: <http://wavec.org/index.php/17/technologies> [Accessed: 10 June 2010]

Wave Energy Centre (sa). Potential and Strategy for the Development of Wave Energy in Portugal. [Online].

Available at: <http://www.wavesenergy.com> [Accessed: 26 May 2010]

Wave Energy Group (2005). Wave Energy. [Online].

Available at: <http://www.wavesenergy.com> [Accessed: 26 May 2010]

Wilson, C. (2010). Choosing your History: Wave Energy Development in the UK. [Online].

Available at: <http://www.historyandpolicy.org> [Accessed: 26 May 2010]

Appendices

Appendix A

Existing Point Absorbers

The existing point absorbers are listed in Figure A.1.



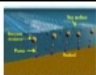


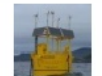


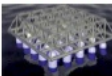










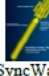


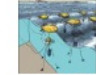






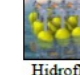








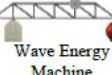








LOCATION	DEVICES				
Nearshore	 PS Frog	 Seadog	 CETO II	 PelagicPower	 EGWAP
	 AquaBuOY	 AWS	 FO3	 Manchester Bobber	 PowerBuoy
Offshore	 FWEPS	 LOPF	 Wavebob	 Wave Catcher	 Triton, Neptune
	 Aegir Dynamo	 Brandl Generator	 PM	 SurfPower	 SyncWave
Near- & Offshore	 Linear Generator	 Sloped IPS	 MHD	 Leancon	 PSP
	 MRC - 1000	 LG - WEC	 OMI	 WET-NZ	 Hydroflot
	 Sperboy	 MotorWave	 IPS OWEC	 WavePumps	 WAP
	 DECM	 WET EnGen	 Wave Star	 Wave Energy Machine	 IWave
	 DCEM	 Seabased AB	 Wave Energy Buoy	 Triton	 Ocean Treader
	 Burin	 CETO 3			

Figure A.1: Existing point absorbers

Appendix B

Values for design parameters

Table B.1: Values for design parameters

Design parameter	Optimal value	Description
a	0.0375 m	Amplitude of wave
T	1 sec	Wave period
r_o	0.075 m	Radius of buoy
m	0.115 kg	Mass of buoy
v	1 m/s	Speed of wave
d	0.45 m	Water depth
k	90 N/m	Spring constant
$C_{d,s}$	0.1	Drag coefficient in surge
$C_{d,h}$	0.1	Drag coefficient in heave
$C_{d,s}'$	0.01	Damping coefficient in surge
$C_{d,h}'$	0.01	Damping coefficient in heave
μ_s	0.65	Added mass coefficient in surge
μ_h	0.55	Added mass coefficient in heave
ϵ_s	0.5	Radiation damping coefficient in surge
ϵ_h	0.63	Radiation damping coefficient in heave

Appendix C

Concepts

Concept 1 (C1)

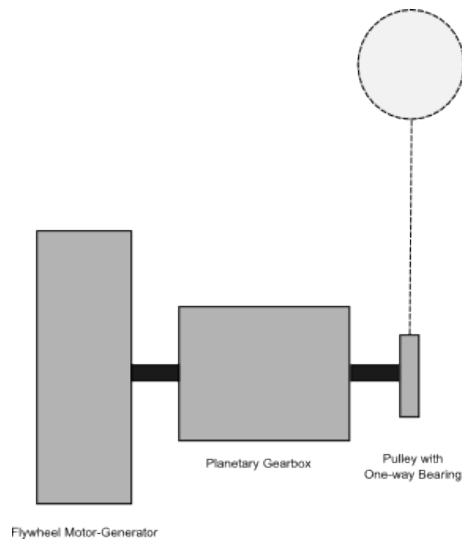


Figure C.1: Concept 1 - Mechanical device

Mechanical power take-off systems may be used in point absorber designs. The system in Figure C.1 uses a pulley to convert the vertical motion into rotating motion. A one-way bearing in the pulley is mounted on the shaft to convert the oscillating rotation into a unidirectional rotation. A planetary gearbox is used to increase the shaft speed, allowing the flywheel-motor or generator to turn at optimal speed. The generator is fitted with a flywheel, enabling the system to store kinetic energy and to have the potential to provide filtered power output.

Concept 2 (C2)

The buoy is connected to a hydraulic piston that is able to pivot around a single point. This allows the power take-off system to follow the movement of the buoy, maximising power output. The hydraulic circuit includes high- and low-pressure accumulators, hydraulic pump or motor, one-way valves and a generator. The advantage of this design is

APPENDIX C. CONCEPTS

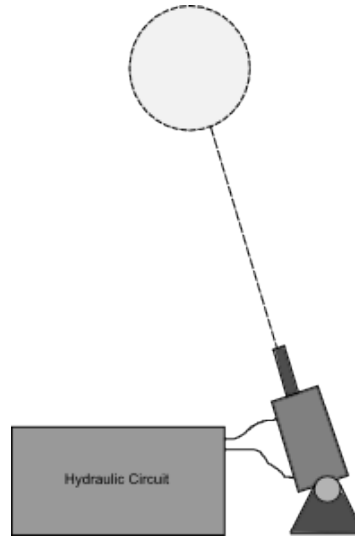


Figure C.2: Concept 2 - Hydraulic device

that there is no rope friction, but one major disadvantage is that the buoy can only be retracted for a short distance that is equal to the piston's stroke length.

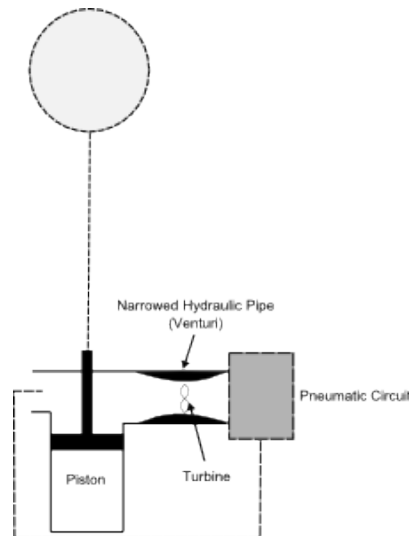
Concept 3 (C3)

Figure C.3: Concept 3 - Pneumatic device

This is a venturi-based design. As the buoy moves upward, air is forced through the venturi. According to the conservation of mass law, the fluid's velocity must increase as it passes through this constriction. The venturi-shaped duct therefore acts as an accelerator, causing an increase in the energy captured by the impulse turbine's blades of given diameter. As the buoy moves downward, air is sucked into and stored in the piston, ready for the next cycle.

APPENDIX C. CONCEPTS

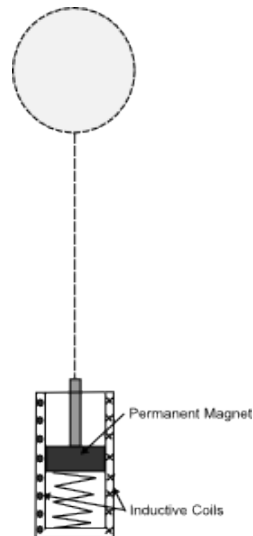
Concept 4 (C4)

Figure C.4: Concept 4 - Linear generator device

In this linear generator system the coils are anchored to the sea floor whilst the permanent magnet is secured to the mooring cable. When the waves cause the buoy to move up-and-down, the permanent magnet moves up-and-down relative to the fixed inductive coils. A voltage is induced and electricity is generated.

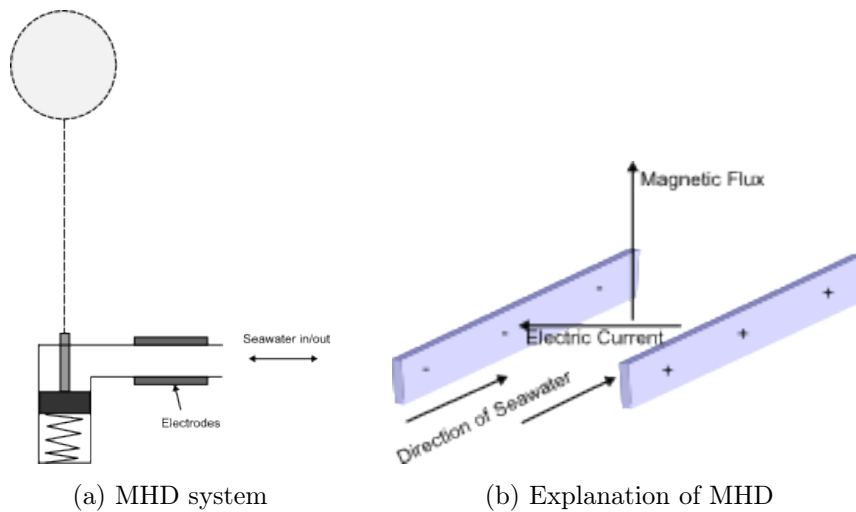
Concept 5 (C5)

Figure C.5: Concept 5 - MHD device

This generator design comprises a vertical piston and horizontal duct arranged to channel the flow of the seawater horizontally in response to the vertical motion of the piston. Two electrodes are mounted on opposite sides in the horizontal duct to apply a strong

APPENDIX C. CONCEPTS

magnetic field perpendicular to the longitudinal axis of the duct and, as a result, to the flow of the water through the duct. The electrodes are in contact with the sea water so that it receives electrical energy generated by the magneto-hydrodynamic phenomenon as explained in Section 2.6.2.2. The electrical energy is conveyed from the electrodes through electrical cables to an external load. One must keep in mind that the polarity of the electrodes change as the direction of sea water flow changes.

Concept 6 (C6)

Figure C.6: Concept 6 - EAP device

This device uses deflectable material, such as electro-active polymers (EAP), that is a stretchable synthetic material (SSM). This material generates electricity when it is stretched. The lower part is anchored to the sea floor, while the upper part is connected to the mooring cable of the buoy. This allows it to move vertically and thereby stretches and relaxes the synthetic materials. The device may even be mounted on a pivot point, allowing it to follow the movement of the buoy in order to maximise power output.

APPENDIX C. CONCEPTS

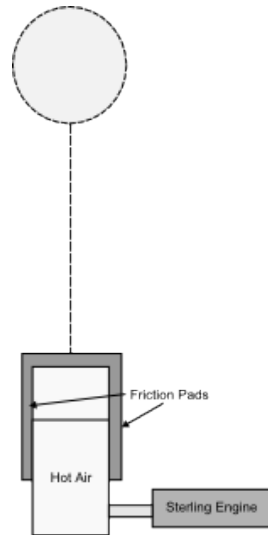
Concept 7 (C7)

Figure C.7: Concept 7 - Friction/ heat device

A friction pad is connected to the mooring cable. As the buoy moves up-and-down, the friction pads cause the air in the pocket to warm up. The warm air can be used to drive a sterling engine.

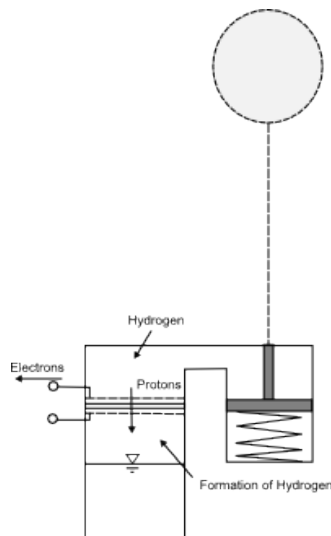
Concept 8 (C8)

Figure C.8: Concept 8 - Hydrogen device

In this configuration the buoy is connected to a piston. The upward movement of the buoy, and therefore the piston, is used to vary the pressure of the upper cavity that is filled with hydrogen gas. As the pressure increases in the upper cavity, the hydrogen penetrates the perforated tinfoil and dissociates at or near the interface between the disk and a protonic

APPENDIX C. CONCEPTS

conductor. The hydrogen ions conduct through the conductor that separates the upper and lower, or low pressure, cavities and the electrons are conducted away through an external circuit. Electrical energy, which is the flow of electrons, is generated. In the lower cavity, or low pressure, the electrons and protons meet again to form hydrogen gas.

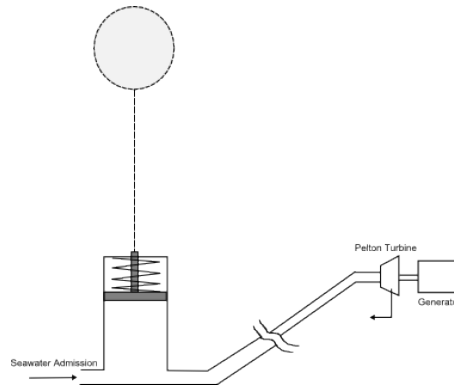
Concept 9 (C9)

Figure C.9: Concept 9 - Sea water pump device

The upward movement of a piston enables the admission of sea water. When the piston returns to its normal position with the buoy moving downward and falling to the trough of the wave, the sea water is pushed through high-pressure pipes. These pipes lead to a pelton turbine that is situated and mounted onshore. The pelton turbine turns a generator, thereby generating electricity. The sea water in the turbine flows back into the ocean.

Appendix D

Concept Evaluation

Table D.1: Decision matrix for wave energy device

Criteria		Importance	Alternatives								
			C1	C2	C3	C4	C5	C6	C7	C8	C9
1	Cost	10		+	-	-	+	-	-	-	-
2	Weight	5		+	-	+	+	+	-	0	-
3	Variable force	9		+	0	0	0	-	0	0	0
4	Complexity	6	R	+	-	+	+	0	-	0	0
5	Availability of components	7	E	0	-	0	0	0	-	-	0
6	Feasibility	10	F	0	-	0	0	-	-	-	-
7	Efficiency	10	E	-	-	-	-	-	-	-	-
8	Adaptability to wave conditions	10	R	-	-	-	-	-	-	-	0
9	Manufacturability	8	E	0	-	0	0	0	-	-	0
10	Assembly time	8	N	0	0	0	0	0	0	0	0

APPENDIX D. CONCEPT EVALUATION

Criteria		Importance	Alternatives (Continued)								
			C1	C2	C3	C4	C5	C6	C7	C8	C9
11	Robustness / Lifetime	10	C	0	0	0	0	-	-	0	-
12	Maintenance	10	E	+	0	+	-	-	-	+	0
13	MTBF	10		0	0	0	0	0	0	0	0
14	Environmental impact	9		-	0	+	+	0	0	+	+
15	Retraction of buoy	10		-	-	-	-	-	-	-	-
Total +			-	5	0	4	4	1	0	2	1
Total -			-	4	9	4	4	8	11	7	6
Overall total			-	1	-9	0	0	-7	-11	-5	-5
Weighted total			-	1	-76	10	-10	-74	-96	-56	-46

Appendix E

Concepts C1 and C2

E.0.0.1 Design of Concept C1

A more detailed schematic of the mechanical power take-off device is provided in Figure E.1. This system will need to increase the rotation speed with a ratio of approximately 125:1. It is impossible to achieve this multiplication in speed using only one gearbox due to the increase in friction angles. As the friction angles increase, the efficiency of the gearbox decreases. At some stage the friction angles will become so high that it will cause the gearbox to come to a complete standstill. A series of industrial gearboxes must therefore be coupled to each other. In this case there will be three gearboxes, each with a gear ratio of 5.6:1.

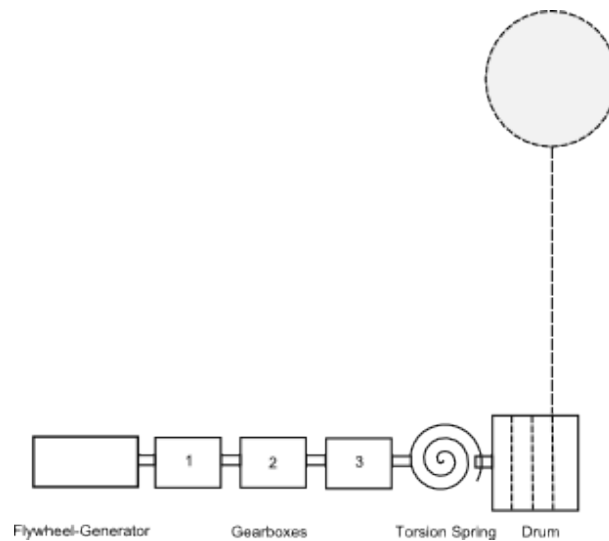


Figure E.1: Schematic of concept C1

As mentioned before, to achieve the motion described in Section 3.3, a positive force must be exerted on the buoy when the buoy's velocity along the cable is positive, otherwise it must be zero (0). As a result the buoy experiences an intermittent force as shown in Figure E.2.

APPENDIX E. CONCEPTS C1 AND C2

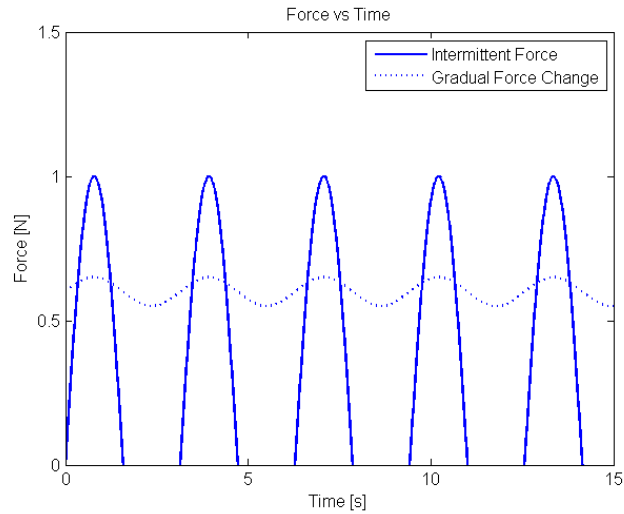


Figure E.2: Intermittent forces versus gradual force changes

The intermittent forces must somehow be converted into more gradual, "continuous" forces, depicted in Figure E.2. This will allow the gearboxes to experience gradual torque changes and not sudden jerks causing high torques. Another reason for having a more gradual output is that if the device is connected directly to the national grid, one would not want to feed a few kilowatts into the grid and then nothing, again a few kilowatts and nothing, and so forth. One would want to have a continuous feeding of power supply into the grid.

This could be achieved by implementing a flywheel into the design as illustrated in Figure E.1. Figure E.3 shows an approximate power output when only a flywheel is incorporated into the design. The power output is slightly better as it is a continuous function, but it still oscillates too much.

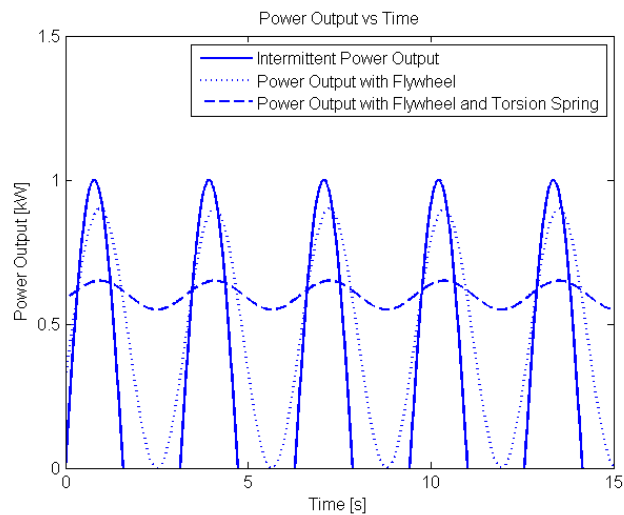


Figure E.3: Power output changing with flywheel and torsion spring

APPENDIX E. CONCEPTS C1 AND C2

Another problem arises when one only uses a flywheel. It must be kept in mind that the upward motion of the buoy is damped. The system therefore experiences an upward pulling force, increasing the speed of rotation of the flywheel. When the buoy moves downward, nothing happens. The system therefore experiences no force and the flywheel's speed is reduced as the kinetic energy of the flywheel is absorbed by the generator and converted into electrical energy. As the flywheel is constantly turning at a variable speed, the upward velocity of the buoy must exceed the rotational velocity of the flywheel for the system to capture and store the energy from the waves in the flywheel. Figure E.4 shows that a certain amount of energy is lost when flywheel's rotational speed exceeds the cable's velocity. The lost energy is illustrated with shaded areas in the figure.

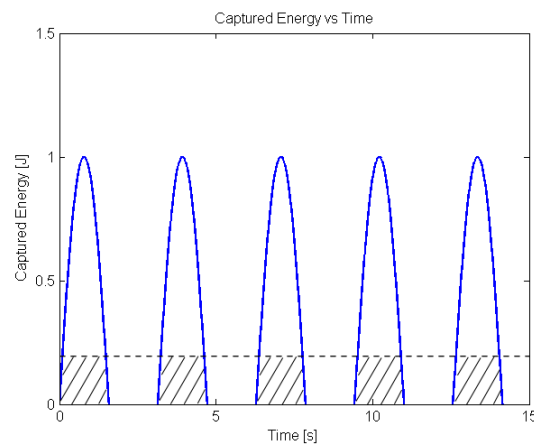


Figure E.4: Energy capture using only a flywheel

Two problems therefore arise: (1) The output is still not gradual or more constant; and (2) energy is lost. One can overcome these difficulties by incorporating a torsion spring into the design, as shown in Figure E.1. The torsion spring will not only change the intermittent output to a more gradual output (Figure E.3), but will also store the energy that is lost when the flywheel's rotational speed exceeds the cable's linear speed. Whereas no energy is effectively lost, complexity is introduced into the system.

E.0.0.2 Design of Concept C2

A more detailed schematic of the hydraulic power take-off device is provided in Figure E.5. As the buoy moves upward, the single-acting cylinder pushes hydraulic fluid through the hydraulic circuit. The hydraulic fluid has a damping effect on the buoy's motion. The piston cylinder is spring-actuated which means that as the trough of the wave passes over the buoy, a tension spring pulls the piston downwards; thereby filling the top chamber with hydraulic fluid. There is a minimal damping effect.

APPENDIX E. CONCEPTS C1 AND C2

Banks of accumulators are used to minimise pulsations and to absorb shocks. This means that an intermittent input will become more gradual, allowing the hydraulic motor to turn constantly. Nitrogen gas bottles are connected to the accumulators with a ratio of approximately 15:1 to increase the effective gas volume while keeping the size and cost of the piston accumulator at a minimum.

High- and low-pressure accumulators are installed on either side of the motor to ensure that hydraulic fluid will constantly flow through the hydraulic motor. As in the case of the mechanical system where the flywheel's rotational speed is higher than the rotational speed of the drum, the pressure in the hydraulic system may be lower than the pressure in the accumulator bank when the buoy starts moving upward.

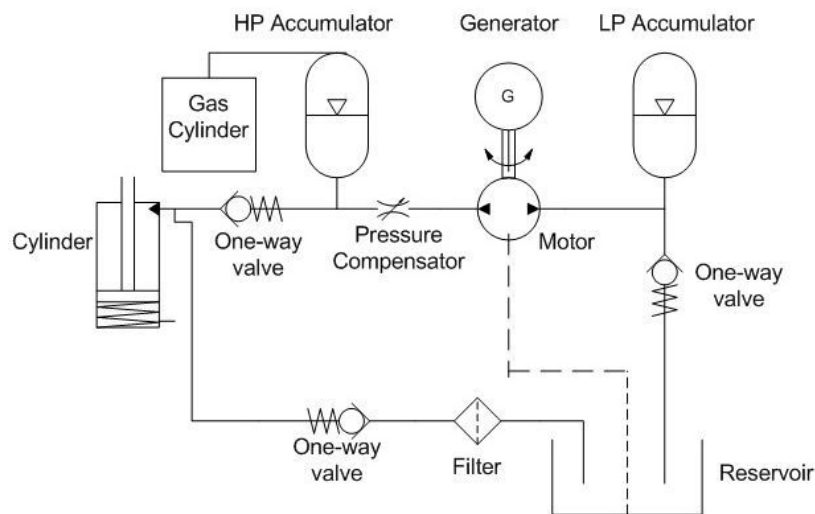


Figure E.5: Schematic of concept C2

A smaller accumulator that is the hydraulic equivalent of the torsion spring, with a lower pre-pressure rating than that of the high-pressure accumulator bank, can be installed to absorb this lost energy.

APPENDIX E. CONCEPTS C1 AND C2

E.0.0.3 Sizes*Concept C1 - Mechanical*

The velocity along the cable is approximately one (1) to two (2) m/s for a full-scale model. The diameter of the drum is chosen to be 2.8 m. The angular velocity of the drum can then be calculated as:

$$\omega = \frac{\nu}{r} \quad (\text{E.0.1})$$

where ν is the velocity along the cable and r is the radius of the drum, respectively. Three industrial gearboxes, each with a gear ratio of 5.6:1, will be connected in series. The gearboxes are rated for a 250 kW output and have input shafts with a diameter of 80 mm. Bearings and couplings are sized according to this specification.

Table E.1: Sizes of components: hydraulic vs mechanical

Hydraulic system		Mechanical system	
<i>Component</i>	<i>Size</i>	<i>Component</i>	<i>Size</i>
Piston	ϕ 0.25 x 3.3 m	Drum	ϕ 2.8 x 2 m
HP accumulator	ϕ 0.45 x 3.5 m	Gearboxes	0.5 x 0.65 x 3
Gas cylinder	ϕ 0.23 x 1.8 m	Flywheel-generator	ϕ 1.5 x 2 m
Motor	ϕ 0.34 x 0.55 m	Spring	ϕ 1.5 x 0.5 m
Reservoir	2 x 1 x 0.5		
Generator	ϕ 0.4 x 0.2 m		
<i>Total Size</i>	2 x 2 x 3.5 ($l \times w \times h$)	<i>Total size</i>	8 x 3 x 3 ($l \times w \times h$)
<i>Total volume</i>	14 m^3	<i>Total volume</i>	74 m^3

Concept C2 - Hydraulic

All hydraulic components are sized according to an internal pressure of 350 bar. The dominant wave height along the South-West coast of South Africa varies between two (2) and three (3) metres. The piston cylinder therefore has a stroke length of three (3) metres.

The approximate sizes of the main components for both the mechanical and hydraulic systems are provided in Table E.1.

E.0.0.4 Mass of Each Component

The weights of the components listed in Table E.1 and the South African suppliers of these components, are given in Table E.2.

APPENDIX E. CONCEPTS C1 AND C2

Table E.2: Weights of components: hydraulic vs mechanical

Hydraulic system			Mechanical system		
<i>Component</i>	<i>Company</i>	<i>Weight</i>	<i>Component</i>	<i>Company</i>	<i>Weight</i>
Piston	Hytec	1000 kg	Drum	Fabrinnox	4500 kg
HP accumulator	HYDAC	1600 kg	Gearboxes	Renold Crofts	2100 kg
LP accumulator	HYDAC	300 kg	Flywheel- generator	-	600 kg
Gas cylinder	HYDAC	300 kg	Spring	-	1000 kg
Motor	Hytec	200 kg	Other (shaft, bearings)	Fabrinnox, Stamcor	100 kg
Reservoir	HYDAC	500 kg			
Generator		100 kg			
Other (oil, fit- tings)	HYDAC	500 kg			
<i>Total weight</i>		4500 kg	<i>Total weight</i>		8300 kg

E.0.0.5 Costs

The approximate costs (including VAT) of each component are provided in Table E.3

Table E.3: Costs of components: hydraulic vs mechanical

Hydraulic system		Mechanical system	
<i>Component</i>	<i>Cost</i>	<i>Component</i>	<i>Cost</i>
Piston	R95 000	Drum	R450 000
HP accumulator	R50 000	Gearboxes	R600 000
LP accumulator	R35 000	One-way bearing	R45 000
Gas cylinder	R20 000	Flywheel-generator	R100 000
Motor	R325 000	Spring	R20 000
Hoses	R2 000	Shaft	R10 000
Check valves	R2 000	Bearings	R21 000
Flow regulator	R3 000		
Filter	R20 000		
Generator	R80 000		
<i>Total cost</i>	R632 000	<i>Total cost</i>	R1 246 000

Appendix F

Engineering Specifications

Table F.1: Engineering specifications

Specification	Unit	Prototype	Model 1/7
<i>Physical characteristics</i>			
Mass (buoy, max)	kg	30 000	10
Mass (PTO, max)	kg	30	10
Buoy diameter (max)	m	10	0.25
Width of PTO (max)	m	1	0.5
Height of PTO (max)	m	1	0.4
Length of PTO (max)	m	2	2
Material	-	HDPE/ steel/ fiber reinforced plastics	HDPE/ steel/ fiber reinforced plastics
Number of parts	#	15	15
Number of moving parts	#	7	7
Control	-	Control movement of buoy for maximum power output (desired path). Pull buoy under water during inclement weather conditions.	Control movement of buoy for maximum power output (desired path). Pull buoy under water during inclement weather conditions.
Complexity	-	Low	Low

APPENDIX F. ENGINEERING SPECIFICATIONS

<i>Performance criteria</i>			
Ave power output (max)	W	250 000	4 000
Survivability/ reliability	-	High	High
Overall efficiency (min)	%	40	40
Pressure (max)	kPa	1 610	120
Impulse force due to buoy movement (buoyancy, max)	kN	5 000	5
Vertical linear speed (max)	m/s	1 – 2	0.2
Rotational speed (max)	rpm	1500	1500
Gear ratio	-	1:200	1:8 – 1:4
Direction of shaft rotation	-	Unidirectional	Unidirectional
Drag	-	Low	Low
Rope friction	-	Low	Low
<i>Manufacturing</i>			
Manufacturing time (max)	hrs	480	20
Assembly time (max)	hrs	2	2
Installation time (max)	hrs	24	5
Tests	months	2	2
Manufacturability	-	High	High
<i>Operating conditions</i>			
Wave period (min, max)	s	9 – 15.5	3.4 – 5.8
Wave length (min, max)	m	126 – 375	18 – 53
Wave height (min, max)	m	1.5 – 5	0.2 – 0.7
Water depth (max)	m	120	17
Flux (max)	W/m	40 000	350
Operating temperature	°C	-5 – 50	-5 – 50
Water resistance	-	High	High

APPENDIX F. ENGINEERING SPECIFICATIONS

<i>Other</i>			
Lifetime (min)	years	20	10
Maintenance (short-term, regular checks)	years	1	1
Maintenance (long-term, full)	years	5	5
Maintenance time	hrs	72	2
Cost (system)	R	10 000 000	10 000
Cost (maintenance)	R	200 000	1 000
Replacement cost of components (percentage of total)	%	10	10
Withstand corrosion (material loss PA, max)	g	10	10
Environmental impact	-	Low	Low
Feasibility	-	High	High
Cost of electricity	R/kWh	1.80	1.80

Appendix G

Parameter Values

Table G.1: PTO model parameters

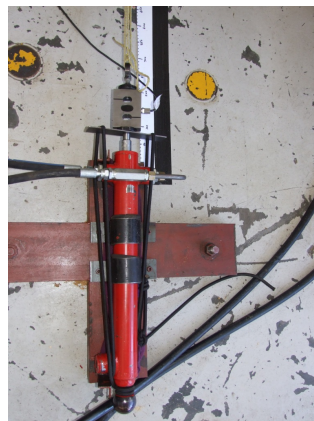
Parameter	Value	Description
f	1 Hz m^2	Wave frequency
r_{amp}	0.2 m	Amplitude of stroke length
K	1.1	Friction force coefficient
c_v	10 s/m	Transition coefficient
F_{pre}	100 N	Preload force of cylinder
$p_{pre,HP}$	20 bar	Precharge pressure of accumulator
$p_{pre,LP}$	1 bar	Pressure in reservoir
C_D	0.75	Discharge coefficient
Re_{cr}	2300	Critical Reynolds number
Re	900	Reynolds number
ν	15 cSt	Kinematic viscosity
ρ_{oil}	0.87 kg/l	Oil density
β_f	15 000 bar	Bulk modulus of oil
β_a	1.42 bar	Bulk modulus of air
β_h	4 700 bar	Bulk modulus of hose
$d_{pipe,in}$	0.008 m	Inlet pipe diameter
$d_{pipe,out}$	0.025 m	Outlet pipe diameter
L_g	4 m	Pipe geometrical length
L_{eq}	1 m	Aggregate equivalent length
J	14.6×10^{-6}	Inertia of motor
T_g	1 Nm	Generator torque

Appendix H

Hydraulic Model



(a) Strain gauge



(b) Load cell

Figure H.1: Sensors

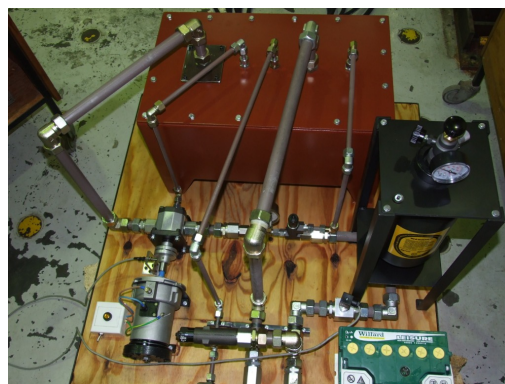
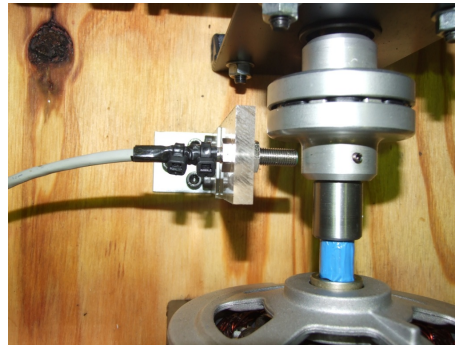


Figure H.2: Hydraulic PTO

APPENDIX H. HYDRAULIC MODEL



(a) Pressure transducer



(b) Proximity sensor

Figure H.3: Sensors



(a) Pressure regulator



(b) Pressure relief valve

Figure H.4: Pressure devices

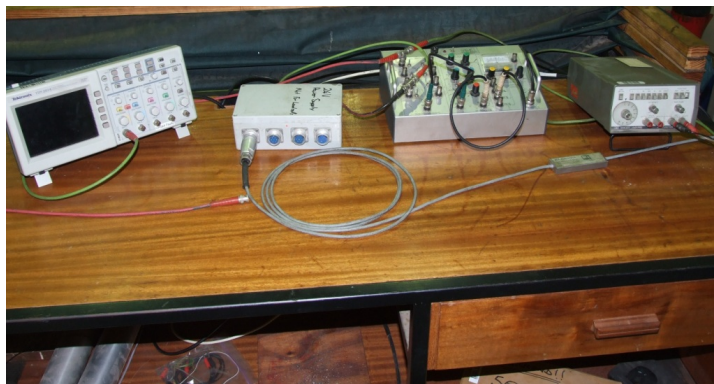
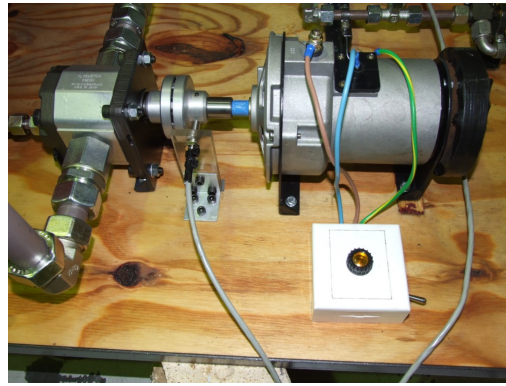


Figure H.5: From left to right: Scope; power supply; PID controller; and signal generator

APPENDIX H. HYDRAULIC MODEL

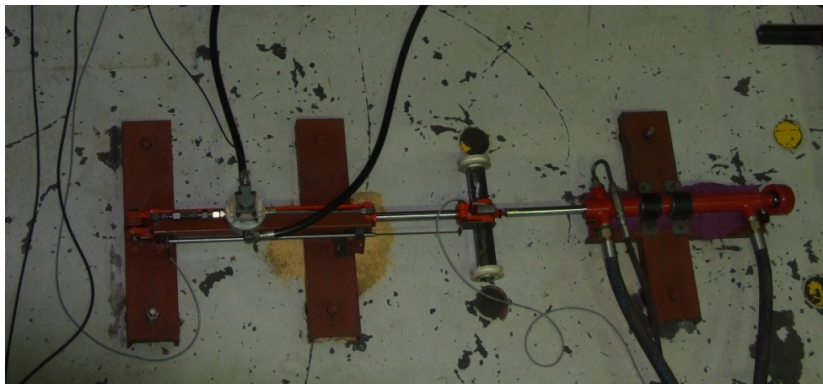


(a) Accumulator

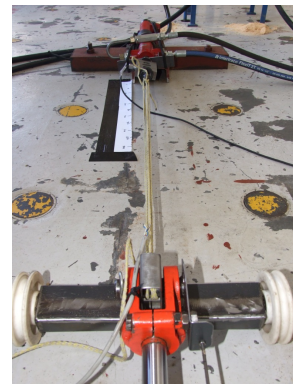


(b) Gear motor and alternator

Figure H.6: Accumulator, gear motor and alternator



(a) Direct coupling



(b) With rope

Figure H.7: Single-acting cylinder (or pump) connected to actuator

Appendix I

Laboratory Tests - Results

I.0.1 Flywheel

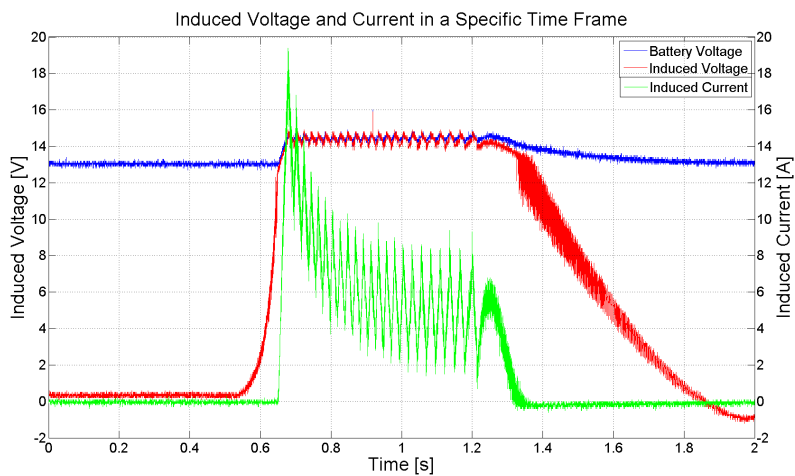


Figure I.1: Induced voltage and current with 2 kg-flywheel

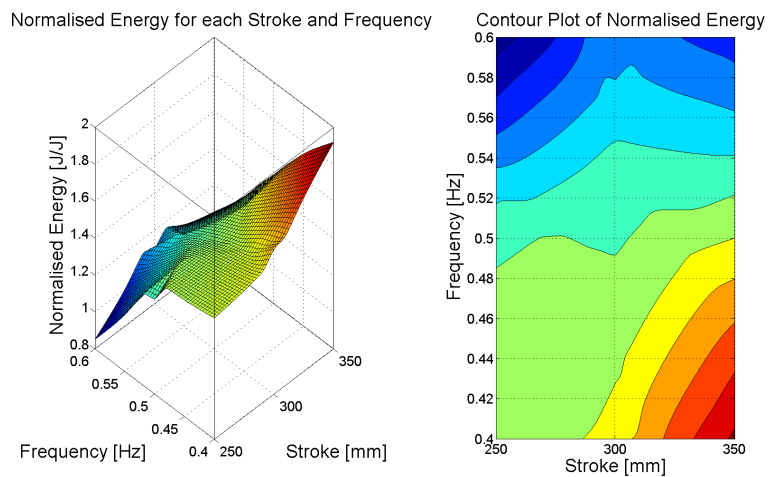


Figure I.2: Normalised energy with 2 kg-flywheel

APPENDIX I. LABORATORY TESTS - RESULTS

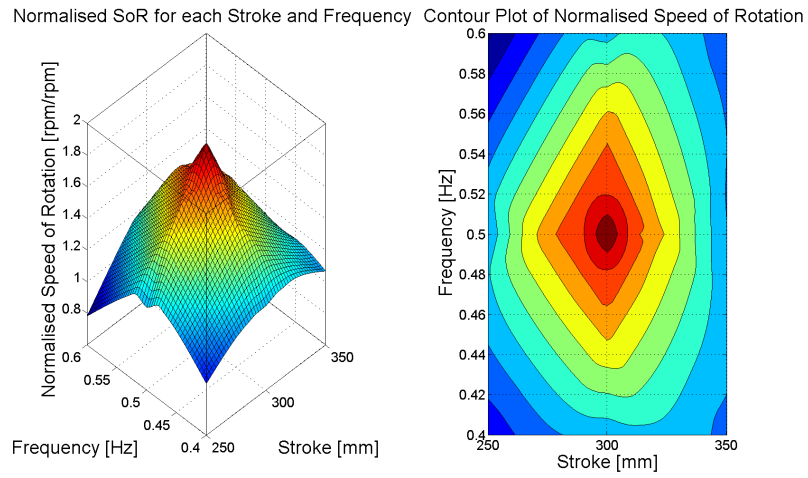


Figure I.3: Speed of rotation with 2 kg-flywheel

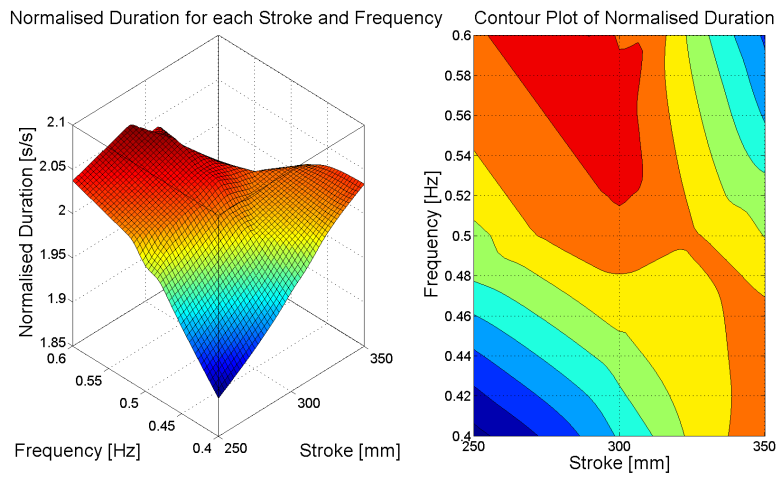


Figure I.4: Duration of rotation with 2 kg-flywheel

APPENDIX I. LABORATORY TESTS - RESULTS

I.0.2 Flow Restrictor at Outlet

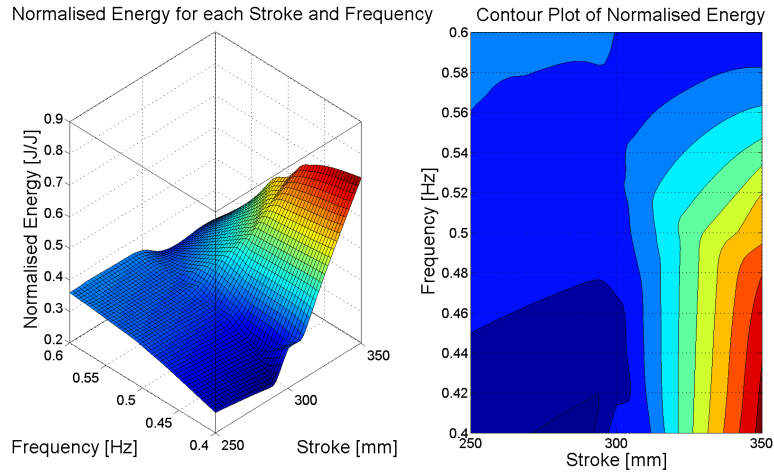


Figure I.5: Normalised energy with back-pressure and 2 kg-flywheel

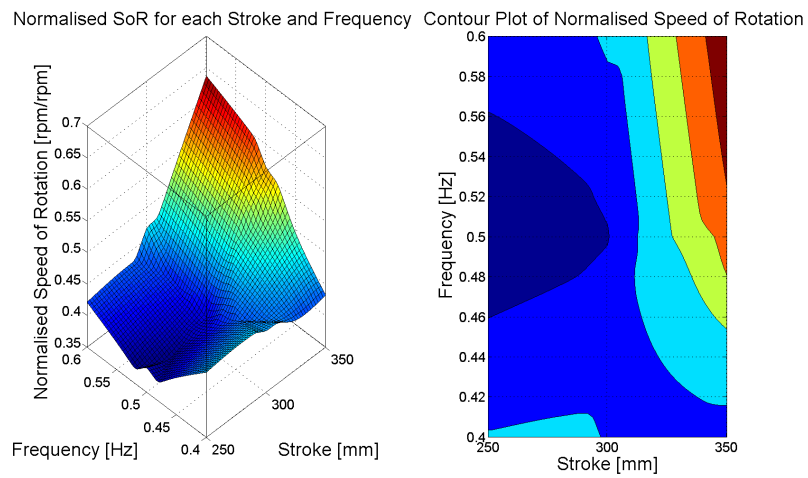


Figure I.6: Speed of rotation with back-pressure and 2 kg-flywheel

APPENDIX I. LABORATORY TESTS - RESULTS

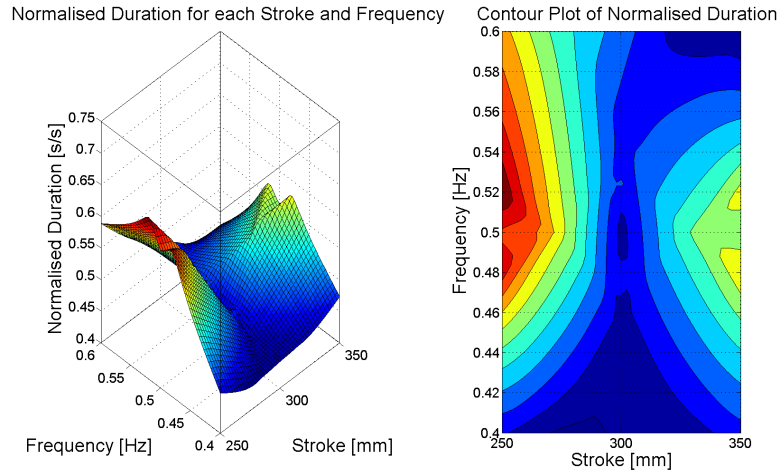


Figure I.7: Duration of rotation with back-pressure and 2 kg-flywheel

I.0.3 Flow Restrictor at Inlet

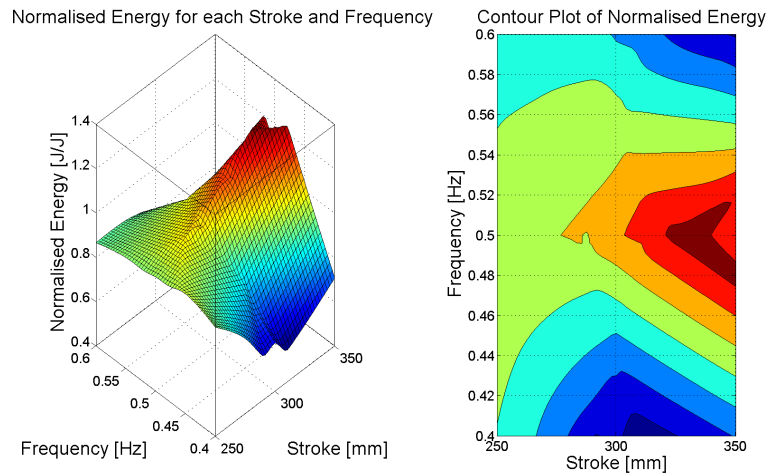


Figure I.8: Normalised energy with flow restrictor at inlet and 2 kg-flywheel

APPENDIX I. LABORATORY TESTS - RESULTS

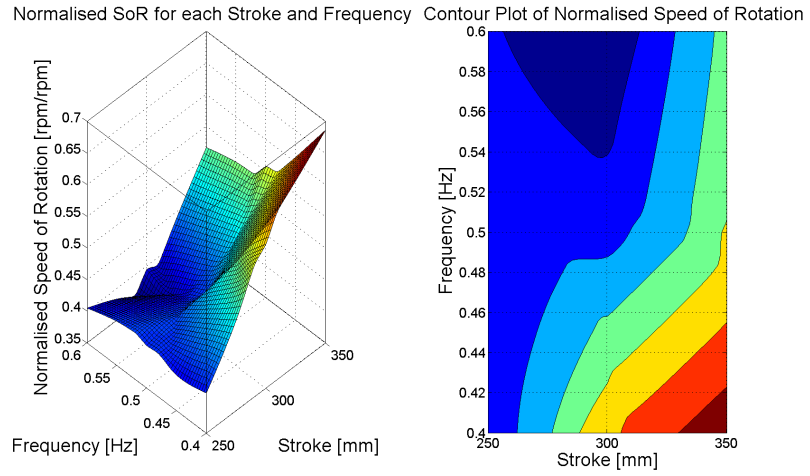


Figure I.9: Speed of rotation with flow restrictor at inlet and 2 kg-flywheel

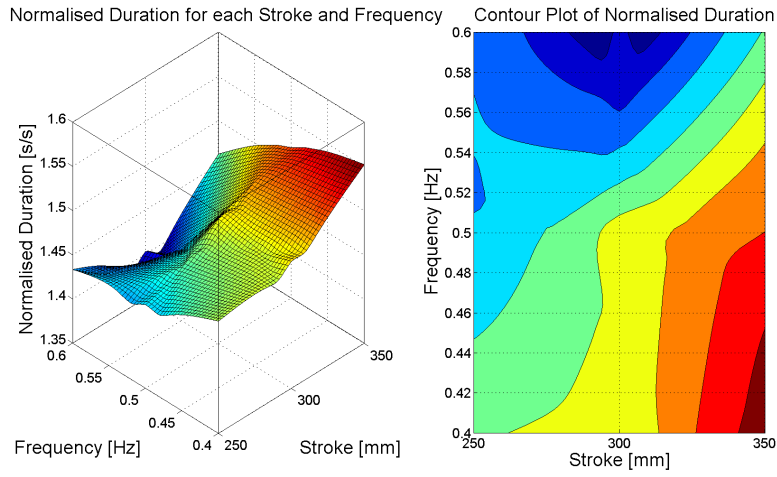


Figure I.10: Duration of rotation with flow restrictor at inlet and 2 kg-flywheel

APPENDIX I. LABORATORY TESTS - RESULTS

I.0.4 Smaller Motor

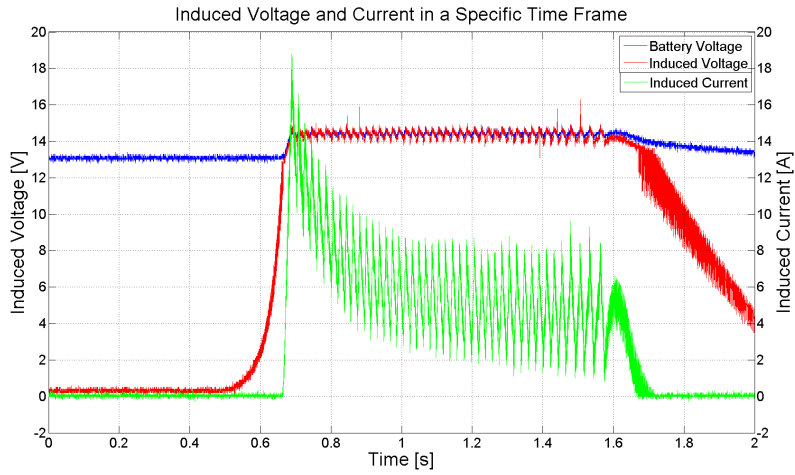


Figure I.11: Induced voltage and current with 6 cc motor and 2 kg-flywheel

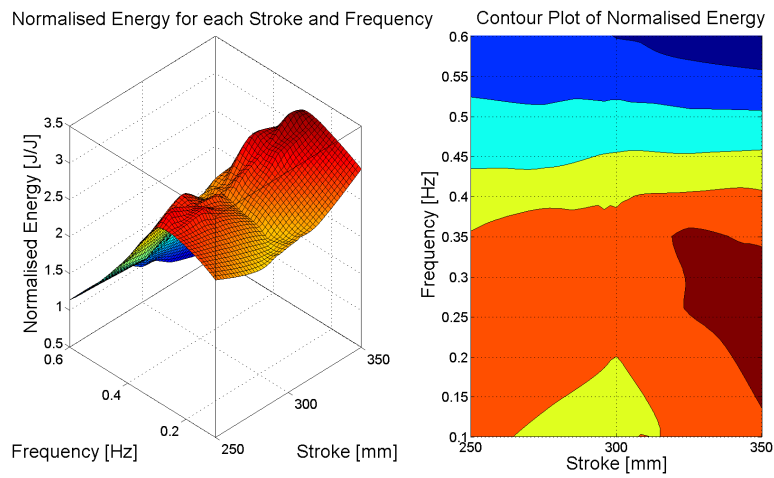


Figure I.12: Normalised energy with 6 cc motor and 2 kg-flywheel

APPENDIX I. LABORATORY TESTS - RESULTS

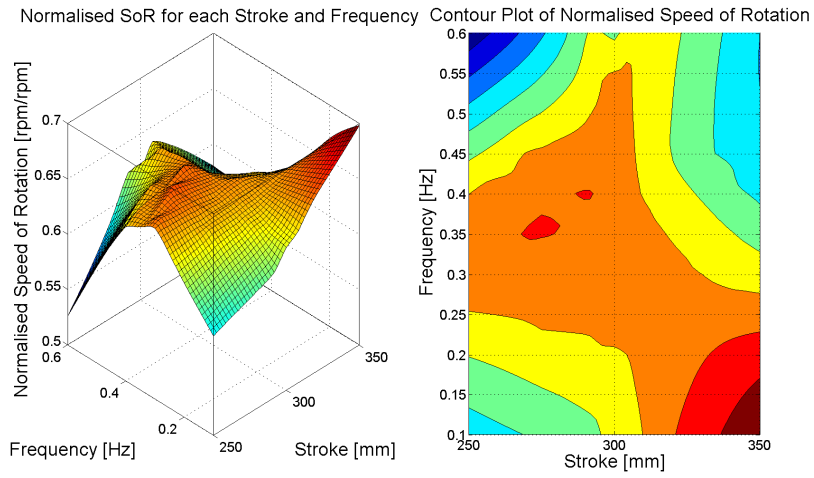


Figure I.13: Speed of rotation with 6 cc motor and 2 kg-flywheel

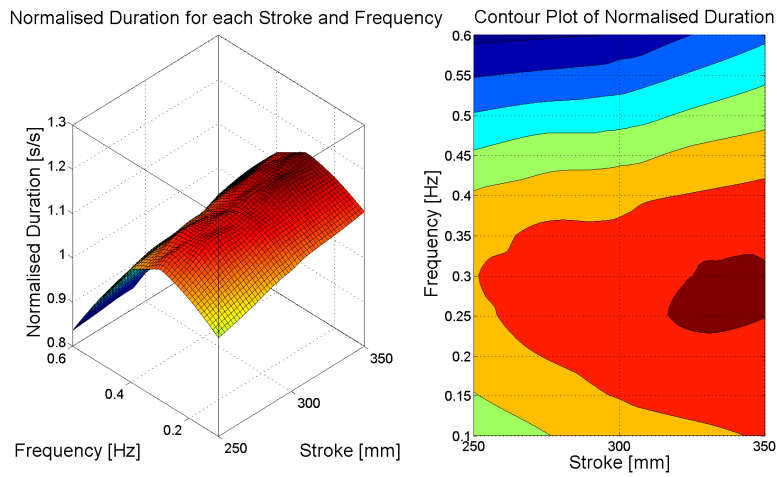


Figure I.14: Duration of rotation with 6 cc motor and 2 kg-flywheel